**Perception-Based Synthetic Cueing for Night-Vision Device
Rotorcraft Hover Operations**

by

Edward N. Bachelder

S.B., Aerospace Engineering
San Diego State University, 1986
S.M., Aeronautics and Astronautics
Purdue University, 1987

SUBMITTED TO THE DEPARTMENT OF AERONAUTICS AND ASTRONAUTICS IN
PARTIAL FULFILLMENT OF THE REQUIREMENTS FOR THE DEGREE OF DOCTOR OF
PHILOSOPHY IN AERONAUTICS AND ASTRONAUTICS
AT THE
MASSACHUSETTS INSTITUTE OF TECHNOLOGY
SEPTEMBER, 2000

Signature of Author: _____
Department of Aeronautics and Astronautics, July 17, 2000

Certified by: _____
Professor R. John Hansman
Professor of Aeronautics and Astronautics
Thesis Supervisor

Approved by: _____
Professor Walter M. Hollister
Professor of Aeronautics and Astronautics

Approved by: _____
Duane T. McRuer

Approved by: _____
Professor Laurence R. Young
Apollo Program Professor of Aeronautics and Astronautics

Approved by: _____
Greg L. Zacharias
Principal Scientist, Charles River Analytics

Accepted by: _____
Professor Nesbitt W. Hagood
Associate Professor of Aeronautics and Astronautics
Chairman, Department Graduate Committee
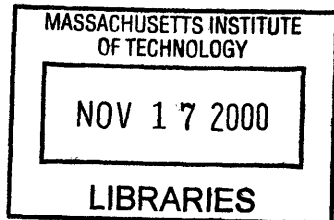
**Perception-Based Synthetic Cueing for Night-Vision Device
Rotorcraft Hover Operations**

by

Edward N. Bachelder

Submitted to the Department of Aeronautics and Astronautics
on July 17, 2000
in partial fulfillment of the requirements for the degree of
Doctor of Philosophy in Aeronautics and Astronautics

Abstract

Helicopter flight using night-vision devices (NVDs) is difficult to perform, given evidence by the high accident rate associated with NVD flight compared to day operation. A mishap analysis of NVD-related helicopter accidents was conducted which found approximately 70% of the accidents attributable to pilot misperception of the flight environment, with the most frequently misperceived states being spatial in nature and in the hover regime. While hardware changes such as increasing the field of view or image resolution may alleviate some of the problems, it is unlikely that they will address all of the perceptual issues. The approach proposed in this thesis is to augment the NVD image with synthetic cueing, whereby the cues would emulate position and motion in an ecological fashion and appear to be actually occurring in physical space on which they are overlaid. Synthetic cues allow for selective enhancement of perceptual state gains to match the task requirements. The perceptual gains examined were aircraft positional error along the three translational axes.

A hover cue set was developed based on an analogue of a physical target used in a flight handling qualities tracking task, a perceptual task analysis for hover, and fundamentals of human spatial perception. The display was implemented on a simulation environment, constructed using a virtual reality device, an ultrasound head-tracker, and a fixed-base helicopter simulator. Seven highly trained helicopter pilots were used as experimental subjects and tasked to maintain hover in the presence of aircraft positional disturbances while viewing a synthesized NVD environment and the experimental hover cues. The simulation employed a number of unique techniques that enabled identification of visual perception and division-of-attention effects. Measures of hover performance and subjective ratings were collected, and frequency analysis was used to measure system (i.e., pilot/display/vehicle suite) stability and bandwidth.

Significant performance improvements in NVD flight were observed when using synthetic cue augmentation. Subjective ratings showed longitudinal control to be more difficult than in the other axes for both single and multi-axis control. This thesis demonstrates that artificial magnification of perceptual states through synthetic cueing can be an effective method of improving night-vision helicopter hover operations.

Thesis Supervisor: R. John Hansman, Jr.
Title: Professor of Aeronautics and Astronautics

Acknowledgements

Acknowledgement

To my parents

To Laura

Table of Contents

List of Figures

List of Tables

Notation

Symbols

dB	Decibels, $20\log_{10}(\ )$
e(t)	Error as a time function
e_n	Error component due to remnant
i(t)	System forcing function as a time function
K	Open-loop gain
n_e	Remnant, referred to pilot input
t	Time
T_L	General lead time constant of human pilot describing function, specialized by subscript
x	Longitudinal displacement
y	Lateral displacement
Y	Transfer function or describing function, specialized by subscript
z	Vertical displacement
ε	Magnification factor
δ	Pilot control input
θ	Pitch angle
ρ_n	Relative remnant
σ	Standard deviation
τ	Pure time delay
φ	Roll angle
φ_M	Phase margin
ω	Angular frequency, rad/sec
ω_c	System crossover frequency, i.e., frequency at which $|Y_pY_c| = 1$

Subscripts

cmd	Commanded
err	Error

Acronyms

ANVIS	Aviators Night Vision Imaging System
FOV	Field of View
GPIP	Glide Path Intercept Point
GPS	Global Positioning System
IHADSS	Integrated Helmet and Display Sighting System
LOS	Line of Sight
NVD	Night Vision Devices
NVG	Night Vision Goggles
UAV	Unmanned Aerial Vehicle
UCE	Usable Cue Environment
VFR	Visual Flight Regulations

They're like us ... do you suppose such men would have seen anything of themselves and one another other than the shadows cast by the fire on the side of the cave facing them?

— Plato

Chapter 1

Introduction

Helicopter flight using night vision devices (NVDs) is difficult to perform, given evidence by the high accident rate associated with NVD flight compared to day operation shown in Figure 1.1. Analyzing summary reports of 367 NVD-related helicopter
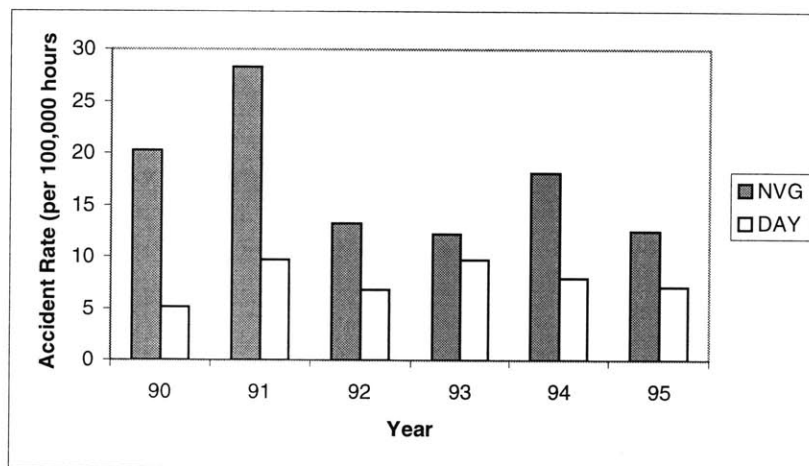
Figure 1.1. Flight accident rate for U.S. Army helicopters, 1990-1995 (Army Safety Center).

accidents from the U.S. Army, Navy and Marines that occurred during 1984-1996 (U.S. Army and Navy Safety Centers), it was found that approximately 70% of the accidents were attributable to pilot misperception of the flight environment. Figure 1.2 categorizes these perception-related accidents according to the misperceived state and flight regime as interpreted from the accident summary reports (note that more than one state may contribute to an accident). While showing NVD hover operation to be more difficult than day operation, Figure 1.2 also indicates hover to be the most challenging NVD flight regime. Of these hover accidents, the states most frequently misperceived were spatial in

nature, and, significant to this study's findings, a number of incidents involved rearward drift.
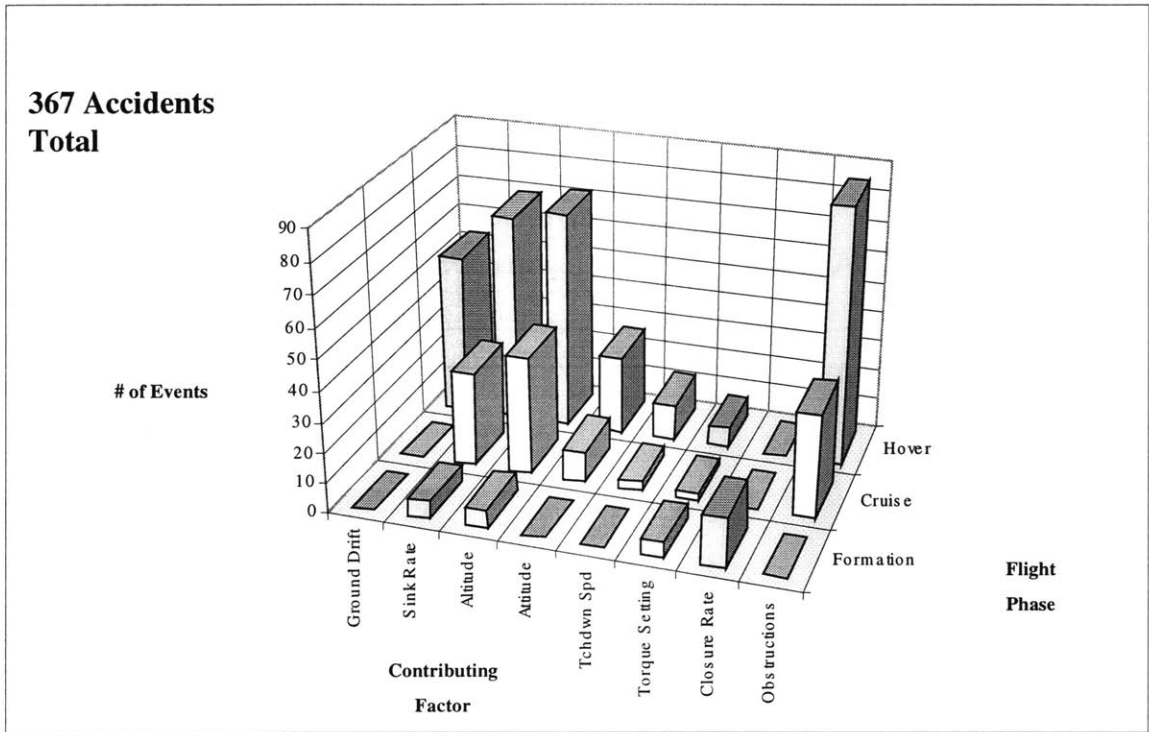
Figure 1.2. NVD-related helicopter accidents for U.S. Army, Navy and Marines, 1984-1996 (Army and Navy Safety Centers).

Figure 1.3 shows an example of an image viewed with night vision goggles. Three key factors contributing to NVD spatial misperception are: (1) limited field of view (FOV), (2) poor contrast, and (3) poor display resolution. Numerous studies have been conducted to identify FOV effects and areas of the visual field that are responsible for various spatial perceptual functions (Gillingham, 1986); however, these are difficult to apply directly to NVD flight given the confounding factors of poor contrast and display resolution. One study (Hoh, 1984), however, investigated the effects of FOV, macrotexture (large, well-defined objects), and microtexture (fine-grained texture) on subjective ratings during precision, aggressive low speed and hover tasks. Interestingly,

Figure 1.3. Night vision goggle image.

microtexture was found to be the critical factor to inner-loop control (attitude, position

rate), with FOV being of secondary importance beyond ± 20 degrees. The findings of

this study are summarized in Figures 1.4 and 1.5. Figure 1.4 is a simplified model

showing the channels of sensing and perception available during day flight. In Figure 1.5

only the channels available for NVD flight are shown. Comparing Figures 1.4 and 1.5, it

is seen that the pilot's perception of velocity, depth and height during NVD operation

becomes degraded since much of this information is normally sensed through peripheral

vision. Also, due to poor display resolution much of the information from microtexture

(velocity and attitude rate) is also lost. The pilot must therefore visually sense all spatial

information, primarily from macrotexture, using central vision.

In terms of the compensatory, precognitive and pursuit paradigm (McRuer, 1974),

this combination of factors tend to bias pilot behavior toward compensatory control, as

pilot maneuvers are restricted to error information without being able to take advantage

of cues stemming from display of background reference frames and/or preview aspects of

wide FOV visual flight.
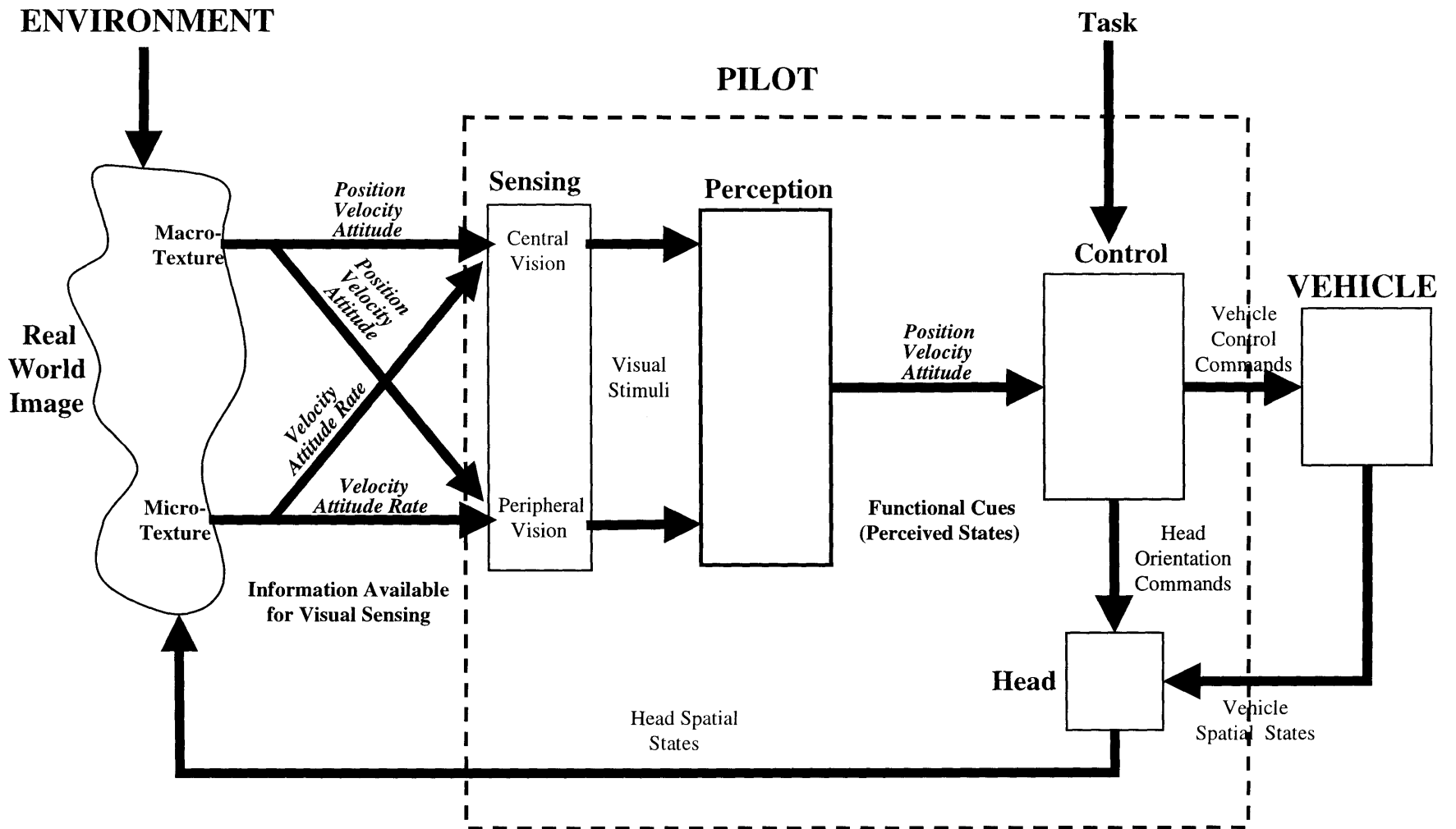
Figure 1.4. Visual sensing and perception channels during day hover.
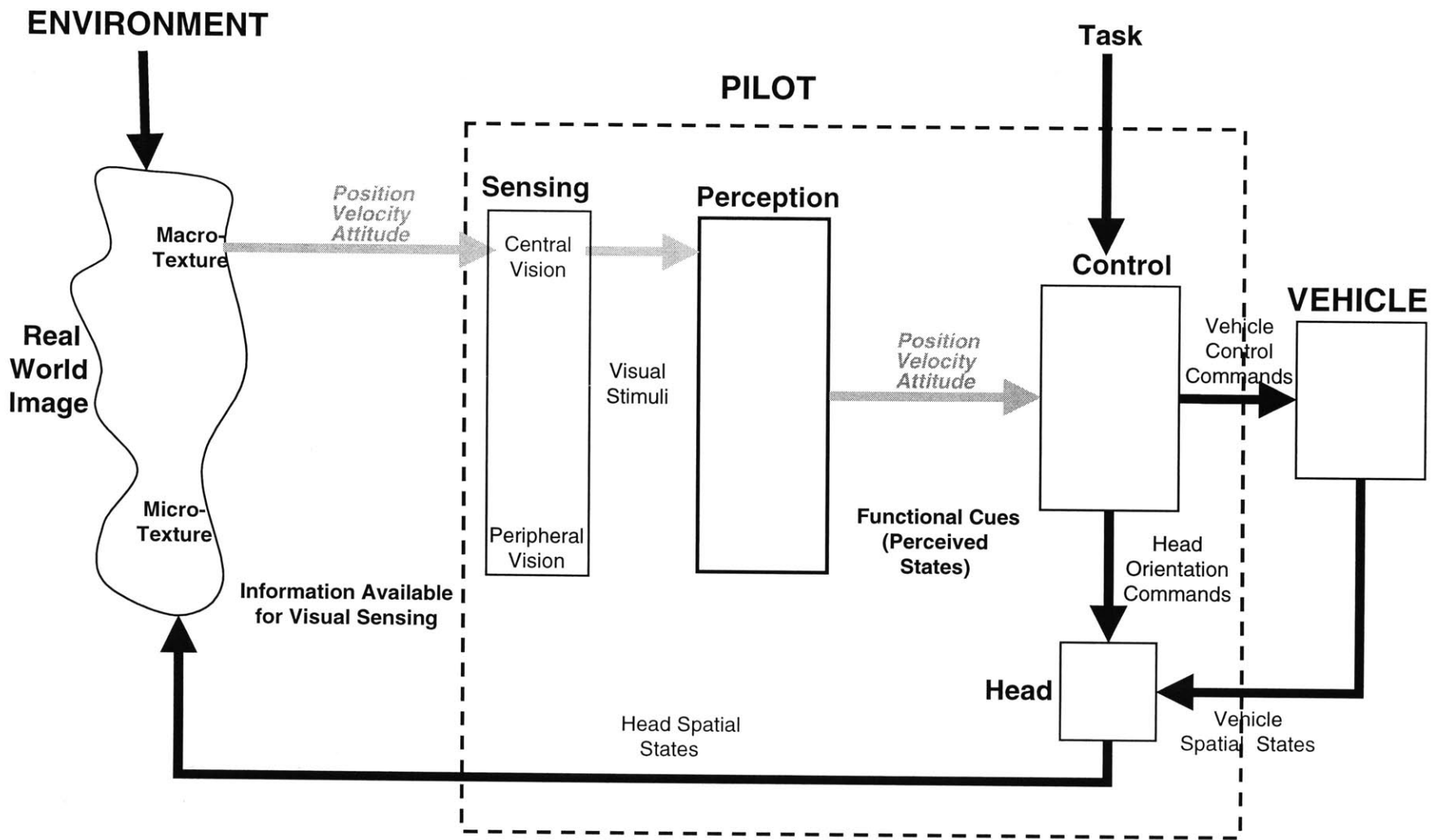
Figure 1.5. Visual sensing and perception channels during NVD hover.

In addition to reduced spatial awareness, static and dynamic visual illusions can occur during NVD flight (Miller, 1992; Crowley, 1992). While hardware changes such as increasing the FOV or image resolution may alleviate some of these problems, it is unlikely that they will address all of the perceptual issues. A favored current approach (e.g., Hoh, 1986) is to employ degrees of aircraft stabilization based on what is defined as the Usable Cue Environment (UCE) for a given display system (Figure 1.6 provides the definition of UCE found in the Army's "Handling Qualities Requirements for Military Rotorcraft"). But this approach can also introduce some unfavorable features. For instance, the conclusion reached by this study was that "the use of attitude command augmentation was found to be effective as a way to make up for display deficiencies. However, a corresponding loss of agility occurred with the tested attitude command/attitude hold system resulting in unfavorable pilot comments. Hence, the favorable control display tradeoff must be interpreted in the context that the best solution would be to improve the vision aid. Such an improvement would require an increase in the visible microtexture, an advancement in display technology which is unlikely to be available in the foreseeable future." (Hoh, 1986).

The approach proposed in this thesis is illustrated in Figure 1.7, whereby the NVD image is augmented with synthetic spatial cueing. These cues would emulate position and motion in an ecological fashion (van Paasen & Mulder, 1998), and appear to be actually occurring in the physical space on which they are overlaid. Ecological interface design (EID) (Vicente, 1992) employs some basis of perception in the physical world, where evolved perceptual capabilities are used to make inferences about the state of the world, for instance, or a HUD-presented attitude symbol or runway, or highway-in-

3.2.2.1 **Determination of the Usable Cue Environment.** The displays and vision aids provided to the pilot shall be assessed to determine their effectiveness for stabilization and control. The visual cue ratings shall be determined using all displays and/or vision aids that are expected to be operationally available to the pilot, in the Degraded Visual Environments specified in Paragraph 3.1.1. The usable cue environment (UCE) is defined in Figure 2(3.2) using the visual cue ratings obtained from the Figure 1(3.2) scale during the flight assessments specified below. Points falling on a boundary in Figure 2(3.2) will be considered to lie in the region of numerically higher UCE.

The translational rate visual cue rating to be applied to Figure 2(3.2) is the poorer (higher numerically) of the horizontal and vertical axis ratings obtained from Figure 1(3.2). The visual cue ratings (VCRs) are to be made by at least 3 pilots and the UCE shall be obtained by using the mean VCRs in Figure 2(3.2). The test rotorcraft must meet the requirements for a Rate Response-Type as defined in Paragraph 3.2.5 and have a Level 1 mean pilot rating (Figure 1(2.8) scale) by at least 3 pilots operating without any vision aids in good visual conditions (UCE=1) and negligible turbulence. The following Mission-Task-Elements shall be flown when making the UCE assessments: hover, vertical landing, pirouette, acceleration and deceleration, sidestep, bob-up and bob-down. The task descriptions and performance limits specified in Sections 4.4 and 4.5 for each of these maneuvers shall apply when making the VCR ratings except that the maneuvers may be flown in calm winds.
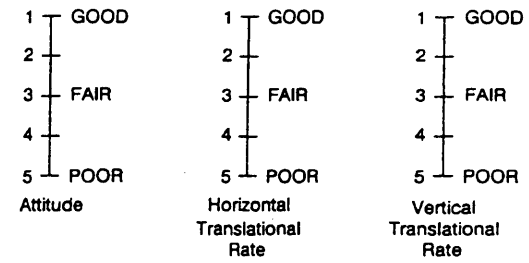
DEFINITIONS OF CUES

X = Pitch or roll attitude and lateral, longitudinal, or vertical translational rate.

Good X Cues: Can make aggressive and precise X corrections with confidence and precision is good.

Fair X Cues: Can make limited X corrections with confidence and precision is only fair.

Poor X Cues: Only small and gentle corrections in X are possible, and consistent precision is not attainable.

Figure 1(3.2). Visual Cue Rating (VCR) Scale to be Used When Making UCE Determinations
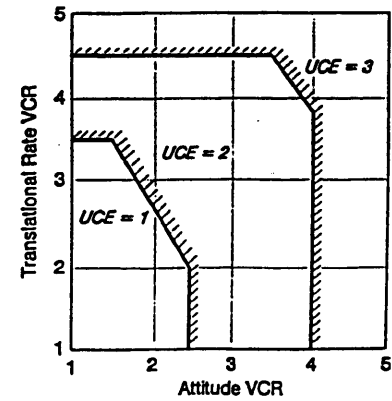
Figure 2(3.2) Definition of Usable Cue Environments

Figure 1.6. Definition of Usable Cue Environment (ADS-33D)
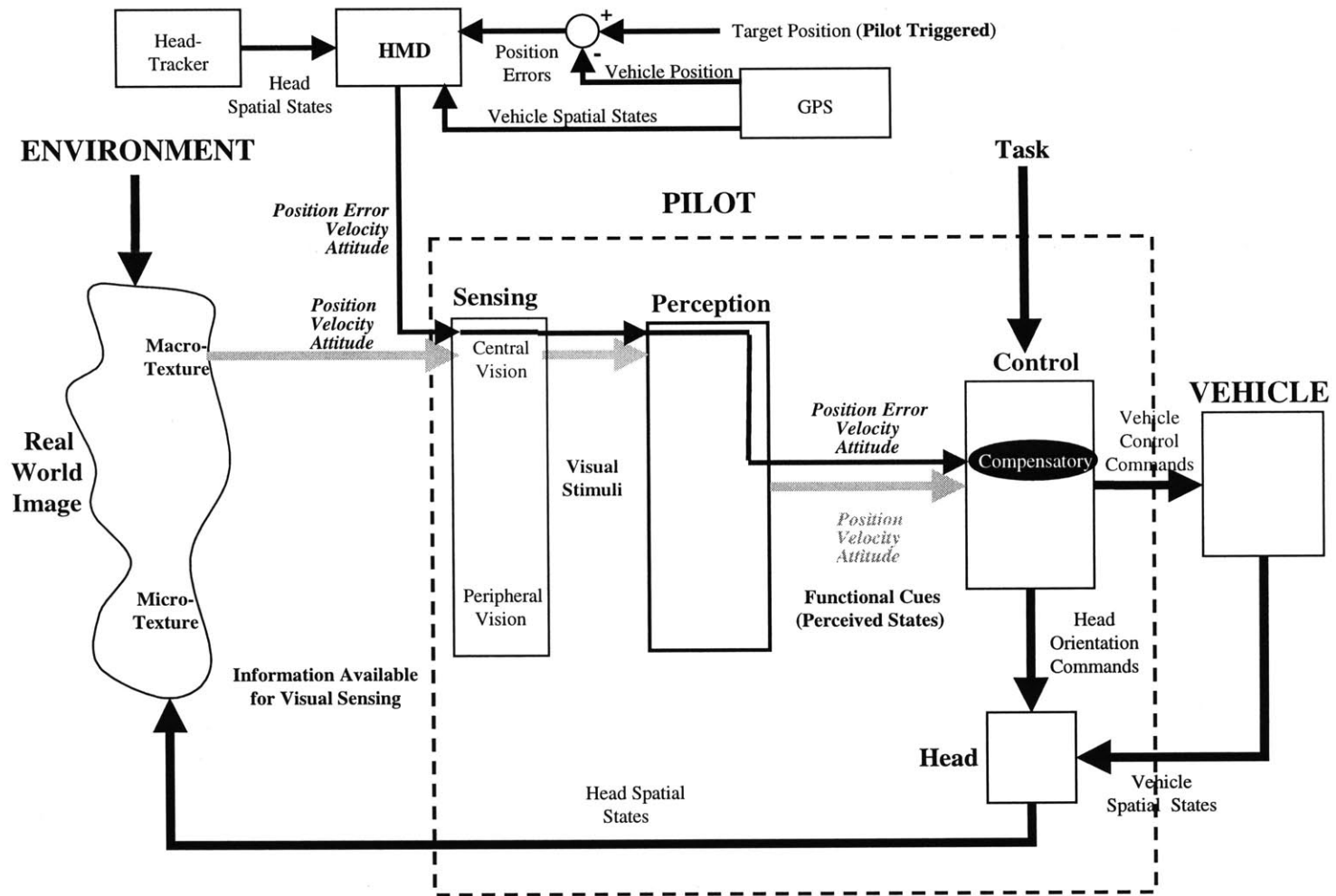
Figure 1.7. Role of synthetic cues during NVD hover.

sky. This contrasts with a conventional display, where symbology (i.e., alphanumerics, dials, light strips) behaves in ways that are meaningful through convention.

Among the cognitive and reliability engineering communities, it is widely accepted that information can be interpreted in three mutually exclusive ways – as signals, signs, or symbols – and that the way in which information is interpreted determines which of the three levels of cognitive control (skill-based, rule-based, or knowledge based behavior) is activated. Two advantages of ecological interface design are: (1) mental economy – the rule-based level of cognitive control involves less effort than the knowledge-based level, and (2) because there is a 1:1 mapping between symbols and signs (a fundamental principle of EID), the operator can exhibit what looks like knowledge-based behavior by merely relying on rule-based behavior. The advantage of knowledge-based control is that its applicability is not restricted to specific conditions (e.g., frequently encountered scenarios) as rule-based control often tends to be. The 1:1 mapping therefore allows the operator to take advantage of the cognitive economy of rule-based behavior while, at the same time, preserving the wide applicability of knowledge-based behavior (Vicente, 1992).

In the synthetic spatial cueing approach, sensing systems measure aircraft and head spatial states that are relayed to an onboard computer, which performs coordinate transformations and generates hover-aiding symbology overlaid on the NVD image. Both the synthetic cues and NVD image enter the pilot's perceptual field and prompt control actions.

A number of advances have made synthetic cueing technically feasible. Global Positioning System (GPS) enables precise measurement of position and attitude that can

be used for driving the display symbology. In the absence of GPS (i.e., due to signal masking), an onboard inertial system could provide rate information and position relative to a reference point and attitude, with altitude being sensed by radar. Head tracking systems allow symbology to be head-referenced so pilots can see spatial information in its natural context. The display used in this thesis was set up for non-coupled, tightly attitude-controlled helicopters. State-of-the-art helicopter design already employs these dynamics – the challenge today is presenting the proper synthetic visual cues to improve impoverished Usable Cue Environments. On a display/control tradeoff, it is proposed that this display concept could be used with state-of-art helicopter dynamics to provide a Usable Cue Environment of 1.

1.1 Research Objectives and Approach

While there currently exist operational hover displays that are overlaid on a sensed image, such as the Apache Integrated Helmet and Display Sighting System (IHADSS) discussed in §1.3, it does not appear that a study to date has been conducted for an ecological display for use with an NVD. Research has shown important advantages when spatial information is presented in its natural context rather than represented abstractly (McCann, 1995; van Paasen & Mulder, 1998). Using the helicopter NVD problem as an area of focus, this thesis investigates key perceptual issues regarding the use of synthetic spatial cues that are displayed ecologically for helicopter hover. Synthetic cues allow perceptual gains to be selectively adjusted in different axes to match the task, but while this is ecological it is only pseudo conformal in that motion along specific axes is artificially enhanced. In this thesis, the states adjusted were aircraft positional error along the three translational axes, which allowed pilot position error

sensitivity to be adjusted as a gain. This raised a number of issues that have not been previously addressed in the context of helicopter hover, such as: Can gain be changed along one axis independent of the other two without having negative consequences? What is the range of perceptual gains for which the pilot can maintain relatively steady performance? Is there an optimum gain region (i.e., based on subjective ratings and performance) that is shared by pilots? If such an optimum region exists, what factors would influence its location? Will control behavior be identical for each axis given the same perceptual gains? How do axes compete for control attention? Will gain mixing (e.g., assigning different gains to separate axes) give rise to perceptual conflict when the synthetic cues are overlaid on a natural scene?

In order to investigate these questions a hover cue set was developed based on a functional requirements analysis of a hover display, fundamental principles of human spatial perception, and expansion of a concept employed in a flight handling qualities tracking task. The display was implemented on a simulation environment, constructed using a virtual reality device, an ultrasound head-tracker, and a fixed-base helicopter simulator. Fixed-base simulation does not provide pilots with the vestibular feedback present in actual flight, so that performance between the two environments may differ. The results of this study are nonetheless useful for indicating trend behavior for full-motion flight. Its findings are directly applicable toward fixed-base, virtual-reality environments, although for remotely piloted operations the issue of transmission time delay (not addressed here) can introduce severe performance limitations.

Seven highly trained helicopter pilots (four with extensive NVD experience) were used as experimental subjects tasked with maintaining a hover in the presence of aircraft

positional disturbances while viewing a synthesized NVD environment and the experimental hover cues.

The simulation conceptually employed a number of techniques that made it uniquely different from previous helicopter simulation studies. The vehicle dynamics were completely decoupled so that vehicle translation along a given axis did not interact with motion of another axis. In order to provide the pilot with realistic feedback the aircraft was allowed to *virtually* (i.e., visually) roll and pitch in response to cyclic inputs – the actual rotational motion of the vehicle was frozen in all axes so that motion in response to control inputs was purely translational. An automatic heading hold kept yaw constant. If the helicopter had been allowed to actually rotate, then a maneuver such as left translation along the aircraft body axes (involving a left roll) would create both a left and vertical translation component in the geographic axis system – to maintain altitude the pilot would have to make a control adjustment in the vertical (collective input). By only allowing the aircraft to *virtually* roll and pitch, the aircraft coordinate system remained rotationally aligned with the geographic axes.

The positional disturbances were geographically referenced (North-East-Down) so that the full component of each axis' disturbance would be acting along the intended aircraft axis. The positional disturbances imposed on the helicopter were designed to be both realistic and a diagnostic probe for pilot control behavior. Composed of a sum of non-harmonically-related sine waves, the disturbance was perceived by the pilot as a random process – the result, however, was that the pilot's control response power resided largely at the same frequencies contained in the input disturbances. Each axis

disturbance was unique in frequency content to allow for independent analysis of individual axes.

Yaw was held constant so that: (1) the aircraft and disturbance axes remained aligned, and (2) the pilot's perception of translation would not be skewed or coupled with yaw motion. The vehicle translational dynamics for each axis were made identical (rate commanded), the control gains for collective and cyclic were set equal, and the controls were made spring centering. The intention of the simulation design was to create an environment where differences in performance between axes would be due primarily to visual perception and control strategy differences.

In this study measures of hover performance and subjective ratings were collected, and qualitative observations relating to perception were made possible through the experimental design.

In addition to examining the viability of synthetic-cued hover flight, this thesis conducts a first study of its kind in division-of-attention issues with application toward 3D translational hover control. Based on the Crossover Model, physical explanations are offered for hover control. From this research, limited predictions for hover performance, control behavior, and subjective ratings should be possible for visual flight systems (i.e., remotely controlled unmanned aerial vehicles (UAVs)) using a similar display concept. Lastly, a number of interesting practical measurement and simulation issues were also encountered and examined.

1.2 Night Vision Goggle Hardware and Operational Characteristics

1.2.1 Electro-optical Design

The most widely used night-vision device among pilots in the U.S. Armed Services is the III-Gen ANVIS (Aviator's Night Vision Imaging System), shown in Figure 1.8. ANVIS employs two image-intensifier (I^2) tubes that amplify ambient light reflected from an object and present an intensified image on a phosphor screen – unlike binoculars, direct viewing of objects does not occur. Ambient light entering the I^2 tubes is focused by an objective lens onto a photocathode. The schematic diagram of an I^2 tube is given in Figure 1.9. When photons of ambient light strike the photocathode, which is sensitive to visible and near-IR radiation, electrons are released creating a cascading effect. The electrons are then accelerated and multiplied by a microchannel plate that acts like a large array of photomultiplier tubes. The microchannel plate guides the accelerated electrons to a phosphor screen, which produces an intensified light image. The light intensification capability (amplification) is referred to as the gain of the device. Gain is the ratio of the light delivered to the eye by the phosphor screen to the light striking the objective lens. The output of the phosphor screen is a relatively narrow band peaking at 530 nm, so that the image is essentially monochromatic green and color discrimination between objects is not possible. Finally, the amplified image is made upright by a fiber-optic inverter and focused through the eyepiece lens.
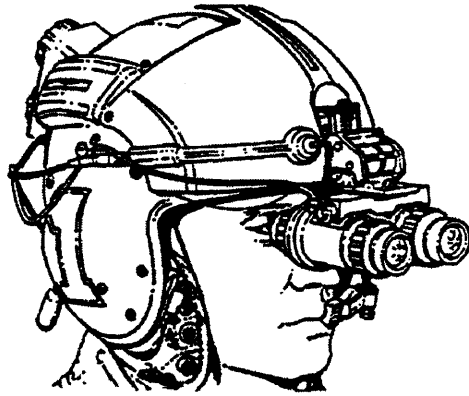
Figure 1.8. ANVIS III-Gen NVG (Miller, 1992).
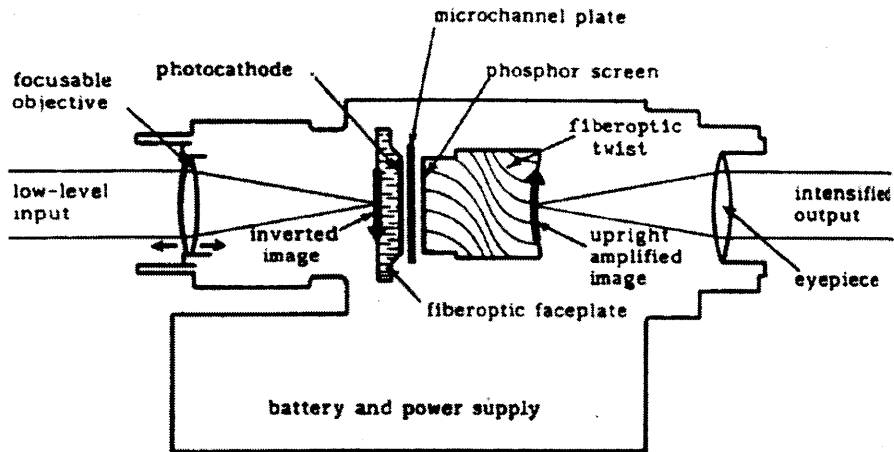
Figure 1.9. Schematic of photocathode tube (Miller, 1992).

1.2.2   Operational Performance and Limitations

The ANVIS is only sensitive to wavelengths in the range of approximately 625

nm to 900 nm (orange, red, and near-IR) shown in Figure 1.10. Also shown in Figure

1.10 are the response profiles for human photopic (day) and scotopic (dark adaptation)

vision. The steep slopes and sharp peaks associated with human vision provide good

contrast, however the relatively flat ANVIS response across its broad sensitivity range

can reduce or completely eliminate contrast gradients.
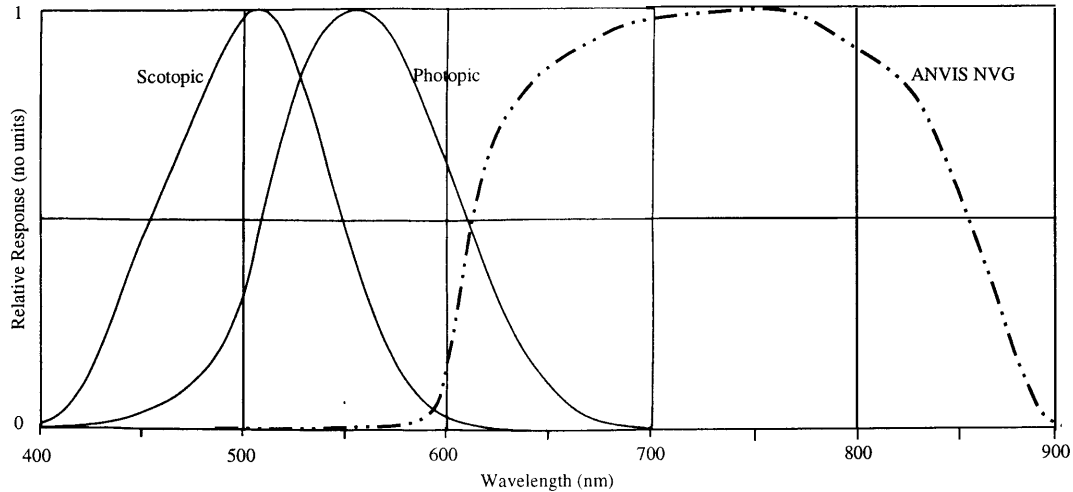
Figure 1.10. Spectral response of human eye and ANVIS III-Gen (adapted from Miller, 1992).

Night vision goggle (NVG) display resolution is 0.77 mrad/cycle (2.8 arcminutes), which would correspond to visual acuity of approximately 20/60 under ideal conditions. One field study (Miller, 1984) revealed that, under ambient starlight conditions, mean visual acuities for high contrast eye charts were reduced to less than 20/80. A more recent laboratory study (Riegler, 1991) showed that visual acuities with low contrast eye charts were considerably worse.

Under binocular conditions, the normal unaided field of view measures approximately 120 degrees vertically by 200 degrees horizontally. For ANVIS the field of view of a single I^2 tube is a circular 40 degrees, and as the tubes have 100% overlap the combined binocular field is also a circular 40 degrees. This value is based on the pilot's ability to obtain minimal eye relief and proper eye positioning with the designed eye positions of the NVG optics (Task, 1991). If eye relief is greater than 20 mm, the field of view for users decreases significantly. Variations in head anthropometry (i.e., deep-set eyes), use of other life-support equipment or protective masks, wearing

corrective spectacle lenses, or improper adjustment of the helmet attachment can

contribute to field of view losses that are not always obvious to the aviator (Miller, 1992).

1.3   Review of Hover Displays

The AH-1 Cobra helicopter employs a HUD, and during NVG ANVIS operation

the HUD symbology (shown in Figure 1.11) can optionally be presented to the right eye.

No head tracker is incorporated, so that all symbology is screen-fixed and referenced to

the nose of the helicopter. Thus the artificial horizon is conformal with the actual horizon

only when the pilot line-of-sight is aligned with the vehicle longitudinal axis.
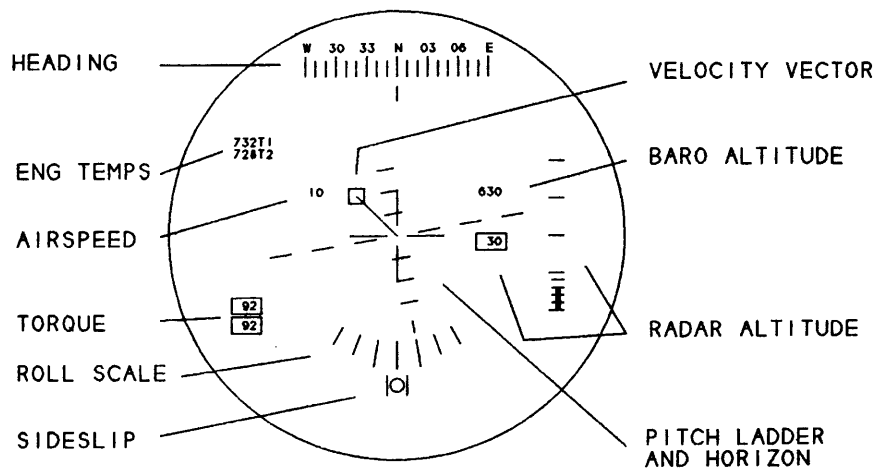
Figure 1.11. ANVIS HUD hover symbology (Newman, 1994).

The AH-64 Apache IHADSS hover symbology is shown in Figure 1.12. While

there is a head-tracker, it is used only to direct the sensor, not orient the display, so that

all symbologies are screen-fixed. This display uses a plan view perspective. A fixed

aircraft head-tracker symbol is shown aligned to the aircraft axis, and a station-keeping

variant of the hover symbology uses a superimposed ground-fixed box denoting a fixed

hover point.
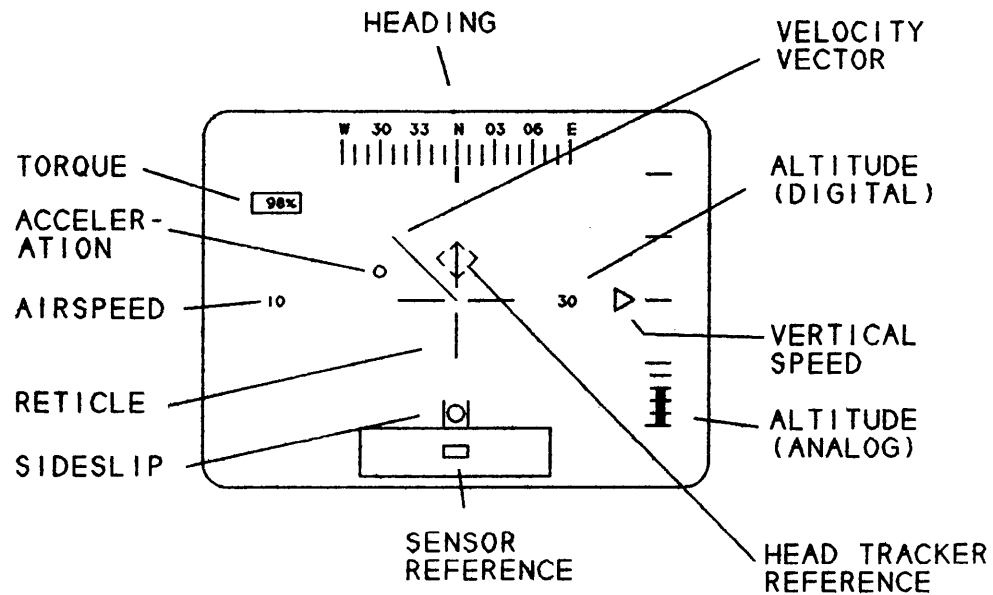
Figure 1.12. Apache IHADSS, hover mode (Newman, 1994).

The box is driven by Doppler radar signals. A velocity vector and acceleration ball also appears on the display relative to the aircraft axes.

In Figure 1.13, an experimental head-up display for shipboard helicopter recovery is shown (Stapleford, 1979). The glide path intercept point (GPIP) symbol is designed to straddle the point where the optical landing system on the ship will appear when visibility conditions permit. During station-keeping over the ship, the window size varies to show fore/aft motion, and the window displacement with respect to the GPIP varies to show lateral and vertical motion.
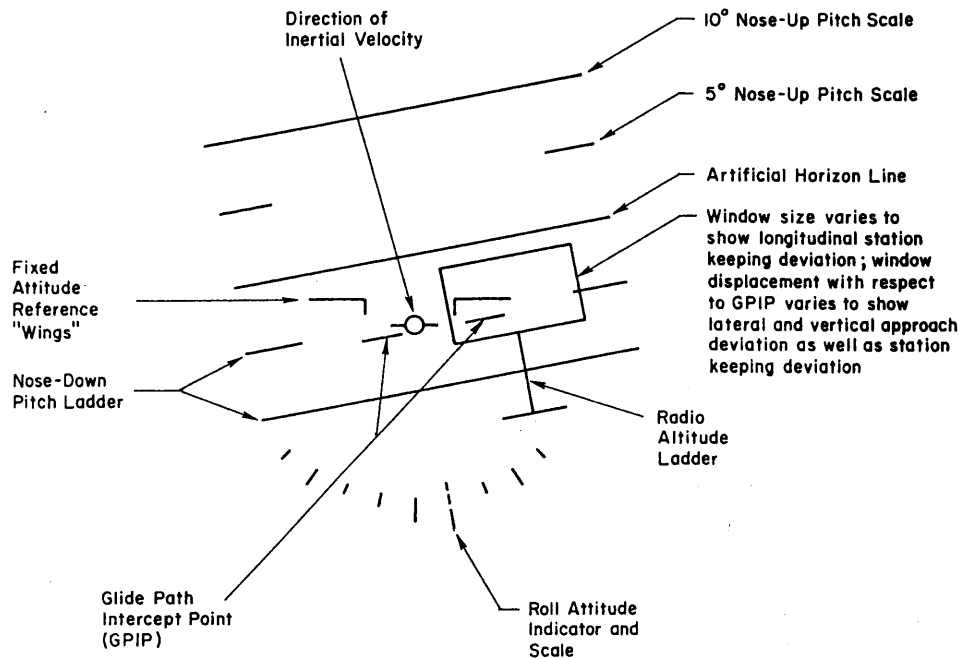
Figure 1.13. Experimental VSTOL Head-Up Display for shipboard recovery (Stapleford, 1979).

An example of an early hover head-down display (Kemp, 1969) using a plan view perspective is shown in Figure 1.14. Altitude error is depicted using a reference window (centered on helicopter, laid on ground level) and a comparator window (centered on and anchored to the helicopter). As the vehicle descends toward the ground, the reference box grows larger, and at zero altitude, the reference box overlays on the comparator box. An "X" depicts the desired hover site. A pitch line and a roll line indicate attitude (in Figure 1.14 down pitch is indicated), with angle of attack displayed by a linear moving pointer.

Predicted attitude is depicted by a line representing the future attitude from the current time until the end of the prediction (approximately five seconds) assuming the stick is returned to neutral position. Position prediction is similarly displayed with lines

indicating the path to the desired hover site. Predicted altitude is indicated by a series of

grid squares that show the size that the grid will be in the future.
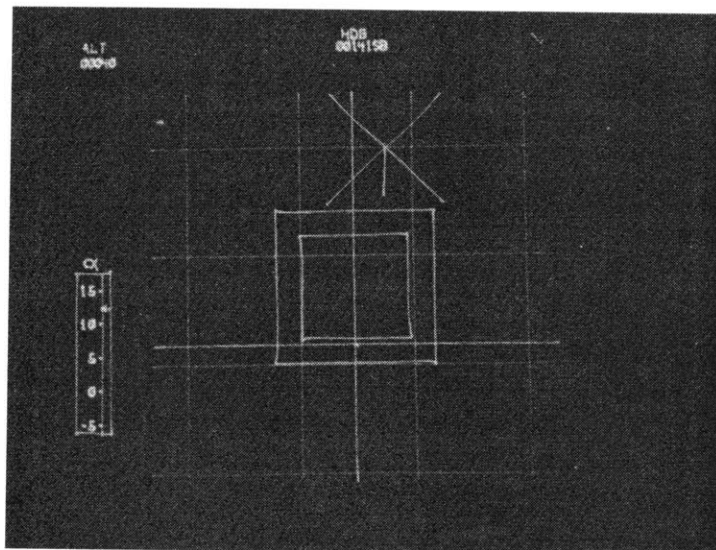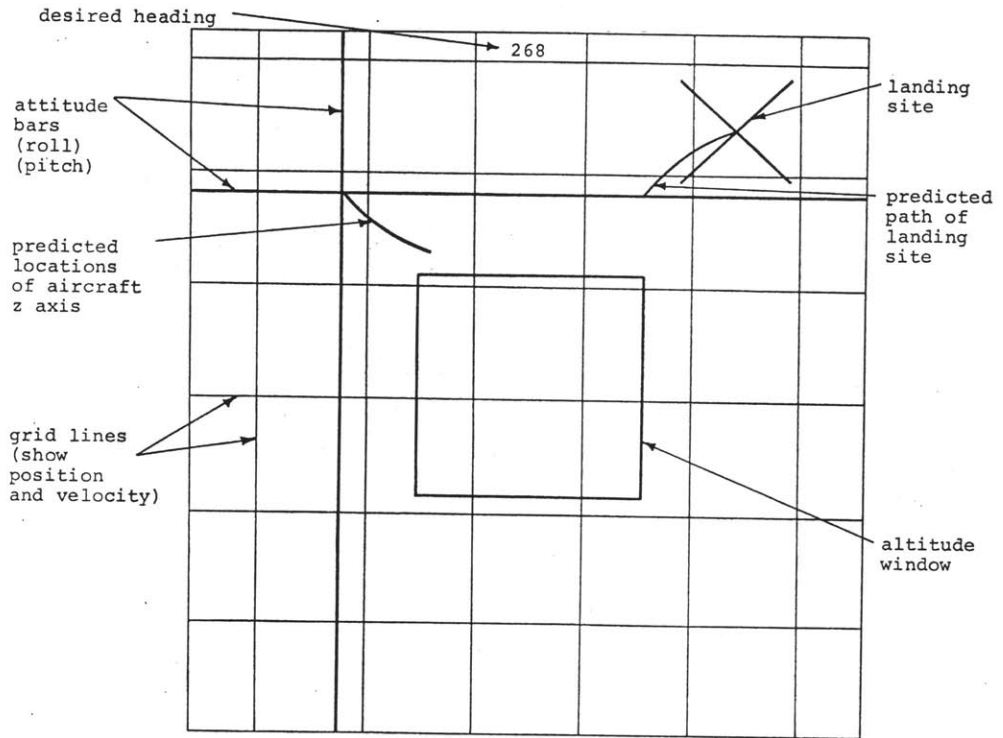
Figure 1.14. Experimental VTOL Head-Down hover director (Kemp, 1969).

An experimental head-up display developed by NASA Ames Research Center

(Dornheim, 1995) for VSTOL 'blind' landings is shown in Figure 1.15. A velocity

vector and velocity predictor ball offer guidance to an initial hovering point, and then to

the pad. The pilot directs the velocity vector by maneuvering to place the velocity

predictor ball on top of the hover "X", after which the aircraft symbol (three inverted
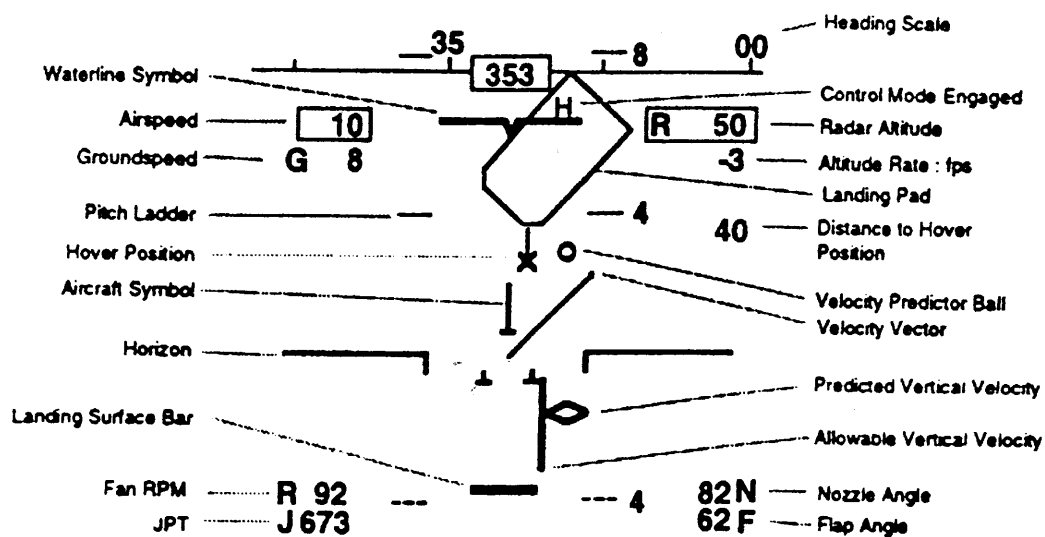
Figure 1.15. Experimental VSTOL (YAV-8B) Head-Up Display, hover mode (Dornheim, 1995).

"T"s) catches up with the predictor. The pilot repeats the same process to hover over the

landing pad. The lower portion of the display represents the vertical situation. Attitude

is depicted with a waterline and horizon symbol.

1.4 Thesis Outline

In Chapter 2 a perceptual task analysis of the manual hover task is performed, identifying what spatial states are required to perform the task. Chapter 3 presents what visual informational sources are normally available for human perception of spatial layout. These are used to design a cue set that expands on the concept of a flight handling qualities tracking task. The chapter concludes with specifics of the display.

Chapter 4 develops the experimental method, detailing vehicle motion constraints, manipulator dynamics, vehicle dynamics, display dynamics, and aircraft disturbance composition. Finally, experimental protocol is discussed.

Chapters 5 presents the results for the experiments conducted in five sections: 1) The effect of display motion gain on single-axis station-keeping; 2) The effect of display motion gain on multi-axis station-keeping; 3) Comparison between single-axis and multi-axis station-keeping results; 4) Performance tradeoff varying display motion gains between axes; and 4) The effect of synthetic cues on station-keeping using a simulated NVG environment. Display conditions address the influence of near-field and far-field reference trees, as well as perceptual conflict when overlaying cue motion set at different gains onto a natural scene. Chapter 6 gives a summary of the thesis' results and conclusions.

Chapter 2

Perceptual and Control Task Analysis for Helicopter Hover

Execution of a complex task such as hover using the external environment for visual cues likely involves a combination of control strategies such as compensatory, pursuit, and precognitive (McRuer, 1974). For the purposes of tractable modeling and analysis, the hover task will be represented as four outer-loop compensatory control tasks shown in Figure 2.1: three in position (longitudinal, lateral, and vertical) and one in heading (yaw), with each outer-loop supported by applicable subsidiary inner-loops. The cues actually selected by the pilot will correspond to the states, which satisfy both guidance and control needs, and certain pilot-centered requirements.
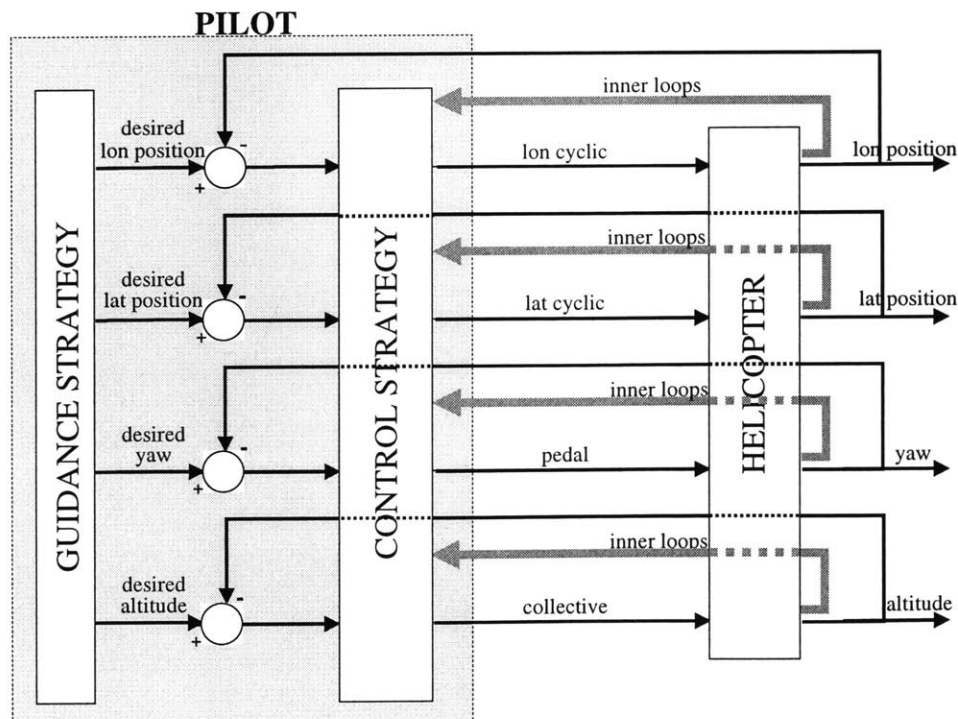
Figure 2.1. Multi-loop structure for hover task.

2.2   Pilot Compensation and Adjustment

The mathematical models describing pilot behavior in continuous control tasks

take into account two kinds of system requirements (McRuer, 1974):

- Guidance and control requirements that are related to system stability and the capability of following a desired path or executing a desired maneuver.

- Pilot-centered requirements that express the abilities and limitations of the human pilot.

The first set of requirements is driven solely by the task and is independent of the fact

that the controller is a human pilot. The second requirements set arises from limitations

on such things as multi-task ability and type and degree of pilot equalization applied to

the perceived vehicle motions.

Humans are limited in their ability to generate lead equalization (i.e., using the

derivative of a perceived state) based on visually perceived aircraft motions. Lead

equalization, as will be shown, is a key ability when guiding a helicopter near the ground

plane.

2.2.1   The Crossover Model

McRuer and Krendel (1974) showed that human tracking behavior follows a

simple set of adjustment rules for a wide variety of single-loop and multi-loop tasks.

These rules are described in what is called the Crossover Model. Referring to the

compensatory tracking task in Figure 2.2, Y_V represents the describing function for the

controlled element (i.e., vehicle), and Y_P represents the describing function for the pilot.

A describing function is a linear, frequency dependent approximation of a complex,

nonlinear element.
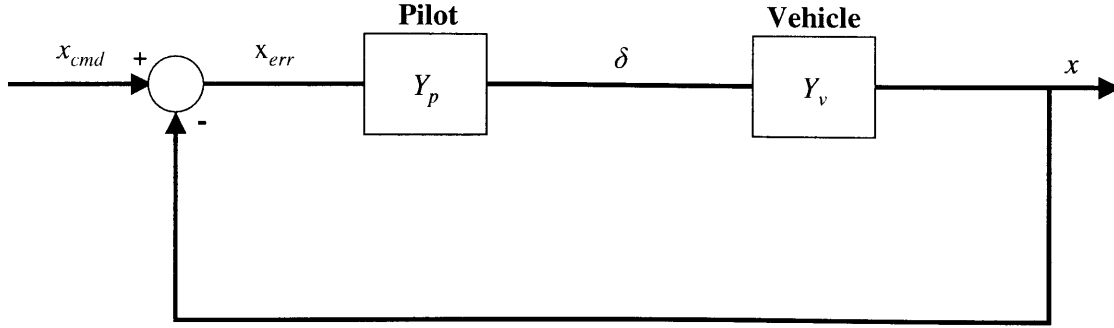
Figure 2.2. Feedback loop for simple compensatory system.

The Crossover Model states that the pilot adjusts the dynamics of Y_P such that the open-loop combined describing function $Y_P Y_V$ approximates a function of the form

$$Y_P Y_V = \frac{\omega_c e^{-\tau s}}{s} \tag{2.1}$$

over a broad frequency range around the crossover frequency ω_c of that loop. The open-loop crossover frequency ω_c is a good approximation of the closed-loop system bandwidth (McRuer, 1973), below which frequency the pilot's compensation is effective at tracking the input signal. Above ω_c the pilot is unable to perform closed-loop tracking effectively and the system is essentially operating open-loop. The pure time delay, τ, includes high frequency vehicle response lags in addition to latencies due to perception, interpretation, and neuromuscular actuation.

The parameters ω_c and τ in (2.1) depend on the pilot equalization required, and on the frequency content (bandwidth) of the disturbance or desired path input. Data show that the crossover frequency is greatest and time delay shortest when pilot equalization is a low frequency lag, i.e.,

$$Y_P = \frac{K_p e^{-\tau s}}{(T_I s + 1)} \quad \text{for } 1/T_I \ll \omega_c \tag{2.2}$$

26

However, when the pilot must generate low frequency lead; i.e.,

$$Y_P = K_p e^{-\tau s}(T_L s + 1) \quad \text{for } 1/T_L \ll \omega_c \tag{2.3}$$

then the crossover frequency is least and time delay is greatest. The major performance cost of pilot equalization is increased time delay, which degrades system stability. There is also an associated cost in pilot subjective rating (McRuer, 1974).

Control engineers often design automatic feedback control loops such that the slope of the open-loop amplitude ratio approximates an integrator (-20 dB/decade) over a broad frequency range around ω_c due to plant uncertainty and variability. For minimum phase systems, a typical specification for phase margin (a stability measure) of 35 to 40 degrees limits the region of ω_c to this amplitude slope ratio (Bode, 1945). Thus the Crossover Model shows the human adopting dynamics that are characteristic of a "good" control system.

2.3   Loop Structure

McRuer (1974) observed that the feedback loops most compatible with pilot control behavior are those that can be closed with pure gain equalization by the pilot. One method for analytically determining what spatial states are required to support a task is to look at the degree of compensation needed by the outer loops – if the pilot equalization does not approximate a gain, additional feedback and feedforward will enter the control loop structure to the extent that supporting visual cues are available. For an assumed set of vehicle dynamics and loop states, McRuer's Crossover Model makes predictions about the degree of equalization the pilot must generate. In order to appropriately model the pilot's control loops, thus gaining a realistic picture for pilot

27

effort and cue requirements, it is necessary to have an understanding for what is happening cognitively with the pilot during the feedforward and feedback processes. To this end, a set of guidelines is developed.

States that are fed forward versus fed back during closed-loop operation is an issue not well addressed in the literature. When a pilot employs a lead adjustment during compensatory tracking, shown in Figure 2.3, the error X_{err} is differentiated and combined with the component generated by pilot's pure gain adjustment. As mentioned earlier, the highest cost to pilot performance and subjective rating is incurred with low frequency lead compensation. This is illustrated in Figure 2.4, where pilot rating decrement (based on a Cooper-Harper scale) is shown as a function of degree of pilot compensation. For open-loop amplitude ratio slopes of +20, 0, -20, -40 dB/decade, the corresponding pilot compensation dynamics are K_p/s, K_p, $K_p s$, and $K_p s^2$, respectively.
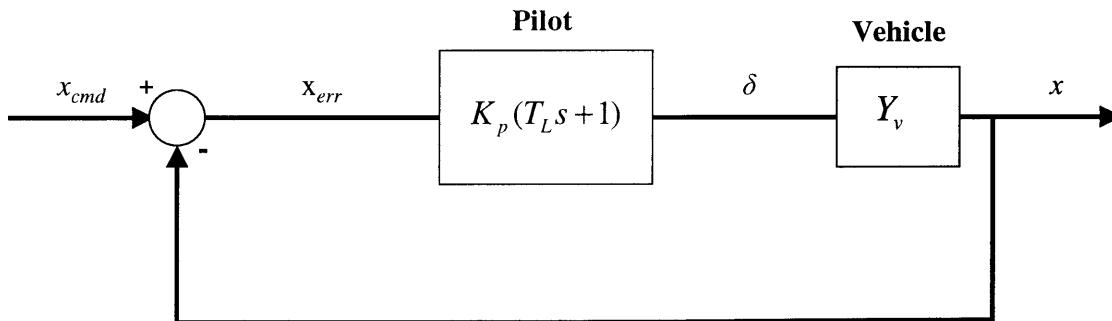
Figure 2.3. Example of lead compensation.

When the Crossover Model implicates lead generation for a given loop, there can exist conditions where the creation of inner-loop rate feedback would eliminate the need for outer-loop lead. To illustrate, consider Figure 2.5, which shows two systems with approximately equivalent closed-loop performance, (x/x_{cmd}). In Figure 2.5a, the pilot
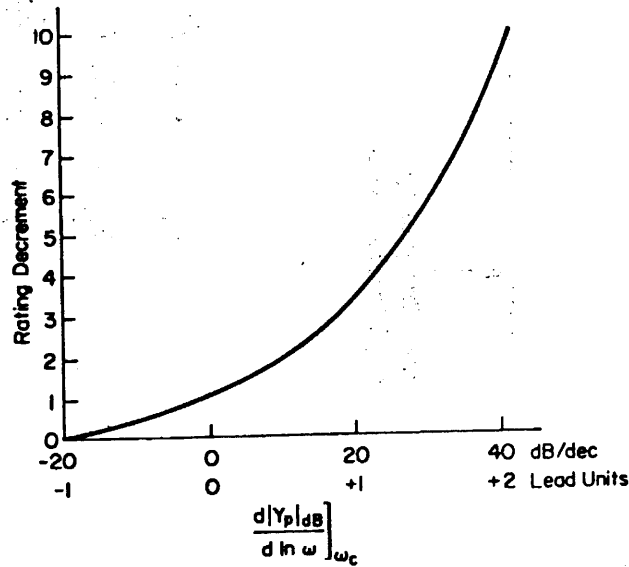
Figure 2.4. Pilot rating decrement as a function of lead equalization (Heffley, 1979).

must generate lead with a time constant of $1/\omega_v$ since the vehicle's pole is situated below

the open-loop crossover frequency. As ω_v decreases pilot workload will increase. In

Figure 2.5b, the pilot produces an internally commanded rate $\dot{x}_{cmd}$ based on x_{err}, and

compares this with the fedback vehicle state $\dot{x}$. In general, the crossover frequency

associated with the loop of a state's derivative ($\omega_{c_{\dot{x}}}$) is higher than that of the state itself

(ω_{c_x}), so that in Figure 2.5b the pilot only has to compensate with a pure gain on the

inner-loop as the open-loop amplitude ratio slope is already –20 dB/decade in the region

of $\omega_{c_{\dot{x}}}$. Figure 2.6 shows the effective outer-loop vehicle amplitude ratios seen by the

pilot, $\left| Y_{v_x} \right|$. The closed-loop transfer function of this inner-loop presents the pilot with a

bandwidth much higher than his outer-loop crossover frequency, so that his outer-loop

compensation is also a pure gain.

29

a.

b.

$$Y_{p_x} = K_1 \qquad Y_{v_x} = \frac{1}{s\left[s + \omega_{c_{\dot{x}}}\right]}, \omega_{c_{\dot{x}}} = (K_2 + \omega_v)$$
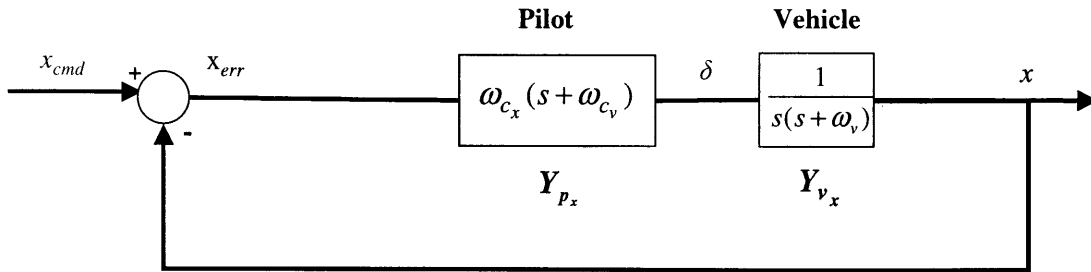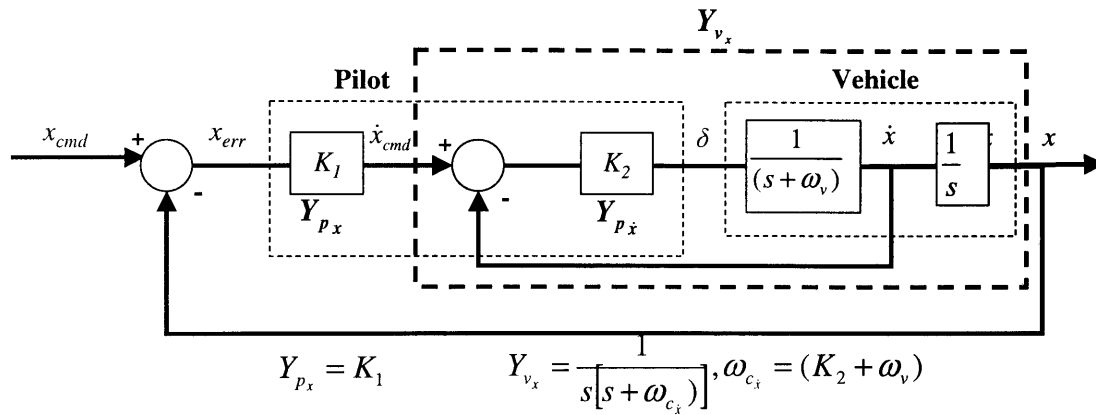
Figure 2.5. Approximately equivalent systems (x/x_{cmd}) using (a) outer-loop lead and (b) inner-loop feedback.

a.

b.
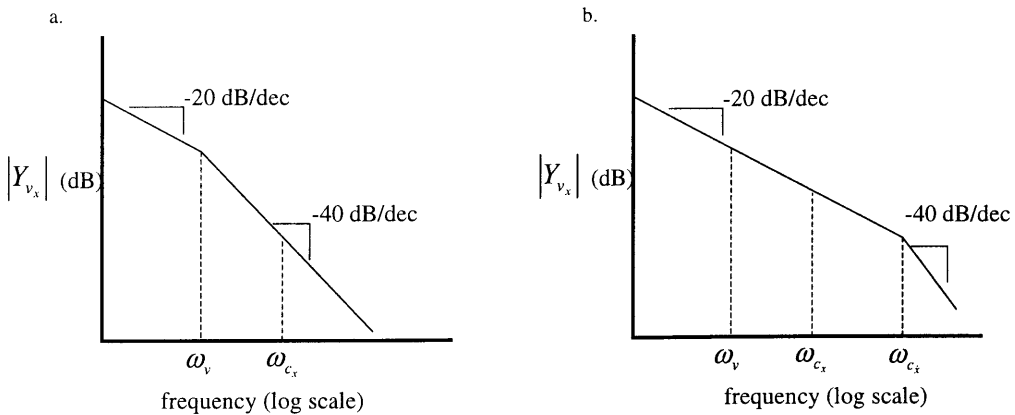
Figure 2.6. Open-loop amplitude ratios for systems shown in Figure 2.5a and b, respectively.

This single example, however, does not make a case for assuming the pilot creates a feedback loop whenever the Crossover Model implicates lead generation. First, vehicle outputs appropriate for inner-loop control must be available to the pilot. These can be direct, as in the above illustration, or it may involve surrogate states. An example of the latter is fixed-wing altitude control, where pitch attitude is approximately proportional to altitude rate, i.e. $h \cong U_0 \theta$. Furthermore, if a state and its derivative's crossover frequencies were not adequately separated, feedback would cause the pilot to experience the same workload for both inner and outer loops as he would with the single feedforward loop.

Anderson (1970) conducted a study correlating pilot rating (Cooper-Harper scale) of VTOL hover dynamics with pilot model parameters and closed-loop performance. Figure 2.7 summarizes the study with a model of the hover tassel and correlated pilot rating functionals. Note that pilot rating is 2.5 times more sensitive to pitch lead time than to position lead time, as well as the ceilings on the pilot ratings.

An implication from Anderson's data on feedforward and feedback loops is illustrated in Figure 2.8. Looking at an inner-loop state ρ, when T_L is small the pilot workload is low because he does not have to start differentiating the error ρ_e until higher frequencies. At higher frequencies we have

$$\dot{\rho}_e = \dot{\rho}_{cmd} - \dot{\rho} \cong -\dot{\rho} \qquad (2.4)$$

31
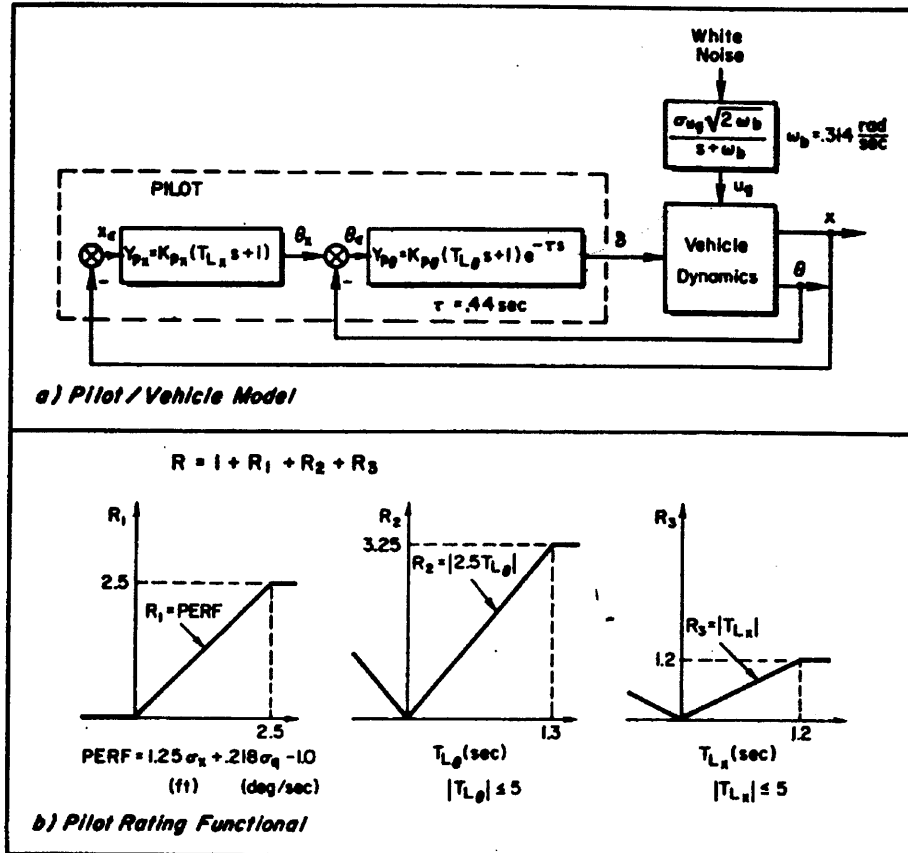
Figure 2.7. Hover regulation task and pilot parameters used in pilot ratings study (McRuer, 1974).
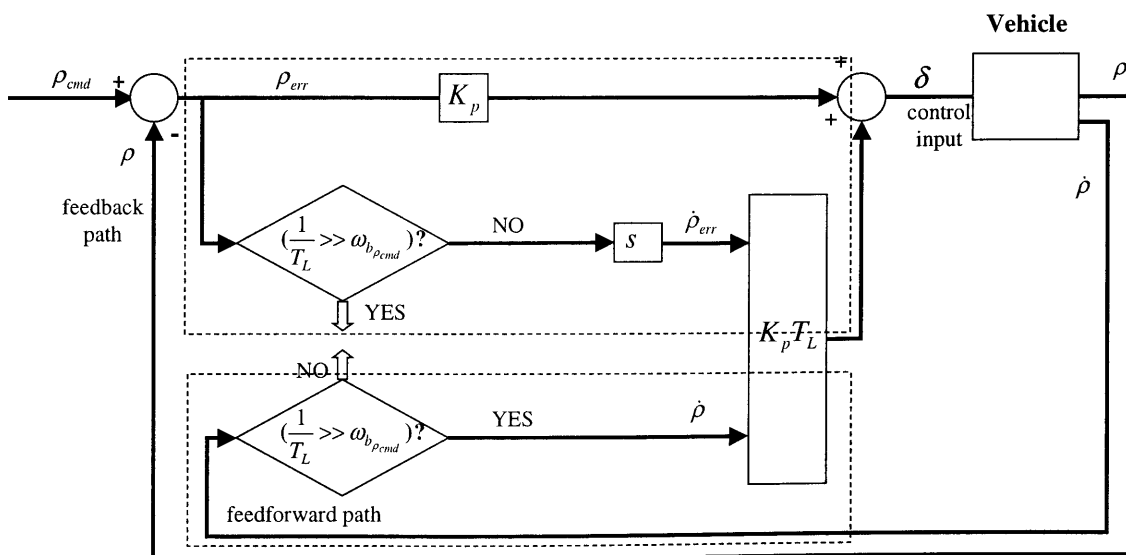
Figure 2.8. Possible feedforward and feedback paths, inner control loop.

32

because the bandwidth of ρ_{cmd}, $\omega_{b\rho_{cmd}}$, is usually considerably lower than the bandwidth of ρ. This means that when

$$\frac{1}{T_L} >> \omega_{b\rho_{cmd}} \qquad (2.5)$$

then effectively a high-pass element acts on the feedforward path and the pilot can simply use any cue providing information on $\dot{\rho}$. An important implication from this is that when (2.5) is satisfied, $\dot{\rho}$ does not require high cue fidelity so that only fair cues are needed.

However, when the lead time constant T_L is high the pilot must differentiate ρ_{err} at low frequencies without the aid of a cue dedicated for $\dot{\rho}$. Thus ρ must have very good cues so it can be compared with ρ_{cmd}, a mentally produced target state. Assuming cues are available, it is much more difficult to differentiate an internally generated error than to use the derivative of the vehicle state, as in (2.4), or a surrogate motion variable such as attitude in the altitude control example cited earlier.

In contrast, a mentally created target rate is directly compared with the actual rate of the state during feedback. With good rate cues, this is especially easy for humans at low frequencies (the region where feedforward presents high workload to operators). One criterion for considering whether feedback is dominating lead compensation would be (2.5).

For the regulation task shown in Figure 2.9, the outer-loop state error x_{err} is simply the negative of the vehicle state,

$$x_{err} = -x \qquad (2.6)$$
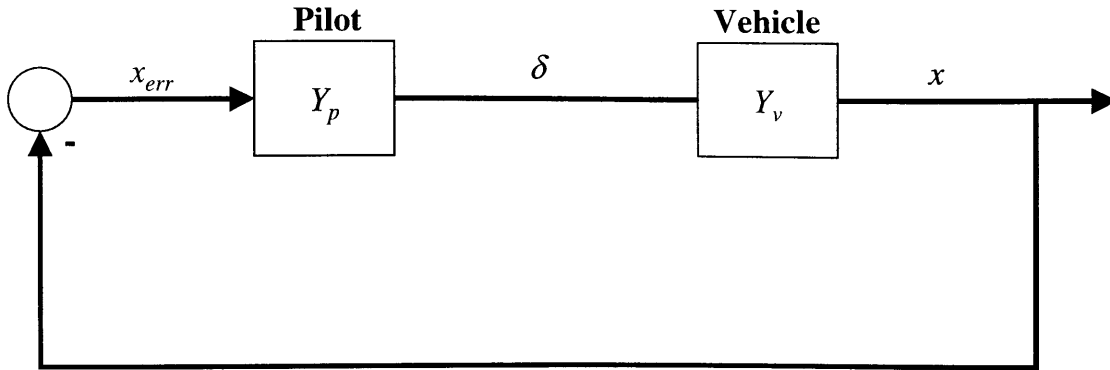
Figure 2.9. Outer-loop of a regulation task.

If lead compensation is required, a special case of (2.4) arises,

$$\dot{x}_{err} = -\dot{x} \qquad (2.7)$$

where the use of $\dot{x}$ is valid for all frequencies (as opposed to high-pass only). This would imply that outer-loop lead generation is easier to perform than inner-loop lead.

Referring again to the pilot rating functional shown in Figure 2.4, equation (2.5) predicts that lead generation for the pitch loop should occur when $1/T_L >> \omega_{bp_{cmd}}$, above which feedback of pitch rate will be employed. Once pitch rate feedback is in place, further changing of vehicle dynamics to alter T_{L_θ} (T_{L_θ} is academic at this point) would have negligible effect on pilot compensation, hence rating. From this it can be inferred that pitch rate feedback has replaced lead generation for values of T_{L_θ} greater than 1.3 seconds.

It should be noted that the pilot rating decrement versus pilot compensation given in Figure 2.4 refers to outer-loop compensatory operation. For inner-loop operation, however, it is possible that pilot ratings would degrade more markedly for the same lead compensation if good rate cues were not available for feedback, since state error must be

directly differentiated (as opposed to just the state itself being differentiated for outer-loop operation).

It should also be noted, looking at the Crossover Model, that employing feedback when high frequency lead compensation can be used increases pilot compensation (thus time delay), which can give rise to second-order effects that degrade system stability and performance.

Applied to multi-loop operation the Crossover Model states that the pilot tends to close loops as a pure gain when cues and dynamics allow. It would seem reasonable that an experienced operator resorts to whichever strategies lends to the easiest task, so that the engineer should model a control task using lead or inner-loop feedback based on relative difficulty and stability.

From the treatment presented in this section the following implications can be drawn (Figure 2.10 repeats Figure 2.8 again for clarity):

i.   Where the Crossover Model calls for high frequency lead compensation

$(1/T_L >> \omega_{b\rho_{cmd}}$, inner-loops), the loop state ρ and its rate $\dot{\rho}$ need only

have fair[**] cueing. If the cues for $\dot{\rho}$ are made too compelling, rate

feedback may occur, thus degrading performance.

[**] The definition of "good," "fair," and "poor" are taken from the Visual Cue Rating Scale (Clement, 1984) and are as follows:
- Good cues are easily and quickly perceived allowing pilot to make aggressive corrections with confidence.
- Fair cues require considerable concentration to perceive accurately, allowing pilot to make only moderate corrections to changes with confidence.
- Poor cues require full concentration to perceive enough information for aircraft control. Only small and gentle corrections are possible, and consistent precision is not attainable.

ii. Where low frequency lead compensation is implicated ($1/T_L \leq \omega_{b\rho_{cmd}}$), the rate of the loop state $\dot{\rho}$ should have good cues so that rate feedback can replace the lead adjustment (in this case cueing for ρ would only have to be fair). In the absence of good rate cues, the loop state ρ should have good cueing.

iii. An additional implication based on crossover regression (McRuer, 1974) is that cues should have spatial frequencies and motion gains which are perceptually consistent with its loop crossover frequency to avoid crossover regression.
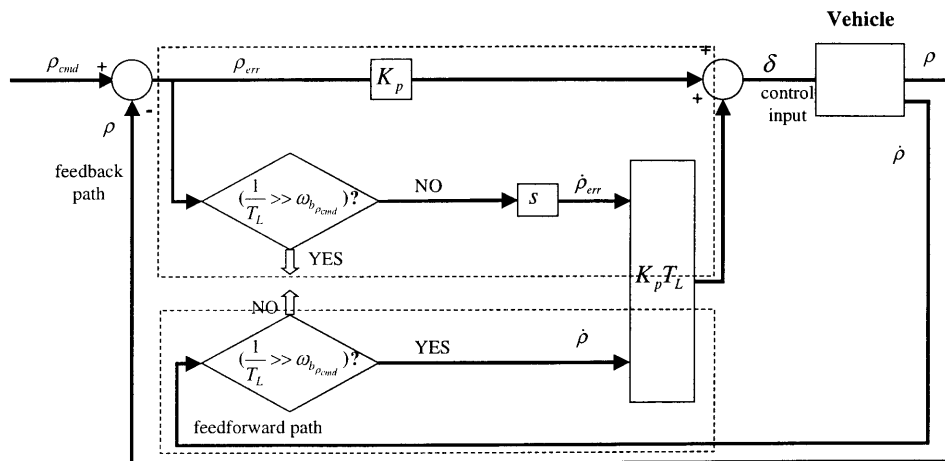
Figure 2.10. Possible feedforward and feedback paths, inner control loop.

2.3.1 Modeling State Feedback and Feedforward for the Hover Task

The loop structures and supporting cues for the hover task will now be discussed. For ease of presentation, it is assumed that vehicle translational and rotational cross-responses to a primary input are perfectly regulated. In addition, yaw is assumed to be

fixed with an automatic heading hold. Figure 2.11 shows the basic control loop structure

for longitudinal station-keeping. Helicopter response to longitudinal control inputs can

be generalized by three modes: phugoid (ζ_{ph}, ω_{ph}), pitch damping (λ_{PD}), and surge

damping (λ_{SD}) (Heffley, 1979). Typical values for these roots are (Heffley, 1979) $\omega_{SD} \cong$

0.02 rad/s, $\omega_{ph} \cong 0.2$ rad/s, $\zeta_{ph} \cong .4$, and $\omega_{PD} \cong 2$ rad/s. Figure 2.12 shows a Bode

magnitude diagram (asymptotes) of the helicopter's stick to longitudinal position (x/δ)

transfer function, Y_{v_x}. For longitudinal position control during hover, typical crossover

values of the open-loop system (ω_{c_x}) range from 0.2 to 0.5 rad/s. The Bode diagram

shows the magnitude slope transitioning from –20 dB/decade to –60 dB/decade at ω = 0.2

rad/s corresponding to the second-order phugoid mode. The Crossover Model states that

the human adopts dynamics such that the open-loop amplitude ratio slope is

approximately –20 dB/decade over a considerable frequency range in the region of

crossover. Because of the lightly damped phugoid mode the actual magnitude in Figure

2.12 would sharply peak then fall off near ω_{c_x}, so that it would be impossible for the

pilot to generate a lag-lead adjustment that produced a well-behaved
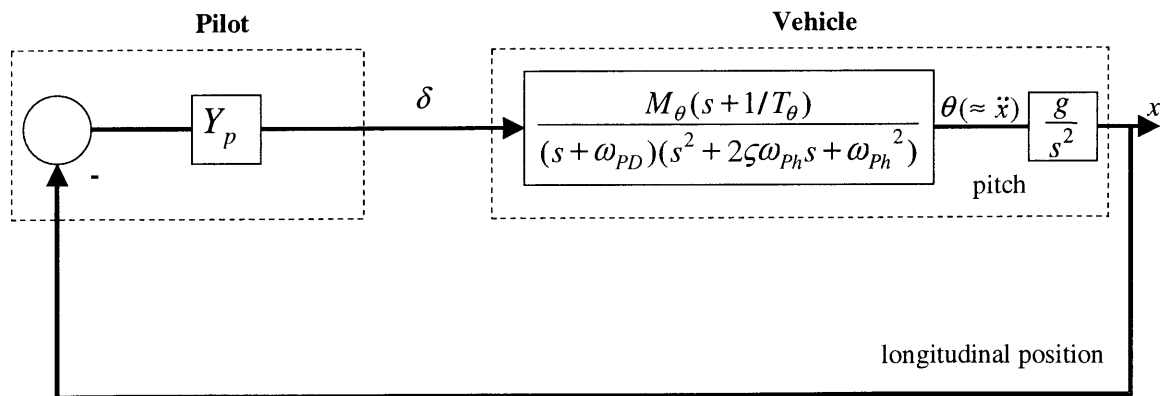
Figure 2.11. Helicopter longitudinal response (generalized).
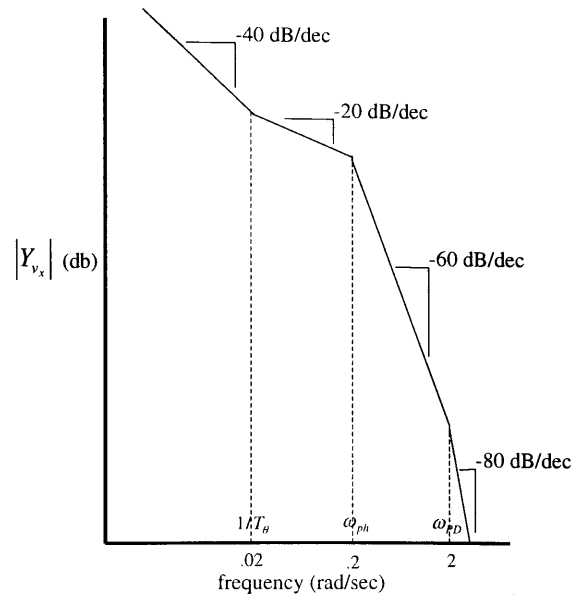
Figure 2.12. Bode magnitude asymptotes of helicopter longitudinal response.

slope in the region of ω_{c_x} . In addition, even if the second-order phugoid mode was

well-damped, the pilot would have to apply an adjustment taking the form

$$Y_P = K_p e^{-\tau s} (\frac{1}{\omega_{ph}} s + 1)^2 \tag{2.8}$$

to offset the –60 dB/decade slope. The pilot's lead equalization in equation (2.8) would

then be +40 dB/decade at ω_{c_x} . Looking back at Figure 2.4, a lead equalization of +40

dB/decade corresponds to a rating decrement of approximately 8 on the Cooper-Harper

scale, so that the pilot cannot control the vehicle longitudinally using only position as a

feedback state.

Position rate as possible inner-loop feedback will now be examined. Feeding

back position rate in Figure 2.11 would create a well-damped phugoid mode so that the

pilot would be required to generate pure lead in this loop. Pure lead generation

corresponds to a pilot rating decrement of approximately 5 seen in Figure 2.4. One might

38

next consider acceleration feedback; however humans do not perceive acceleration well in the visual channel, and without good visual reference the vestibular system can produce spatial illusions (Gillingham, 1993). Figure 2.11 shows pitch to be proportional to acceleration, so that pitch also becomes a surrogate of acceleration. Examining the pitch loop shown in Figure 2.13 a typical crossover value for attitude regulation is ω_{c_θ} ≅ 2 rad/s (Heffley, 1981), so that the pilot must generate lead corresponding to ω_{PD} in order for the open-loop system to behave as an integrator. Thus

$$Y_{P_\theta} = K_{p_\theta} e^{-\tau s} (s + \omega_{PD})$$ (2.9)

Looking at Figure 2.10, the time constant $1/\omega_{PD} = 0.5$ s corresponds to moderate pilot rating and we can assume lead compensation without a pitch rate feedback loop (i.e., pilot uses feedforward with pitch rate). Thus, fair visual cues for both pitch and pitch rate would be required. This initial estimate of pilot rating for determining the type of loop structure can later be tested against (2.4) when the rest of the loop structures have been estimated.

In Figure 2.13, the poles for the closed pitch loop are well-damped ($1/T_{1_{ph}} = .04$, $1/T_{2_{ph}} = 2.12$) so that the amplitude ratio slope for Y_{v_x} is –40 dB/decade in the vicinity of ω_{c_x}. The pilot would then compensate with pure lead if only position were fed back around the pitch loop, thus an additional rate feedback loop is considered necessary. From Heffley a typical crossover frequency for rate control is $\omega_{c_{\dot{x}}} \cong 0.5$ rad/s. The equivalent system for this loop configuration is shown in Figure 2.14b, and it is seen that the pilot adjustment is a gain. Finally the pilot need only generate a pure gain to compensate for the outer position loop of Figure 2.14c.
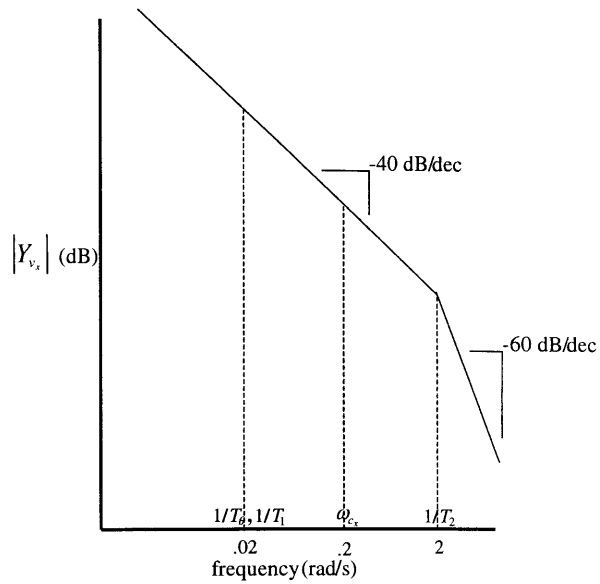
Figure 2.13. Bode magnitude asymptotes of helicopter longitudinal response with pitch loop closed.
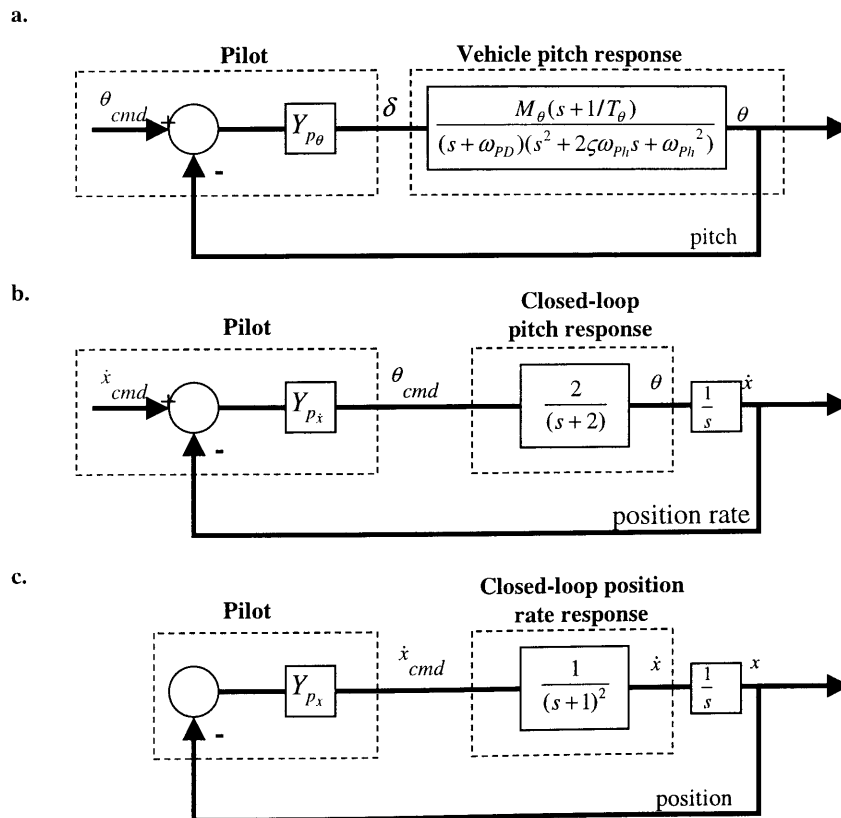
Figure 2.14. Control loops for longitudinal hover: a) inner pitch loop, b) position rate c) outer position loop.

40

An analysis done on the roll axis yielded similar results, but because of the much higher

roll-damping frequency in the vehicle dynamics, there is no need for roll rate cueing.

Looking at the vertical control loop in Figure 2.15, the heave-damping root Z_W is

typically 0.3 rad/s. Since $\omega_{c_x} \cong 0.5$ rad/sec we can expect a lead time constant of $T_{L_z} \cong$

3 seconds. To get an approximate idea of pilot effort associated with this outer loop lead,

Figure 2.10 indicates that feedback is probably occurring, thus fair cues would be

required for altitude rate.

Pilot

Vehicle

$$\frac{Z_\delta}{s(s+Z_w)}$$

δ

Y_{p_z}

z

altitude
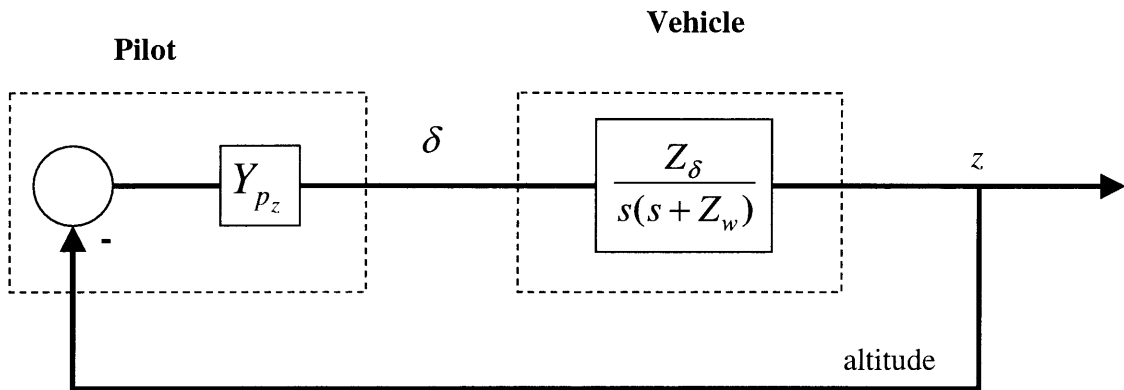
Figure 2.15. Helicopter vertical response.

Table 2.1 lists the required states and cue fidelities that have been identified for a

hover display based on the generalized helicopter dynamics. These requirements are

used in the next chapter as a baseline for developing a hover display used for

investigating fundamental perceptual issues when employing synthetic cues for limited

FOV hovering.

Table 2.1. Cue requirements for hover task (heading hold engaged).

State	Cue Fidelity
θ, Pitch rate	Fair
θ, Pitch	Fair
$\dot{x}$, Longitudinal rate	Good
x, Longitudinal position	Good
ϕ, Roll	Fair
$\dot{y}$, Lateral rate	Good
y, Lateral position	Good
$\dot{z}$, Altitude rate	Fair
z, Altitude	Good

Chapter 3

Synthetic Cue Requirements and Design for NVD Hover

3.1   Synthetic Cue Requirements

Since the nominal outer loop of the hover task is position, a pilot's perception of spatial location is key. Cutting (1994) observes that there are nine information sources available to the human visual system for perceiving the structure of a complex natural scene:

(1)   *Motion parallax* is the relative movement of the projections of several stationary objects caused by observer motion. The motions of a whole field of such objects is called *motion perspective*.

(2)   *Relative size* is the measure of the apparent size of objects that are physically similar in size but at different distances.

(3)   *Relative density* concerns the projected retinal density of a cluster of objects or textures, whose placement is stochastically regular, as they recede into the distance.

(4)   *Occlusion* occurs when one object hides, or partially hides, another from view. For display purposes, this somewhat obscure factor gives rise to a compelling cue for final tuning.

(5)   *Height in visual field* information is in the projected relations of the bases of objects in a three-dimensional environment to the viewer.

(6)   *Aerial perspective* results when moisture, pollutants, or both in the air

cause objects in the distance to become bluer, decrease in contrast, or

both with respect to objects in the foreground.

(7)   *Convergence* is measured by the angle between the optical axes of the

two eyes.

(8)   *Accommodation* is the change in the shape of the lens of the eye,

allowing it to focus on objects near or far while still keeping the retinal

image sharp.

(9)   *Binocular disparity* is the difference in relative position of the

projections of the same object on the retinas of the two eyes.

Figure 3.1 plots the just-discriminable depth thresholds as a function of the log of

distance from the observer for the nine sources of information about layout. In

considering the distances of two objects, D_1 and D_2, the ratio of the just-discernible

difference in distance between them over their mean distance, $2(D_1 - D_2)/(D_1 + D_2)$, is

plotted as a function of their mean distance from the observer, $(D_1 + D_2)/2$. This is done

in order to compensate for the decrease in accuracy with distance.

In Figure 3.1, Cutting segments the layout around a moving perceiver into three

egocentric regions that grade into one another: (1) *Personal space*, which is the zone

immediately surrounding the observer's head, generally within an arm's reach and

slightly beyond; (2) *Action space* is the circular region just beyond personal space and

extends out to 30 m (the utility of motion perspective and binocular disparity decline to

the effective threshold value of 10% at about 30 m), and (3) *Vista space*, which extends

beyond 30 m.
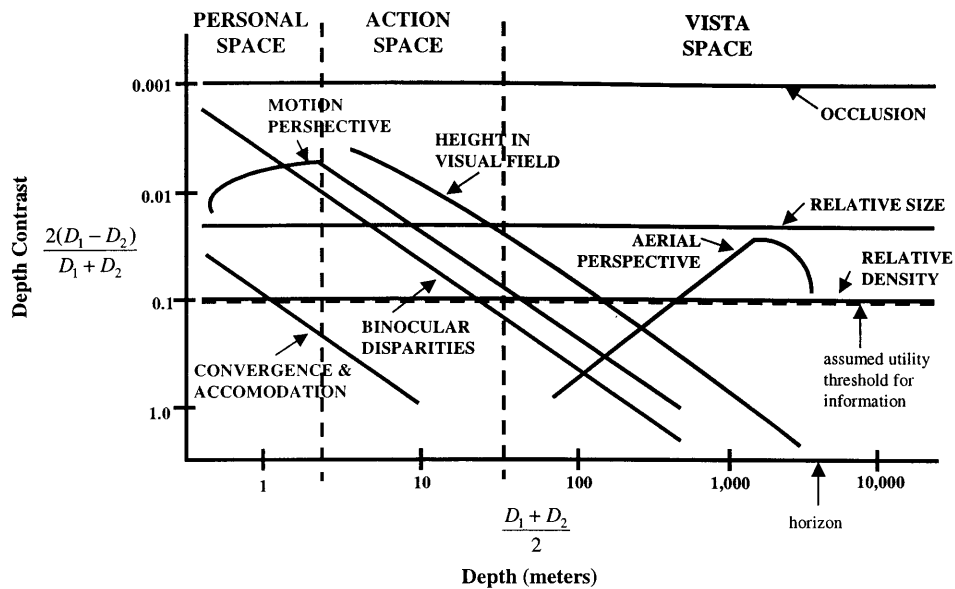
Figure 3.1. Just-discernable depth thresholds as a function of the log of distance from the observer for nine different sources of information about layout (Cutting, 1995).

For NVG operation, height in visual field and motion perspective are limited

sources due to FOV constraints. Both binocular disparity and relative density are

rendered largely ineffective due to poor image resolution. Thus relative size and

occlusion are the dominant cues for spatial layout in the NVG environment.

Examining the nine information sources for applicability to synthetic cueing,

height in visual field would require at least several objects (such as artificial trees) that

have their bases rooted in a model of the terrain – either flat terrain, or one that is

generated from a database. In either case, danger exists for a mismatch between

perceived and actual terrain height and contour. Relative density requires texturing or a

large number of objects to be placed in the image, which would create problems of

obscuration for such a limited field of view. In this experiment the same image was

presented to each due to computational limitations, so that binocular disparity was not an available cue. The remaining layout cues available for synthetic generation are motion perspective, relative size, and occlusion. Occlusion information is ordinal, whereas motion perspective and relative size can provide scaled information. With a restricted field of view, the strength of the first two cues is usually much higher when motion is transverse to the line of sight (LOS) than for motion along the LOS - the geometry of the scene undergoes change more rapidly for transverse motion. This is supported by the results of a study where two sets of external visual cues (microtexture and macrotexture, each observed with a forward-fixed 40 degree field of view) received more favorable pilot ratings when the helicopter moved laterally than longitudinally (Hoh, 1984).

One method that Cutting uses for determining the relative importance of cues within a division of space (i.e., Action space) is to compare the relative areas under each depth-threshold function within that spatial region. Table 3.1 ranks the remaining information found in action space applicable to this study which have depth contrasts above the utility threshold.

Table 3.1. **Relative importance rankings of applicable information sources by the areas under their curves within action space.**

Source of information	Cue rankings in action space
Occlusion and interposition	1
Relative size	2
Motion perspective and motion parallax	3

With a very poor usable cue environment there is clearly an increase in the reliance on the positional aspects of the environment. Those things that are very poorly perceived with NVG operation should be depicted with a minimum abstraction display so

as to enable no-abstraction performance. For at least the last three decades work with driving simulators and landing displays, there has been a continual effort to come up with displays that included the minimum cues – all needed motion perspective (Wier, 1971). Although it ranks third in relative importance in Table 3.1, motion perspective is nonetheless a critical component of spatial and motion perception. Ringland (1981) presents an analysis showing how the interpretation of motion perspective geometry will enable the observer to anticipate changes in the future course of his motion. When present and recognized, these visual elements from motion perspective will enable a controller to provide first and second-order visual lead compensation of his controlled element without the customary intensive psychomotor workload which accompanies visual anticipation of low frequency motions (Heffley, 1981). Second-order lead compensation refers to the adoption of pursuit behavior, which is discussed by Allen (1979).

While undergoing pure translation and looking in the direction of motion, an observer will see cues flowing radially outward from the motion's aimpoint. Precisely at the aimpoint no cue flow will be observed. For an unrestricted FOV, this same helicopter motion will produce cues that flow in lamellar lines when perceived peripherally 90 degrees from the LOS. As noted above, the lamellar cues will generally be moving much faster than the radial cues. An experienced helicopter pilot can perform day visual flight regulations (VFR) hover by looking predominantly out the front of the helicopter using the peripheral lamellar flow for vertical and depth motion detection, and the lamellar flow transverse to the LOS for horizontal motion detection.

When denied peripheral vision during NVG flight, a pilot must determine ground

velocity by fusing together disparate information on rate of motion and direction of

motion. The rate information is found by looking off the velocity axis to pick up lamellar

flow (a LOS 90 degrees from the velocity axis provides view of the most rapid lamellar

flow shown in Figure 3.2). The direction of motion is found at the LOS where cue flow

has effectively ceased. Updating the approximate locations of maximum and minimum

cue flow can account to a large extent why NVG pilots must scan continually from side
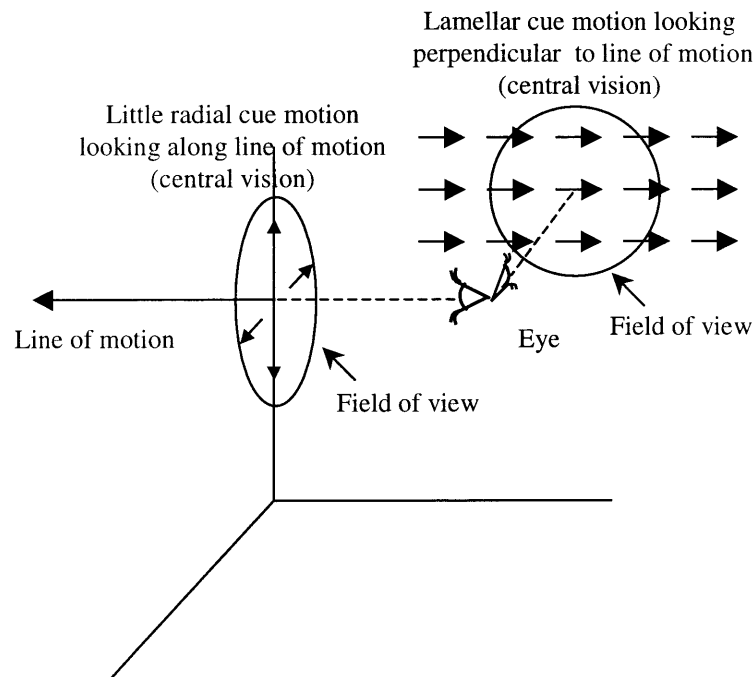
Figure 3.2. Primary visual motion cues during NVG hover.

to side. Reinforcing this is a study (Warren, 1992) in which subjects observed simulated

motion through a field of randomly positioned dots with a $40°$ FOV. Results showed that

estimation of heading angle decreased rapidly as the angle between the LOS and the

velocity vector increased. Another study (Anderson, 1989) suggested that lamellar optic

flow is effective for inducing perceived self-motion when stimulation is limited to the

central visual field. These two studies support the hypothesis that NVG pilots find ground drift information (direction and rate of motion) from different locations in space.

A model of the NVG hover task is presented in Figure 3.3. As noted earlier, the primary source of visual information during NVG operation is macrotexture, which is sensed by central vision and processed to yield perceived information. This information relates primarily to lateral position (with respect to the LOS), and also provides limited lateral rate and attitude information relative to the LOS. Using aircraft-referenced head orientation information, these eye-referenced spatial states must be transformed to geo-referenced (due to the navigational requirement) and aircraft-referenced (due to the control requirement) spatial states. During day flight head orientation is performed with precision primarily using ambient and central vision, an easy and natural task for the experienced pilot. In contrast, because of the loss of ambient vision and peripheral fiducial (reference) cues, NVG flight probably requires that proprioceptive and vestibular feedback play a larger role assisting central vision in the function of head orientation within the cockpit. A study (Bachelder, 1995) indicated that perception of head orientation degraded when cockpit fiducial cues were removed.

It is proposed that extraction of the functional cues shown in Figure 3.3 incurs: (1) continuous lateral head movement to approximate direction of maximum and minimum horizontal cue motion; (2) inaccuracies and added difficulty in head orientation due to reduced FOV; (3) continual mental coordinate transformations going from the LOS reference frame to the aircraft and geographic reference frames, and (4) serial fusing of ground drift information (direction and rate of motion).
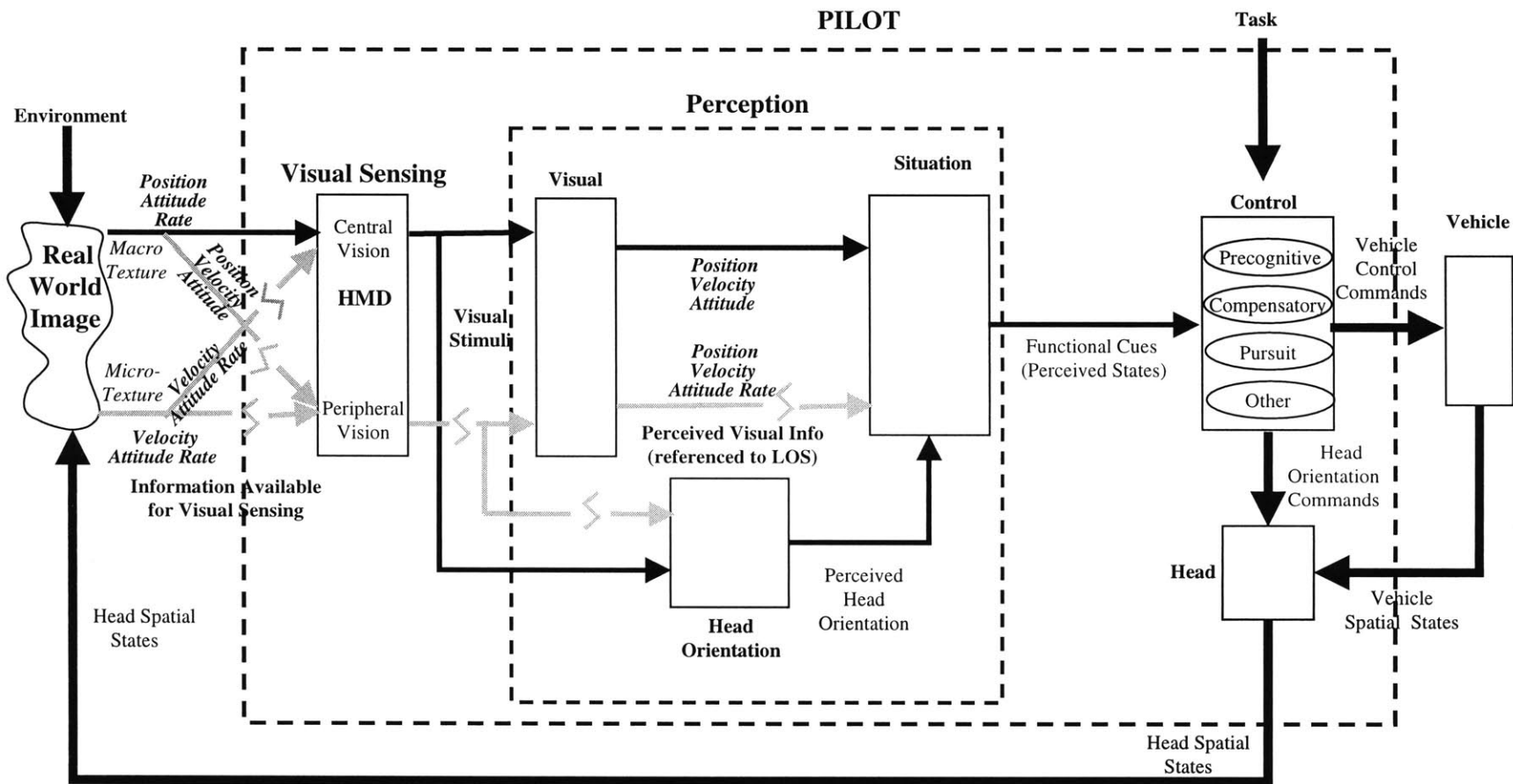
Figure 3.3. Representation of NVG hover task.

The considerably higher workload pilots experience with NVG flight compared to day flight (Miller, 1992) probably owes much to these factors.

3.2   Synthetic Cue Set Design

With the intent to simplify and enhance the perception and control processes, a precision hover display was developed based on an analogue of a physical target used in a flight handling qualities tracking task, shown in Figure 3.4. In this physical system a hover board was moved to command a lateral target position (Ockier, 1996).
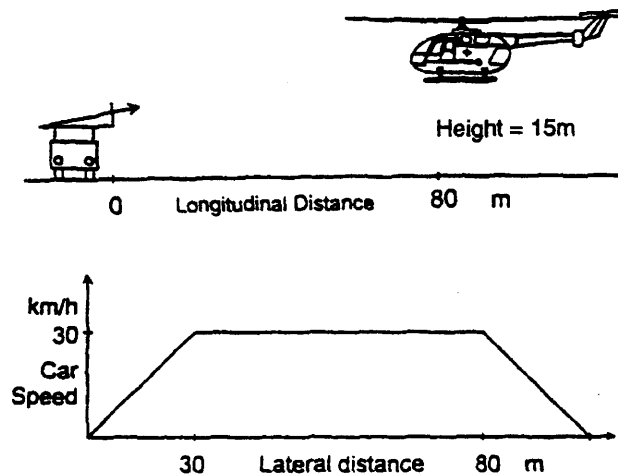
Figure 3.4. Helicopter lateral-position tracking task using a vehicle-mounted hover board (Aviation Safety and Pilot Control, 1997).

Figure 3.5 illustrates the cue geometry for the Synthetic Cue display. The display makes use of two visual alignment systems that are focused on the target hover position. The first alignment system employs two box frames that provide angular displacement information, while the second alignment system incorporates a cube pattern designed to produce compelling flow cues during helicopter motion. The two box frames are located in front of the helicopter's initial hover position, with a one box placed a finite distance

52

Head-on View

Near Box

Near Box

Near Box

Cubes

Side View

Aft of Hover Position

Desired Hover Position

Forward of Hover Position

Near Box

Far Box

5° 3°

∞
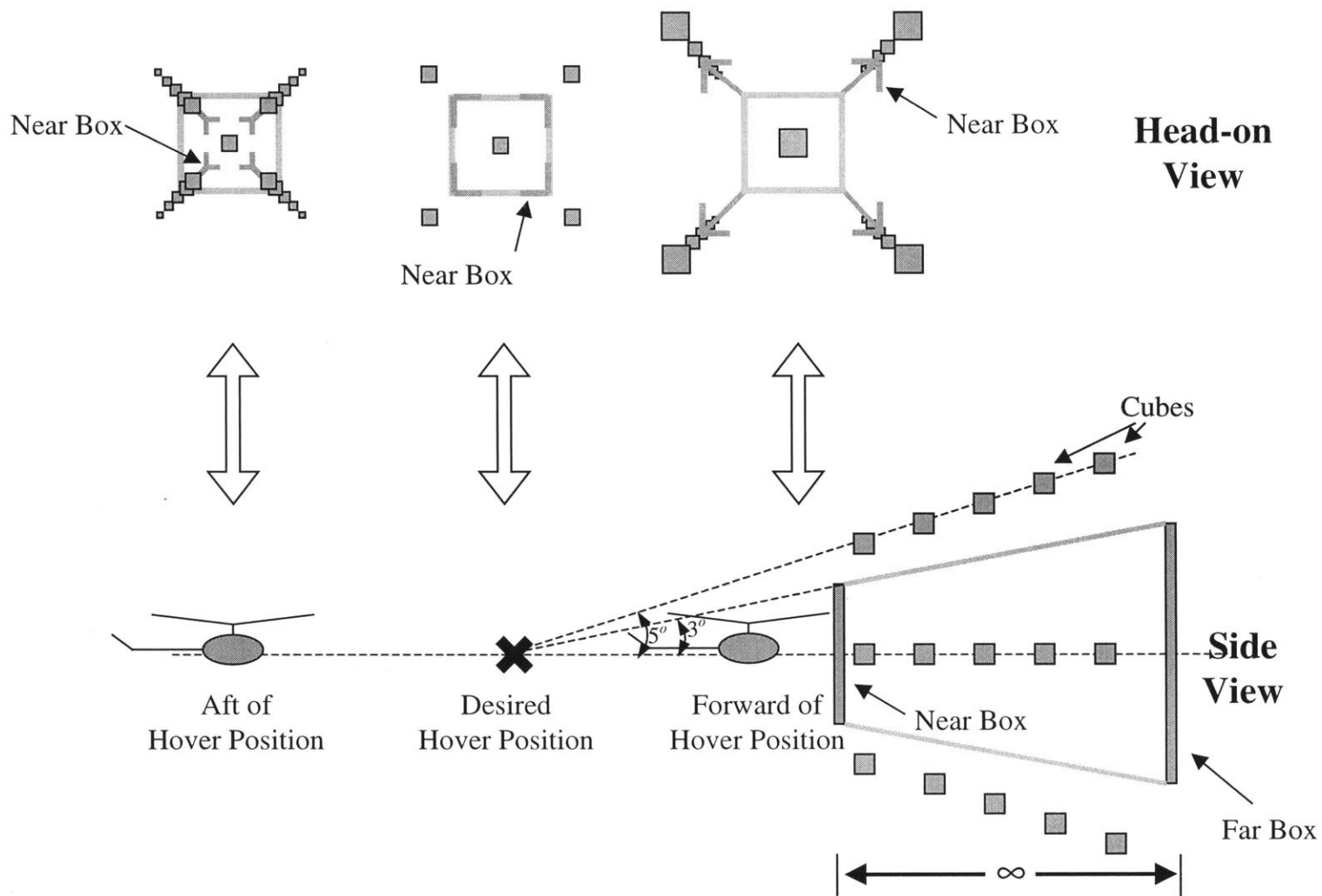
Figure 3.5. Cue geometry for Synthetic Cue display (longitudinal motion).

from the helicopter and the other box placed at infinity. Both box positions are fixed in inertial space. Only the corners of the near box frame are shown to allow precise overlay on the far box frame. The near and far box frames were colored orange and blue respectively to make for easier distinction between the two.

Perspective lines connect the vertices of the boxes - however, with only the boxes and lines shown there can arise ambiguity and object reversibility, a condition known as the 'Necker cube' illusion. This was solved by the second visual alignment system which consisted of five rays of cube that emanating radially from the target position, also shown in Figure 3.5. In addition to eliminating the Necker cube illusion, the rays of cubes introduced relative size cueing and reinforced motion perspective. The cubes also make use of occlusion that enhanced the display's realism. This is an excellent example of high ranking in Cutting's work. When the helicopter is in position, the near box frame corners overlay on the far frame and only the front face of the first cube of each row of cubes is visible. As the helicopter drifts off position along any axis of travel, the edges of the two frames separate and the previously hidden cubes come into view.

Longitudinal motion of the vehicle does not affect the size of the far box as it is placed at infinity. Because the near box is a finite distance from the helicopter, transverse vehicle movement produces parallax as the near box appears to stay motionless while the far box appears to move with the helicopter. Longitudinal motion will cause the near box to contract or expand as the helicopter moves forward or rearward of the desired hover position. As the distance of the near box decreases, the degree of parallax and apparent box expansion (or display gain) increases.

The first cube in each row of cubes was located in-plane with the near box frame, with the remaining cubes being equally spaced behind. The last plane of cubes, located at 3000 ft, appeared to move synchronously with the far box frame.

The far box dimensions were chosen to subtend an angle of 6 degrees on the display screen (this specific value was based on preliminary tests using various box widths) so as to remain within central vision when the eye is looking straight ahead. Visual acuity is highest in the central portion of the eye which extends approximately 10 degrees out from the two-degree wide fovea (Bruce, 1996), beyond which acuity rapidly decreases. To prevent the cubes from obscuring the frames or their connecting lines during nominal helicopter motion, the front cubes were placed two degrees outside of the near box frame.

The display FOV (48 x 36 degrees) limited visible angular cue displacement in the lateral direction to 24 degrees left and right of centerline, and in the vertical direction 18 degrees above and below centerline. When cues reached the screen limits along a given axis of motion, cue motion was frozen along that axis so that usable information in the other axes would still be available. Normal cue motion resumed when the vehicle error was reduced to values that corresponded to nominal cue displacements within the screen FOV.

In Chapter 2 it was determined that fair attitude and pitch rate cues were required for the hover display. Figure 3.6 shows a photo of the attitude reference system used with the hover cue set overlaid on a simulated NVG background. An aircraft-fixed symbol was slaved to the nose of the helicopter, and a horizon line fixed in inertial space spanned the display. It was earlier noted that a study by Hoh (1986) found microtexture

to be a major component of attitude awareness. Since the three-dimensional array of cubes serves to some extent as a substitute for microtexture, it is reasonable to assume the array may also enhance perception of attitude and its rate. To further familiarize the reader with the geometry of the hover cue set, Figures 3.7 and 3.8 show photos of the hover display taken at various positions relative to the desired hover spot.
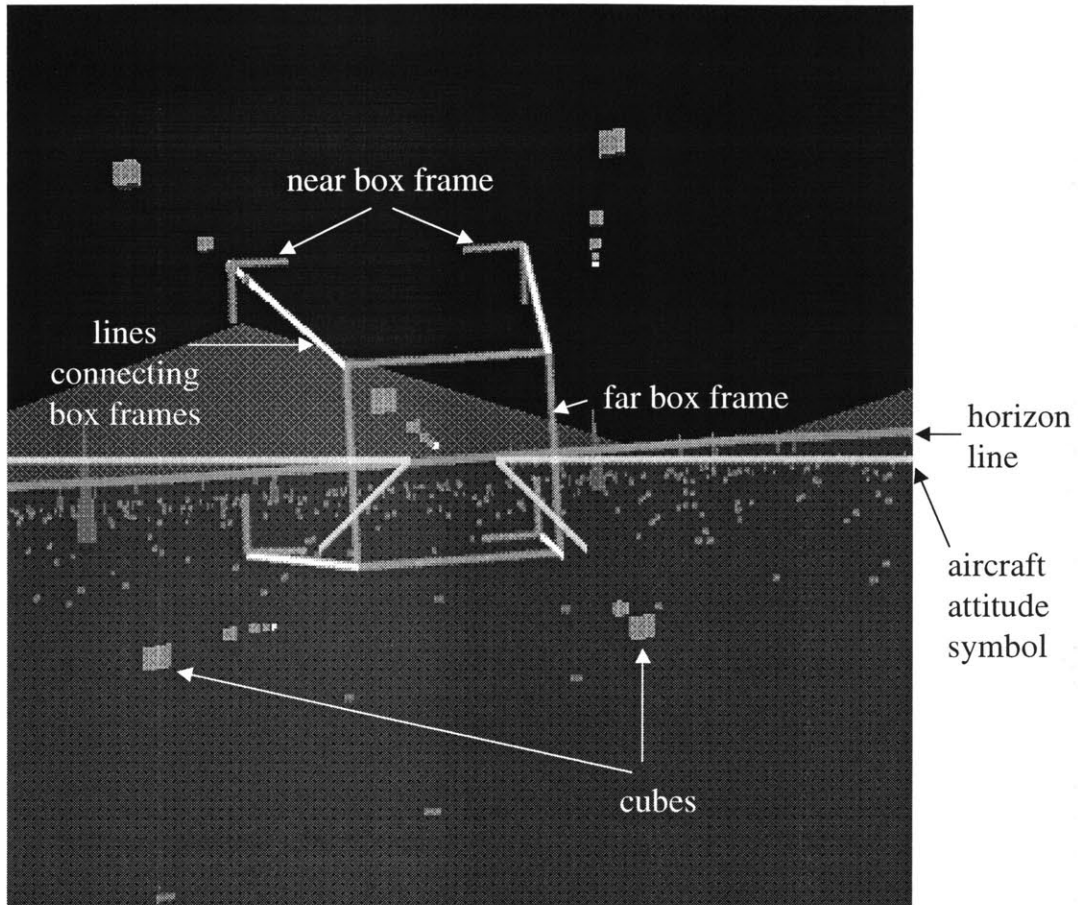
Figure 3.6. Synthetic Cue display overlaid on simulated NVG image.

Aft of Hover Point

At Hover Point
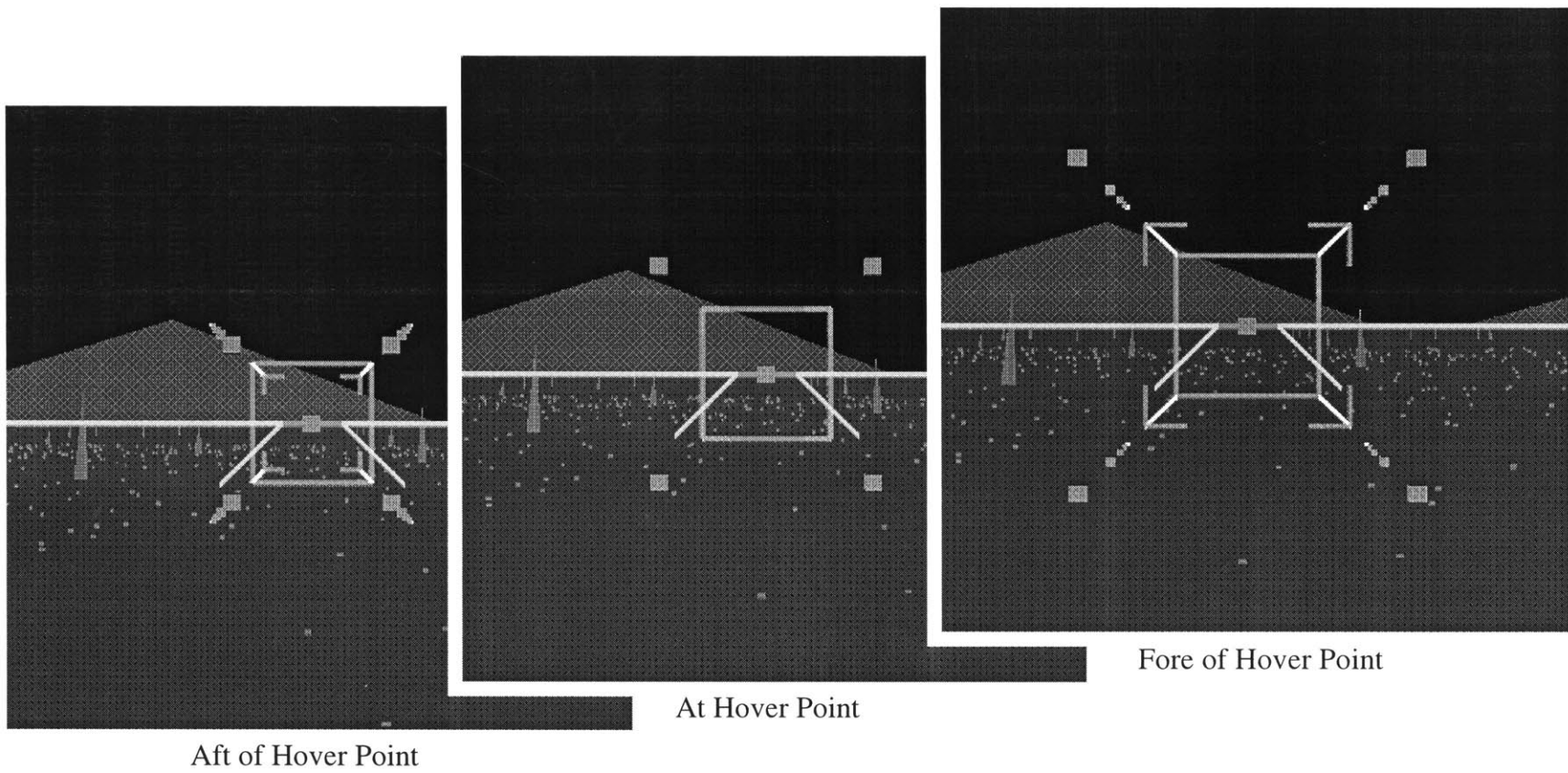
Fore of Hover Point

Figure 3.7. Synthetic Cue display showing depth motion perspective

Up and Left

Up and Right

Down and Left

Down and Right
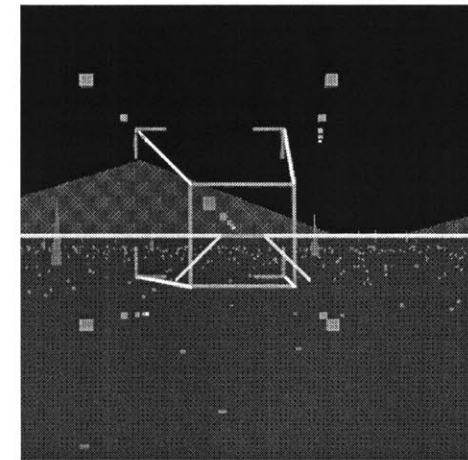
Centered
(Fore of Hover Point)

Figure 3.8. Synthetic Cue display showing transverse motion perspective.

An issue that arises when using this 3D representation of position is differential display sensitivity between transverse motion and longitudinal motion, illustrated in Figure 3.9. For a far box angular width of 6 degrees, the apparent angular separation of the two box-frames for transverse motion will be approximately 20 times greater than when the same distance is traveled along the longitudinal axis. This is true for all near box distances, provided the distance traveled by the vehicle is much less than the near box distance. Doubling the angular width of the far box changes the ratio of transverse/longitudinal sensitivity from 20 to 10, however this also halves the maximum transverse error for which the near box can remain on the screen. Using this representation of position, a narrow FOV such as the one NVGs offer imposes a severe tradeoff between line of sight error sensitivity and overall display utility.

To address the issue of unequal error perception, a technique was developed to vary longitudinal motion sensitivity independently of transverse motion sensitivity. This technique is shown in Figure 3.10, where the actual longitudinal error of the helicopter is multiplied by a factor ε to produce a magnified error gain. The near box frame and cube pattern are then expanded or contracted to give the pilot the same visual perspective as from the magnified error location. Because the expansion is symmetric, perception to transverse motion is essentially unaffected by the longitudinal error magnification, except for gross longitudinal errors where edge separation is so large as to reduce sensitivity to the differential motion. In order to make error sensitivity a design degree of freedom for all axes, the same technique of artificial error magnification was applied in the transverse motion axes, shown in Figure 3.11. Display sensitivity refers to the angular displacement between the edges of the near and far boxes for a linear displacement along. a given axis.

The figure shows a diagram with the following labels:

Far Box

D

Near Box Top Edge

$\Delta X = \Delta Z$

Forward Position Error

$\Delta \beta_X$

θ

Line of Sight to Near Box Top Edge

Line of Sight to Far Box Top Edge

Target Hover Position

ΔX

$\Delta \beta_Z$

ΔZ

Line of Sight to Near Box Top Edge

Line of Sight to Far Box Top Edge

Vertical Position Error

$$Sensitivity \equiv \frac{\text{Angular Displacement of Box Edges}}{\text{Translational Displacement}} \left(\frac{mrad}{ft} \right)$$

For $\theta = 3$ deg,

$$Sensitivity_{X\ axis} = \frac{\Delta \beta_X}{\Delta X} \approx \frac{1}{20D}$$

$$Sensitivity_{Z\ axis} = \frac{\Delta \beta_Z}{\Delta Z} \approx \frac{1}{D}$$

Figure 3.9. Differential perceptual sensitivities for longitudinal and transverse movement.
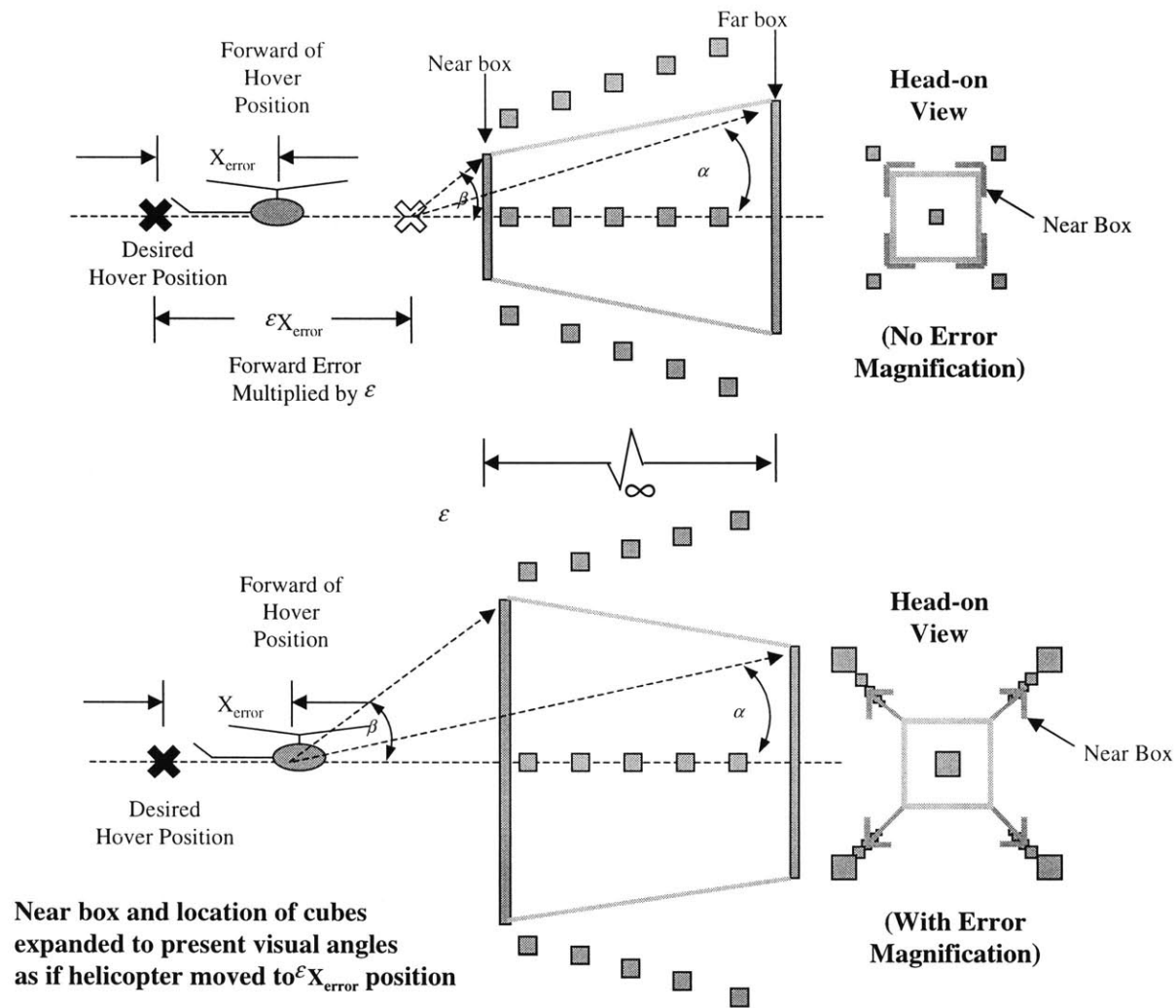
Figure 3.10. Display sensitivity magnification technique, longitudinal axis.

61
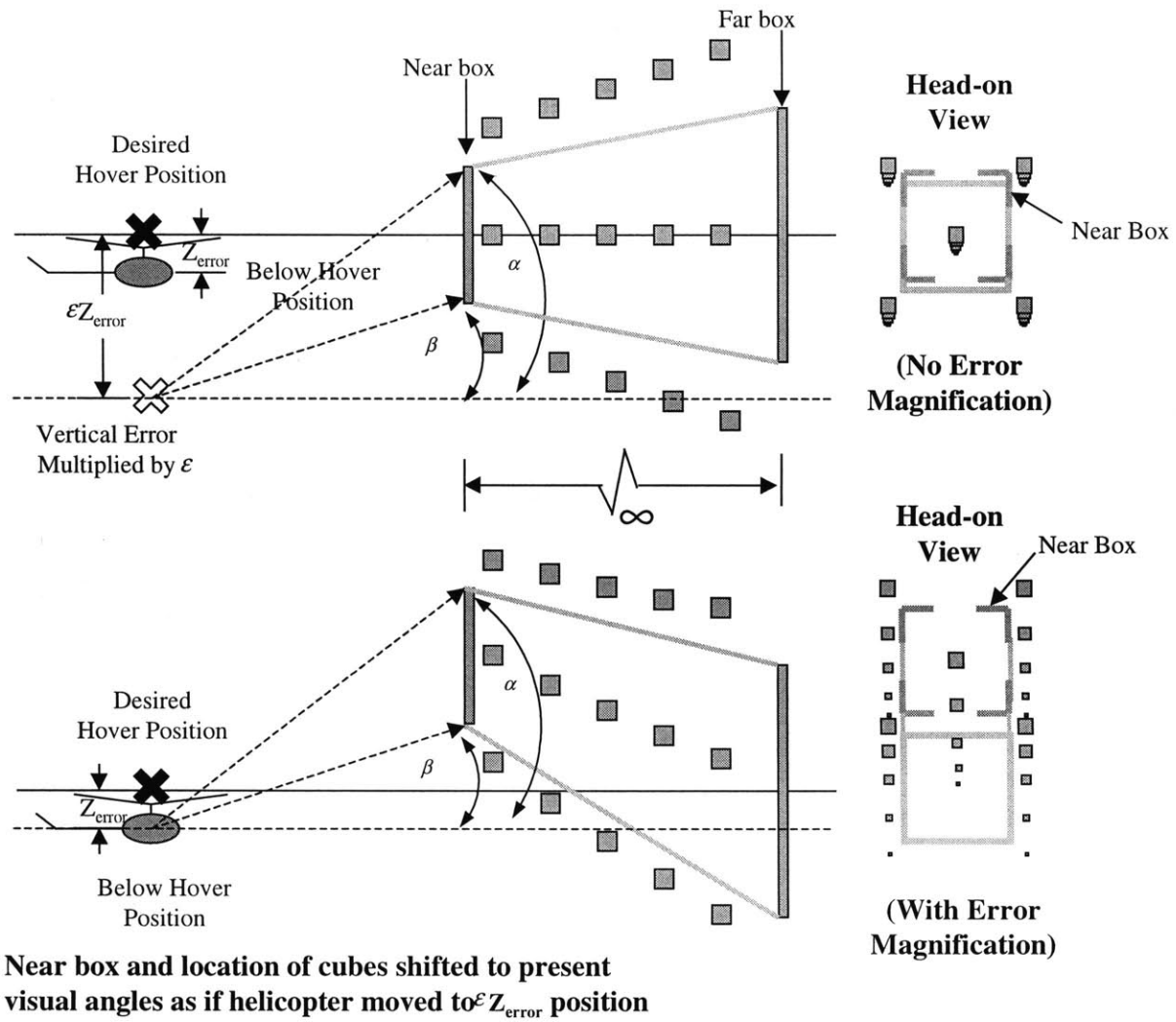
Figure 3.11. Display sensitivity magnification technique, vertical axis.

In Chapter 2 it was determined that strong cues for translational rate in all three axes were required. A primary reason for arranging the cubes in an ordered pattern was to leverage the strengths of occlusion and relative size to enhance motion perspective. Since obscuration, clutter, and terrain misrepresentation were key concerns, synthesizing microtexture was ruled out. Preliminary tests showed placing a limited number of larger objects at random throughout inertial space were effective at imparting rate perception (cubes were chosen because a cube whose faces are made distinct through shading can create its own motion perspective).

Replacing the random cubes with an ordered 3D grid of cubes was seen to improve rate perception, especially when the observer was near-centered on a row of cubes due to occlusion effects. Building on this observation, rows of cubes emanating out from the pilot's perspective were used for imparting rate and position information simultaneously.

By placing all spatial information in one geographically-fixed area off the nose, this design enables the pilot to control the helicopter using a single anchor point in space, thus allowing the surrounding area to be used for object recognition tasks (i.e., navigation, targeting, survivor pickup, etc.). It should be noted that prior to implementation of such a display the issue of cue set initiation must be resolved. This could be performed via pilot-triggering or remote programming. Figure 3.12 shows how synthetic cues have augmented the NVG hover task.

In comparison with the unaided NVG task, extraction of the functional cues that the pilot requires for hover now *no* longer incurs: (1) Continuous lateral head movement

to obtain information on ground drift; (2) Inaccuracies and added difficulty in head

orientation due to reduced field of view; (3) Continual mental coordinate transformations

going from the LOS reference frame to the aircraft and geographic reference frames, and

(4) Serial fusing of ground drift information (direction and rate).
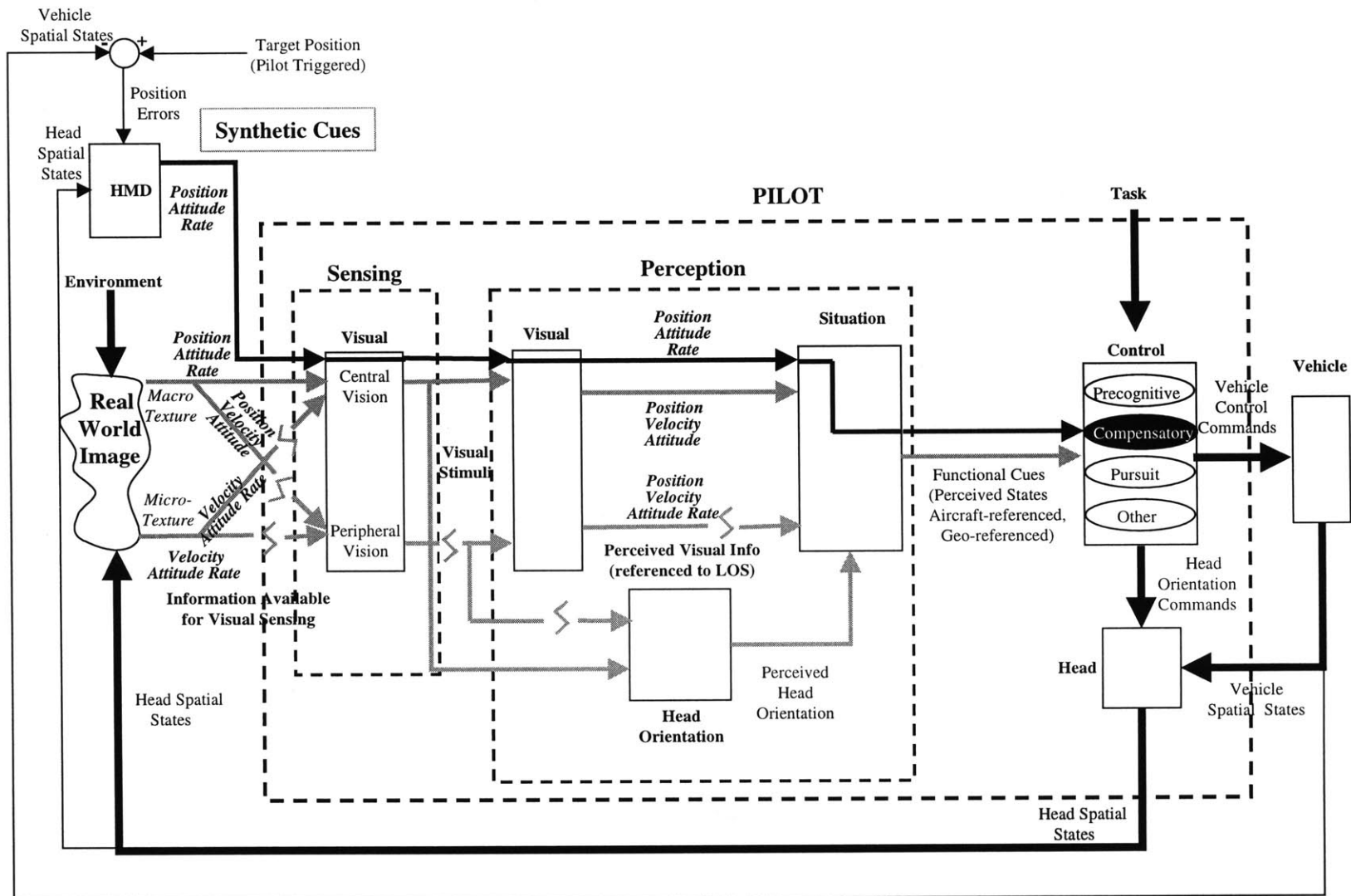
Figure 3.12. Representation of NVG hover task augmented with synthetic cues.

Chapter 4

Experimental Method

4.1 Overview

Synthetic cueing was identified as a major area of opportunity for improving

hover performance. It was proposed that synthetic spatial cues could convey conformal

(or pseudo-conformal) state feedback during night-vision helicopter hover. One of the

objectives of this research was to determine the efficacy of synthetic cueing for helicopter

hover using the night-vision hover problem as a test-bed. The second objective of this

research was to investigate issues of perception and control in the context of synthetic

cueing.

Four experimental studies were conducted. Experiment 1 explored the

relationship between station-keeping and motion gain of displayed synthetic cues when

only one translational axis (longitudinal, lateral, or vertical) was disturbed. In addition,

the effect of these visual cues on pilot control was investigated. Collected performance

measures collected were: (1) station-keeping error and (2) pilot time delay. The

following frequency-domain metrics were derived: (1) open-loop crossover frequency

(a measure of pilot sensitivity to position disturbance), (2) open-loop phase margin (a

measure of control stability), (3) slope of the open-loop amplitude ratio, (4) low-

frequency power of pilot observation noise, (5) break frequency of pilot observation

noise, (6) high-frequency slope of pilot observation noise, and (7) relative tracking error

due to observation noise. Subjective ratings were also collected using a Cooper-Harper

scale (Figure 4.1) for aircraft displays.

AIRCRAFT/DISPLAY CHARACTERISTICS	DEMANDS ON THE PILOT IN SELECTED TASK OR REQUIRED OPERATION	PILOT RATING
Excellent Highly desirable	Pilot compensation not a factor for desired performance.	1
Good Negligible deficiencies	Pilot compensation not a factor for desired performance.	2
Fair – Some mildly Unpleasant deficiencies	Minimal pilot compensation required for desired performance.	3
Minor but annoying deficiencies	Desired performance requires moderate pilot compensation.	4
Moderately objectionable deficiencies	Adequate performance requires considerable pilot compensation.	5
Very objectionable but tolerable deficiencies	Adequate performance requires extensive pilot compensation.	6
Major deficiencies	Adequate performance not attainable with maximum tolerable pilot compensation, controllability not in question.	7
Major deficiencies	Considerable pilot compensation is required to retain control.	8
Major deficiencies	Intense pilot compensation required to retain control.	9
Major deficiencies	Control will be lost during some portion of required operation.	10

Decision flow:

Is it satisfactory without improvement? — YES → (ratings 1–3) / NO → Deficiencies warrant improvement → (ratings 4–6)

Is adequate performance attainable with a tolerable pilot workload? — YES / NO → Deficiencies require improvement → (ratings 7–9)

Is it controllable? — YES / NO → Improvement mandatory → (rating 10)

Pilot decisions

Figure 4.1. Cooper-Harper subjective rating scale (Cooper, 1969).

Experiment 2 explored the relationship between hover performance and display sensitivity when all three translational axes were disturbed simultaneously. The performance, control and subjective metrics used in Experiment 1 were also collected in Experiment 2. Experiment 3 looked at the effect on hover performance using unequal display motion gains between axes. In Experiment 4 the station-keeping performance of the synthetic cueing system was evaluated by comparing a baseline simulated NVG image against the synthetic hover cues overlaid on the NVG image. Two backgrounds were used with each display to investigate the effect of near field objects in the NVG

image. One background presented only far-field trees, and the other background presented both near and far-field trees.

4.2   Display Conditions

The baseline *NVG* display configuration, shown in Figure 4.2 with far-field objects, simulated an NVG image as seen from the pilot's perspective. The objects of the NVG image (mountains, terrain, trees, and airframe) were rendered in monochromatic green with varying intensities for contrast. Trees were positioned at random around the vehicle's initial hover position, starting at a radius of 100 feet out to 1100 feet. Tree height varied randomly between 15 and 50 feet. Ground texture dots appeared at random on the flat terrain starting at a radius of 50 feet from initial hover position.
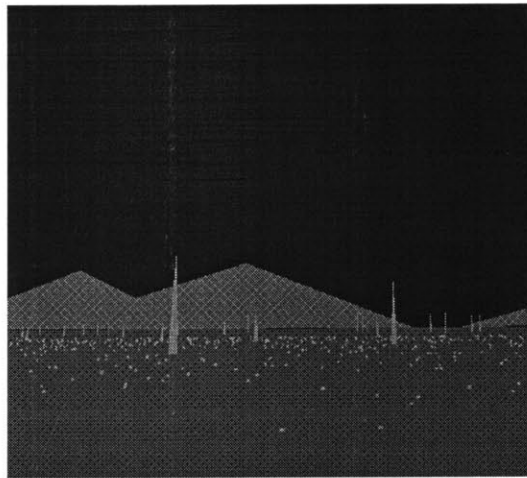
Figure 4.2. *NVG* display with far-field objects.

In Figure 4.3 the *NVG* display is shown at the initial hover position with near-field objects, which consisted of two trees placed 32 and 42 feet away from the pilot, 5 degrees left and 40 degrees right of center, respectively. The *NVG* display offered the pilot a conformal view of the helicopter airframe as well as an instrument panel, which included an altimeter tape, total ground speed readout, and an aircraft attitude indicator.
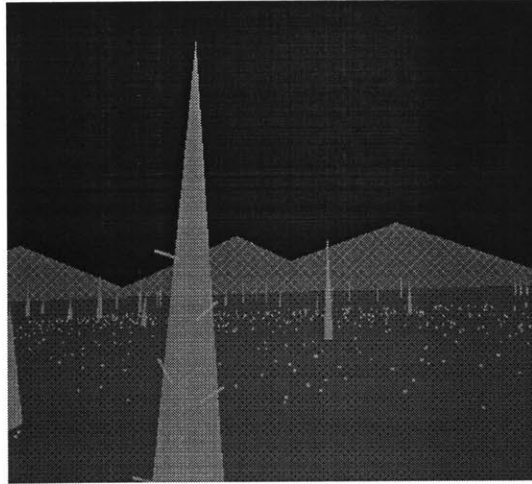
Figure 4.3. *NVG* **display with near-field objects.**

Figure 4.4 shows the Synthetic Cue display overlaid on a black background. The *NVG/* Synthetic Cue display shown in Figure 4.5 combines the Synthetic Cue display with the NVG background.
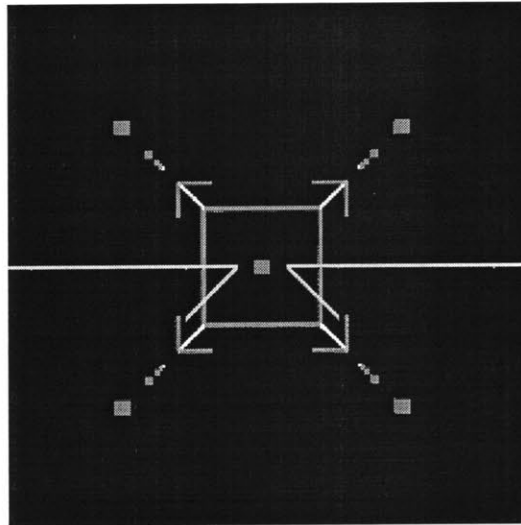
Figure 4.4. Synthetic Cue display.
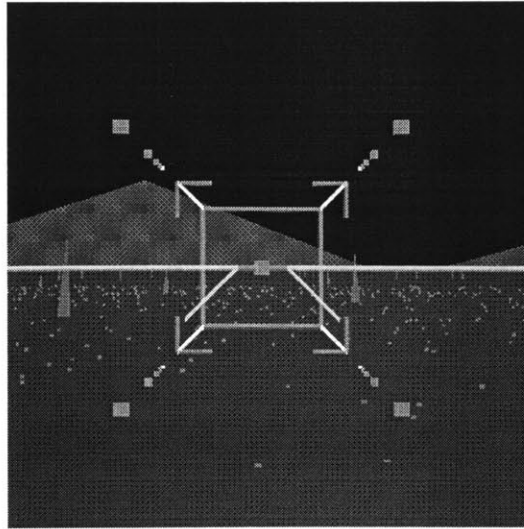
Figure 4.5. *NVG*/**Synthetic Cue display.**

4.3 Simulation Facility Description

The simulation, illustrated schematically in Figure 4.6, employed a number of techniques that made it uniquely different from previous helicopter simulation studies. The vehicle dynamics were completely decoupled so that vehicle translation along a given axis did not interact with motion of another axis. In order to provide the pilot with realistic feedback the aircraft was allowed to *virtually* (i.e., visually) roll and pitch in response to cyclic inputs – the actual rotational motion of the vehicle was frozen in all axes so that motion in response to control inputs was purely translational. An automatic heading hold kept yaw constant. If the helicopter had been allowed to actually rotate, then a maneuver such as left translation along the aircraft body axes (involving a left roll) would create both a left and vertical translation component in the geographic axis system – to maintain altitude the pilot would have to make a control adjustment in the vertical (collective input). By only allowing the aircraft to *virtually* roll and pitch, the aircraft coordinate system remained rotationally aligned with the geographic axes.

70

The positional disturbances were geographically referenced (North-East-Down)

so that the full component of each axis' disturbance would be acting along the intended

aircraft axis. The positional disturbances imposed on the helicopter were designed to be

both realistic and a diagnostic probe for pilot control behavior. Composed of a sum of

non-harmonically-related sine waves, the disturbance was perceived by the pilot as a

random process – the result, however, was that the pilot's control response power resided

largely at the same frequencies contained in the input disturbances. Each axis

disturbance was unique in frequency content to allow for independent analysis of

individual axes.

Figure 4.6. Helicopter simulation environment.

Yaw was held constant so that: (1) the aircraft and disturbance axes remained aligned, and (2) the pilot's perception of translation would not be skewed or coupled with yaw motion. The vehicle translational dynamics for each axis were made identical (rate commanded), the control gains for collective and cyclic were set equal, and the controls were made spring centering. The intention of the simulation design was to create an environment where differences in performance between axes would be due primarily to visual perception and control strategy differences.

Subjects conducted tasks in a fixed-based helicopter simulator. The simulator airframe, shown in Figure 4.7, is an actual forward end of an AH-1 Cobra helicopter. Subjects were seated in the front gunner's seat, shown in Figures 4.8 and 4.9, operating a right side-stick for pitch and roll control and a left collective for altitude control. The side-stick and collective were spring centering.

Figure 4.7. Simulator airframe (AH-1 Cobra).
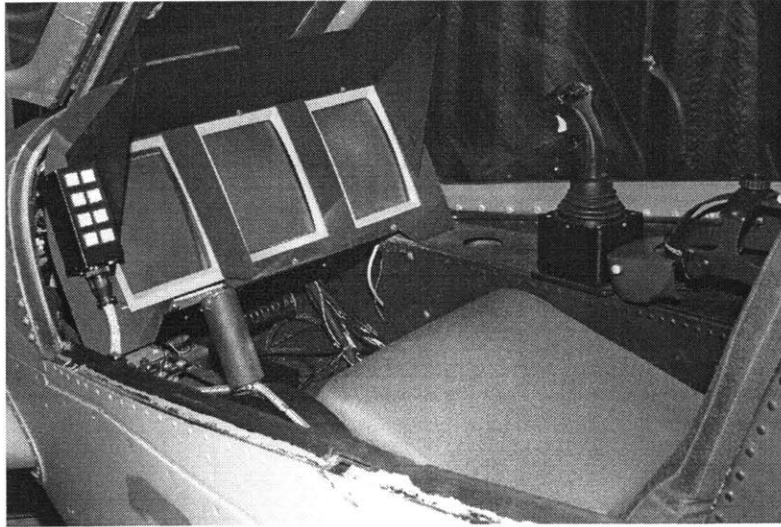
Figure 4.8. Simulator cockpit controls.
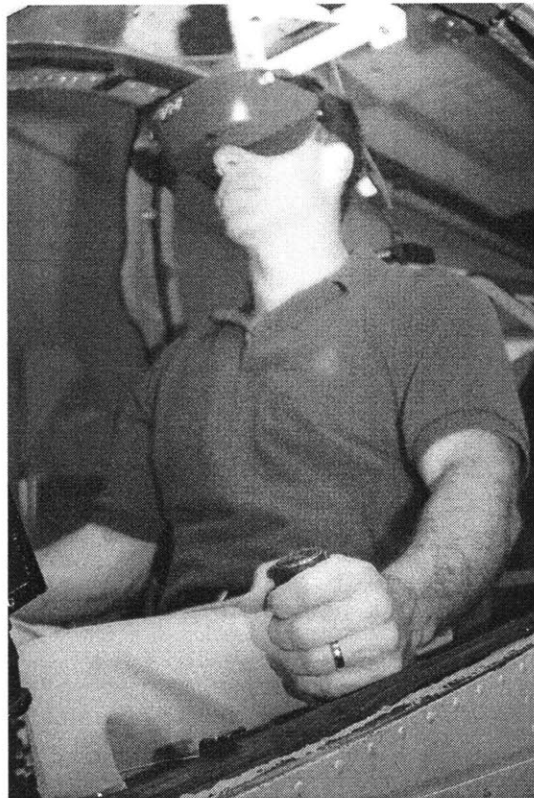
Figure 4.9. Subject pilot at helicopter simulator controls.

Visual scenery was displayed at a frame rate of 20 Hz to subjects with a helmet-

mounted virtual reality device having a 48 X 36 degree FOV. The HMD, made by

Virtual Research Systems (VR4 model) used two liquid crystal displays to provide color images to the pilot's eyes at a 480 x 240 color pixel resolution. The virtual cockpit airframe seen from the pilot's perspective matched the dimensions of an AH-1 Cobra helicopter. Head motion was tracked by a Logitech ultrasound system (see Figure 4.10) at a report rate of 50 Hz and with a resolution of approximately 0.1 degrees in azimuth, pitch, and roll. The cockpit I/O program broadcasted information to the vehicle simulation over a Network DataBase (NDB) at a rate of 30 Hz, and the simulation frequency was 100 Hz. Data was recorded at a rate of 10 Hz. The experiments were conducted at Charles Stark Draper Laboratory.
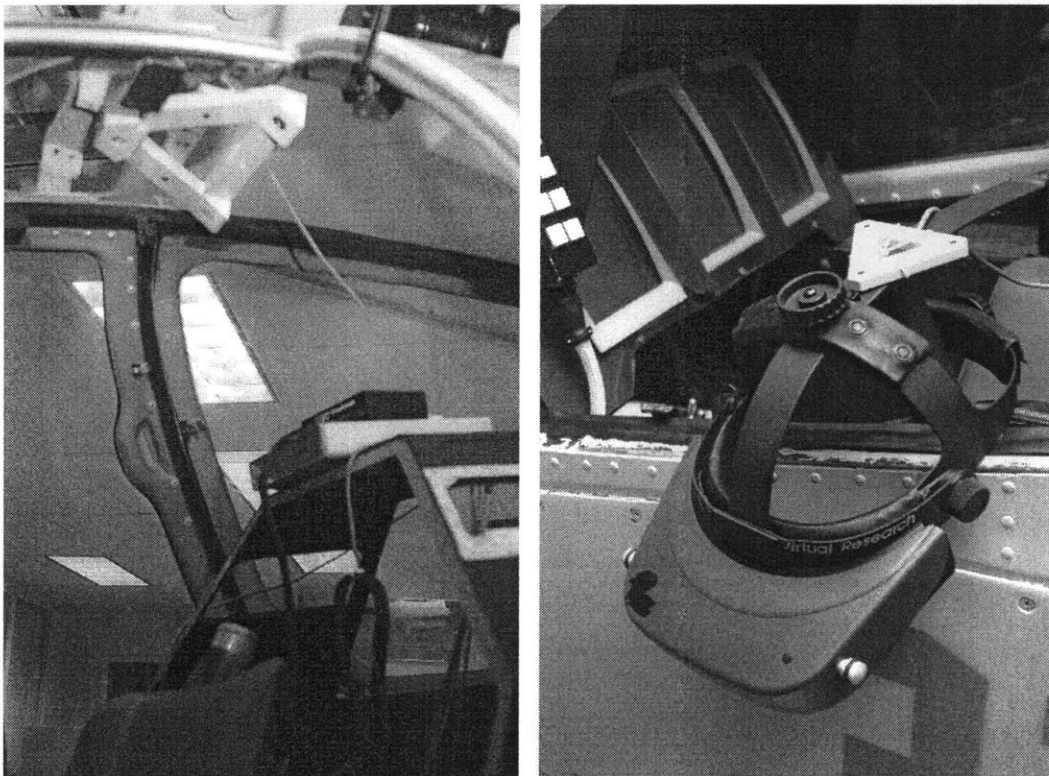
Figure 4.10. Ultrasound head tracker (left) and head-mounted display (right).

4.4　Vehicle Motion Dynamics

Figure 4.11 shows the dynamics used in the simulated helicopter model. The vehicle dynamics were completely decoupled so that vehicle translation along a give axis did not interact with motion in another axis. Vehicle translational dynamics were identical (rate commanded) in each axis, and the control gains for collective and cyclic were set equal. These dynamics resemble state-of-art, highly augmented helicopter dynamics.
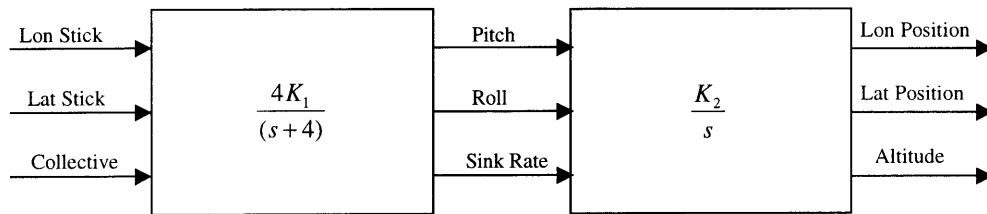
Figure 4.11. Dynamics of helicopter model.

To provide realistic pilot feedback the aircraft was allowed to *virtually* (i.e., visually) roll and pitch in response to cyclic inputs – the actual rotational motion of the vehicle was frozen in all axes so that motion in response to control inputs was purely translational. An automatic heading hold kept yaw constant. Table 4.1 shows the values of K_1 and K_2 used for the attitude and positional gains. These constants were chosen based on one subject's best error performance and pilot rating using a range of values while hovering with disturbances described in §4.5.

Table 4.1. Attitude and positional gains.

	K_1	K_2
Longitudinal	0.1 rad/rad	25/0.1 ft/rad
Lateral	0.2 rad/rad	25/0.2 ft/rad
Vertical	25 ft/(s rad)	1 ft/(ft/s)

4.5 Aircraft Positional Disturbance

Summing 9 sinusoids for Experiments 1, 2, and 3 created the computer-generated disturbance signals injected into the aircraft's positional loops. In Experiment 4 a tenth sinusoid was included whose low frequency created a pseudo steady-state wind. The disturbance signals were each characterized by a "shelf" line amplitude spectrum (see Figure 4.12), whereby amplitudes at frequencies higher than this shelf line were uniformly reduced by 20 dB. To minimize spurious frequency effects in the frequency analysis, the display frequencies were chosen such that two criteria were met: (1) each individual frequency must complete a whole number of cycles during the run-time, and (2) each frequency must not be a low harmonic of any other frequency examined. This meant that each spectral component was a prime multiple of an axis-specific base frequency. For the longitudinal, lateral, and vertical axes, the base frequencies were 1/81 Hz, 1/83 Hz, and 1/85 Hz, respectively, so that the signals were periodic with periods of 81 seconds, 83 seconds, and 85 seconds, respectively. Because of the long periods, the signals were not predictable by the subject, and thus may be termed pseudo-random. The disturbance time history of one axis is shown in Figure 4.13, and Table 4.2 gives characteristics of the three axes' disturbances.
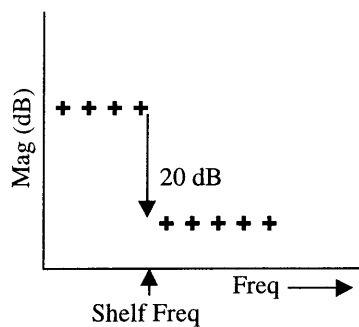
Figure 4.12. Spectral composition of position disturbance.

76
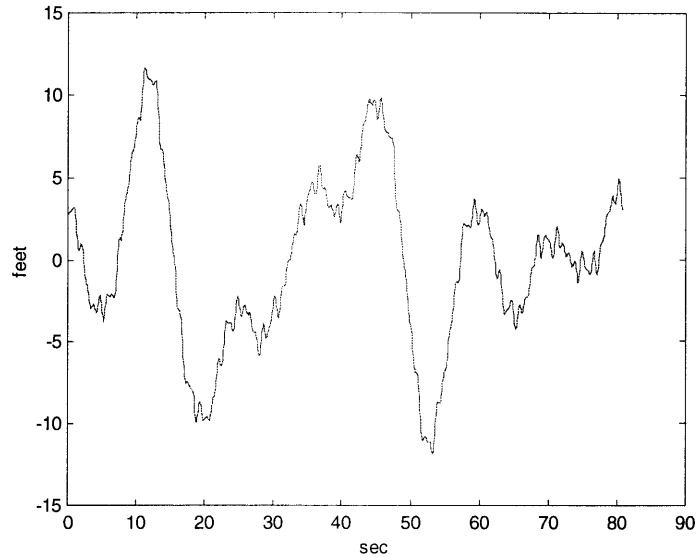
Figure 4.13. Example time history of longitudinal disturbance signal.

Table 4.2. Characteristics of position disturbances.

	Base Frequency (Hz)	Shelf Frequency (Hz)	RMS (ft)
Longitudinal	1/81	7/81	5.14
Lateral	1/83	7/83	5.12
Vertical	1/85	7/85	5.11

4.6   Tasks

In Experiments 1, 2, 3, and 4, the helicopter was automatically positioned and trimmed for a steady-state 15-foot hover. Upon depressing a cyclic button, flight control was transferred to the subject and turbulence initiated. The task objective was to maintain the initial position in space using any visual cues available through the displays. The yaw axis was frozen throughout all flights.

4.7   Experimental Subjects and Protocol

4.7.1   Subjects

Seven pilots participated in all experiments. The helicopter flight experience of

the subject pilots is summarized in Table 4.3. The subjects were not paid.

Table 4.3. Helicopter flight experience of the subject pilots.

Subject	Age	Flight Hours	NVG Hours	Helicopter Experience
A	42	2500	0	R22 Robinson, F28 Enstrom, Bell JetRanger/LongRanger
B	38	10000	50	SA330 Puma, SA316 Allouette, R22/44 Robinson, B206 JetRanger, F20 Enstrom, Single-engine
C	44	5000	300	UH-1, Multi/Single-engine
D	51	3500	125	CH-46, UH-1, Single-engine
E	35	2800	0	SH-2F, TH-57B/C, Single-engine
F	36	2200	75	UH-1H/V, Bell 407,Single-engine
G	36	1000	0	SH-60B, TH-57B/C, Single-engine

4.7.2   Experimental Protocol

The four experiments took place over three days. Table 4.4 shows the

experimental order. Day 1 started with a briefing of all tasks and displays,

Table 4.4. Order and characteristics of experiments.

	Exp1	Exp2	Exp3	Exp4
# Conditions	21	7	8	6
# Measurements	1	1	1	1
Run-time (sec)	90	90	90	90

followed by three familiarization series using the Synthetic Cue display to control

position along a single axis (motion along the other two axes was frozen). Each series

consisted of presenting seven gains (.25, 1, 2, 3, 6, 25, 50 mrad/ft) in ascending order,

each axis receiving three familiarization series. Following the three familiarization runs

subjects were given the option to continue training (no subjects requested additional training), and Experiment 1 was conducted running subjects through the seven display motion gains for each of the three axes. In all experiments each run-time was composed of an initial 5-second period during which startup transients could subside, followed by 85 seconds of actual measurement time. Following each run pilots were asked to give a subjective rating for the display condition. The remainder of Day 1 was used to familiarize subjects with multi-axis hover control using the Synthetic Cue display.

Day 2 started with a briefing of Experiment 2, followed by four familiarization series using the Synthetic Cue display for controlling position along all axes. Each series consisted of presenting seven gains (.25, 1, 2, 3, 6, 25, 50 mrad/ft) in ascending order. Following the four familiarization runs subjects were given the option to continue training (no subjects requested additional training), and Experiment 2 was conducted running subjects through the seven display motion gains. A familiarization series for Experiment 3 (run-time reduced to 20 seconds) was then conducted using eight permutations of two display gains (1 and 3 mrad/ft) applied to the three axes, followed by actual runs that were counterbalanced for gain condition. On Day 3 subjects were given 3 familiarization series with the *NVG* and *NVG*/Synthetic Cue displays using near and far-field objects. Following the three familiarization runs, subjects were given the option to continue training (no subjects requested additional training), and Experiment 4 was conducted with the six display conditions (display condition counterbalanced). Pilot questionnaires were given at the conclusion of Experiment 4, which solicited ideas, recommendations, and criticism pertaining to the displays that had been flown.

4.7   Analysis Methods

Figure 4.14 shows the experimental variables that were measured, as well as the expressions that were used to evaluate observation noise, pilot describing function, and linear coherence. The remnant component of the human pilot's response is generally defined as that portion not accounted for by his describing function, which in Figure 4.14 is denoted as the pilot non-linear stick response. The remnant data for a wide variety of controlled elements and forcing function amplitudes coalesce best when all remnant is reflected to the pilot's input, denoted as pilot observation noise. The total system error e can then be represented as the sum of a linear error component arising from the forcing function, and an error component due to non-linear behavior.

$$\Phi_{ee_n} = \frac{\left|1+Y_pY_c\right|^2}{\left|Y_p\right|^2}\Phi_{\delta\delta} - \Phi_{ii} \qquad |Y_p| = \frac{|\Phi_{i\delta}|}{|\Phi_{ie}|} \qquad \text{Linear} \atop \text{Correl} = \frac{|\Phi_{\delta i}|^2}{|\Phi_{\delta\delta}||\Phi_{ii}|}$$
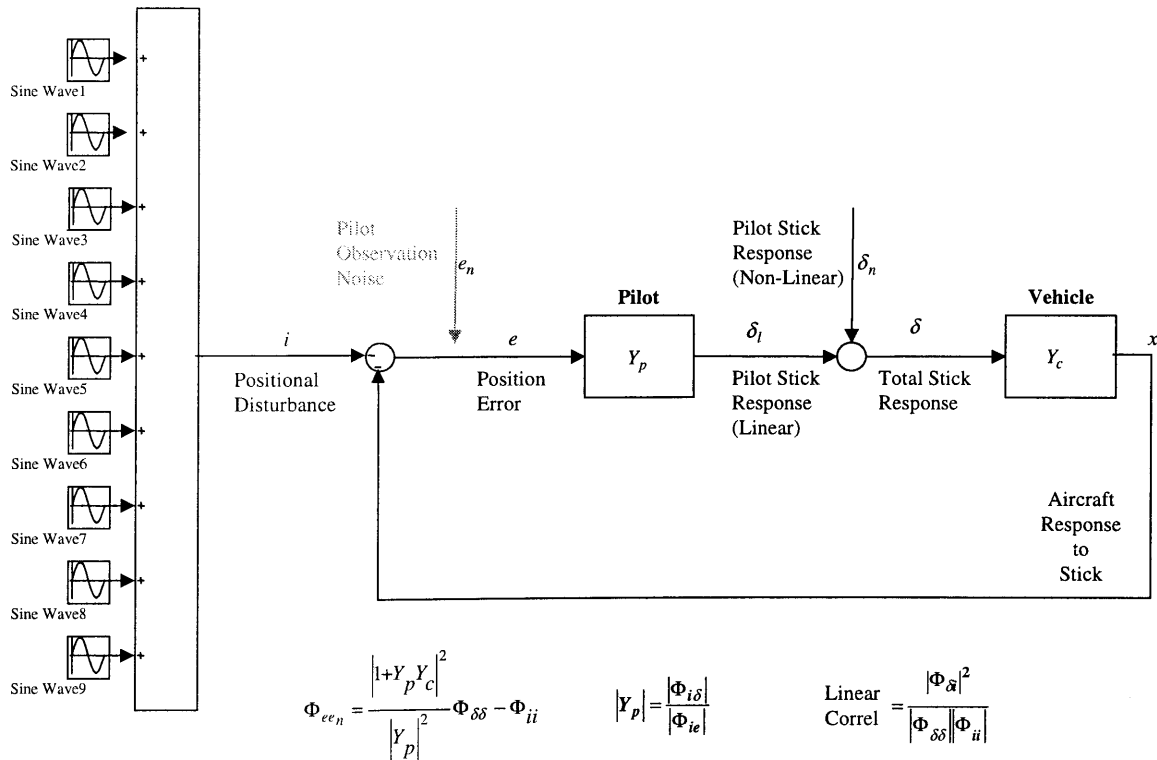
Figure 4.14. Measured experimental variables.

80

Effective pilot time delay τ was computed by cross-correlating position error with stick output, shown in Figure 4.15. The time delay using this method in fact represents the total system time delay, which includes update lags for simulation, display, cockpit control position, in addition to the pilot reaction time. The average time delay due to non-pilot sources (using the update frequencies found in §4.3) was approximately 0.06 seconds.
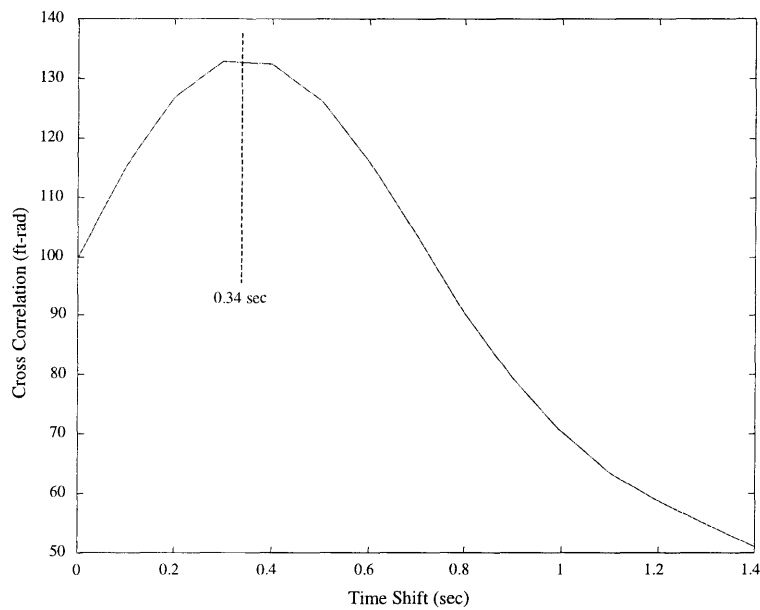
Figure 4.15. Method using cross correlation (position error with stick) for computing effective time delay.

Figure 4.16 shows a sample plot of the open-loop describing function $Y_p Y_c$. Cross-spectral density ratios were used to compute magnitude for the pilot's describing function Y_p at the disturbance frequencies, and these magnitudes were weighted with the linear coherence between the pilot response and disturbance to produce a best-fit line (log-scale frequency) for the amplitude ratio. Crossover frequency, ω_c, was established at the intersection of the best-fit line and 0 dB.
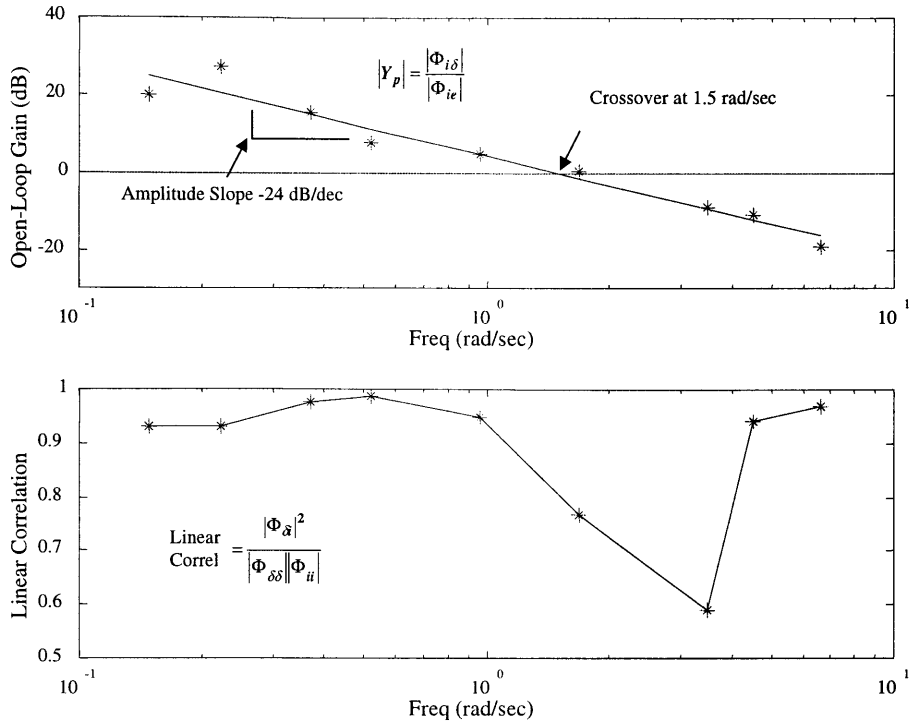
Figure 4.16 Open-loop gain Y_pY_c (pilot-vehicle) using cross-spectral densities.

Phase margin, φ_M, was computed using the crossover frequency and effective

pilot time in the relation:

$$\varphi_M = \pi/2 - \omega_c\tau \tag{4.1}$$

Equation (4.1) holds if the open-loop amplitude ratio (Y_pY_c) slope is approximately –20

dB/dec, which was proved to be valid for this study.

Relative remnant, ρ_n, was computed with equation (4.2) using the linear portion e_l of

the error due solely to the disturbance, which was determined using Matlab simulation by

inserting observed measures of ω_c and τ in the Crossover Model (equation (2.1)).

$$\rho_n = 1 - \frac{e_l^2}{e^2} \tag{4.2}$$

Chapter 5

Results

5.1 The Effect of Display Motion Gain on Single-Axis Station-Keeping

The objective of this experiment was to identify baseline pilot response to display motion gain using the Synthetic Cue display when full attention was devoted to regulating helicopter position along a single axis of translation. These results will later be compared with simultaneous control of the three translational axes to determine divided attention effects during hover. Note that display sensitivity for all plots is given in log scale.

5.1.1 Time Domain Data

Figure 5.1 shows RMS station-keeping error data for all seven subjects as a function of display sensitivity for each of the axes of translation. Display sensitivities were 0.25, 1, 2, 3, 6, 20 and 50 milliradians/foot. The mean data show increasing performance in all three axes with increasing sensitivity until a leveling off near 3 mrad/ft. After 6 mrad/ft the longitudinal error appears to increase slightly while the two other axes remain relatively constant.
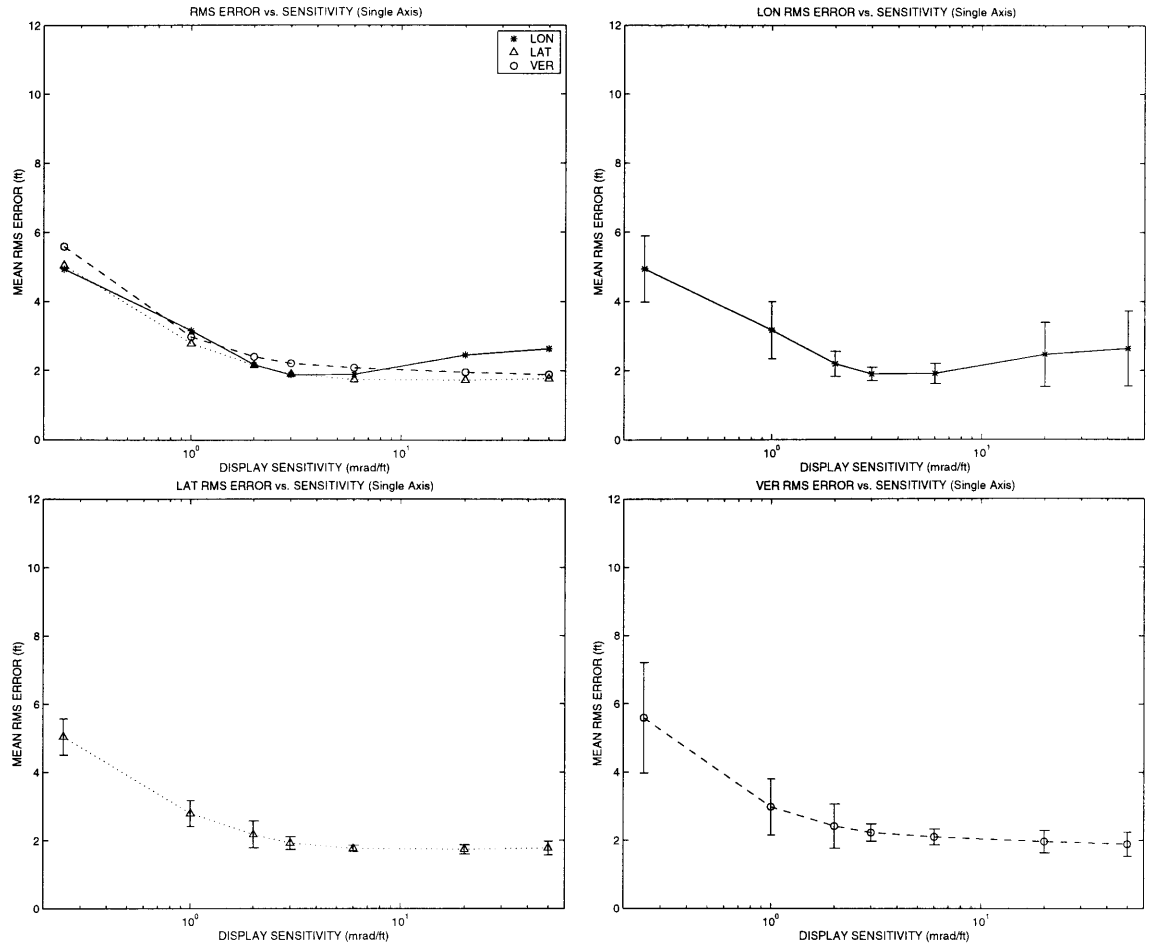
Figure 5.1. Position RMS error versus display sensitivity.

Figure 5.2 shows pilot time delay to decrease monotonically with increasing

display sensitivity in all three axes. There appears to be a general transition in slope in

the vicinity of 3 mrad/ft.
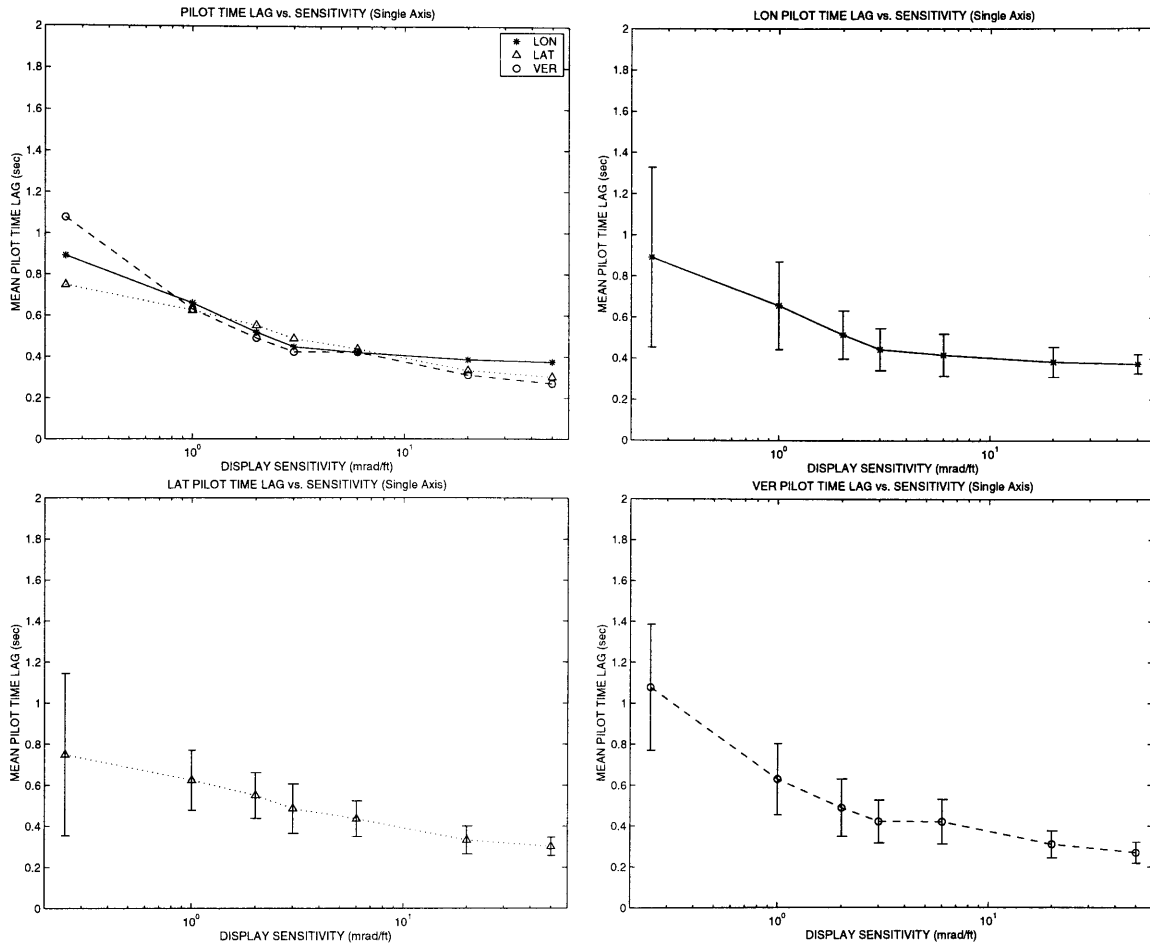
Figure 5.2. Pilot time delay versus display sensitivity.

The display FOV (48 x 36 degrees) limited visible angular cue displacement in

the lateral direction to 24 degrees left and right of centerline, and in the vertical direction

18 degrees above and below centerline. When cues saturated on an axis (i.e., reached or

exceeded the screen limits along a given axis of motion), cue motion was frozen along

that axis so that usable information in the other axes would still be available. Normal cue

motion resumed when the vehicle error was reduced to values that corresponded to nominal cue displacements within the screen FOV. For large displacement errors aft of the target hover spot, cue motion sensitivity along the longitudinal axis effectively became zero. Figure 5.3 shows the mean operation time during which the cue displacement had saturated (i.e., cue motion sensitivity was zero) along a given axis due to large aft errors (longitudinal axis only) and to maximum displacement limits imposed by the screen FOV. At 20 mrad/ft subjects saturated approximately 10% of the time, and at 50 mrad/ft saturation rose to approximately 30% of operating time. This can account in part for the worsening error performance in the longitudinal axis at these sensitivities.

Figure 5.3. Operating times for when cue motion was saturated (90-second total run time).

Cue motion along the longitudinal axis was determined to be essentially linear (i.e., actual display sensitivity was approximately constant and equal to the nominal display sensitivity) for sensitivities until saturation occurred.

5.1.2   Subjective Scores

The median Cooper-Harper ratings (see §4.1 for description) are presented in Figure 5.4. Bars indicate minimum and maximum ratings associated with each median. The acceptability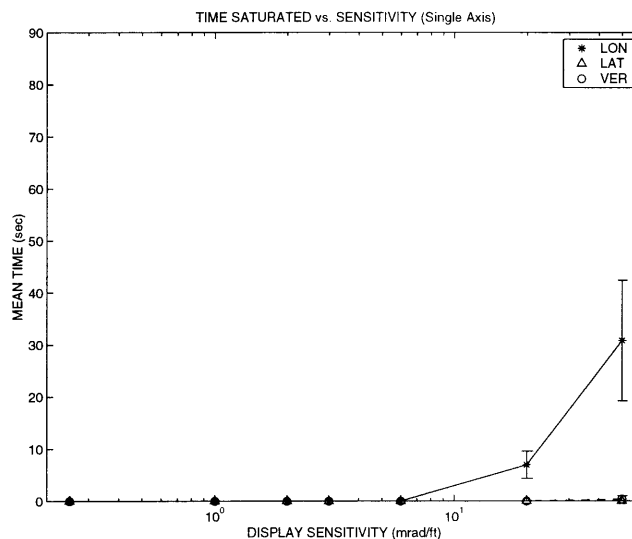 of flying qualities of rotorcraft is quantified in terms of levels (U.S. Army ADS-33D) that are defined for each specific mission task in Figure 4.1. Level 1 represents Cooper-Harper ratings ranging from 1 to 3 ½, which corresponds to minimal pilot compensation required for desired perceived performance. Longitudinal ratings rose significantly above the other axes' ratings for display gains above 3 mrad/ft. At a sensitivity of 50 mrad/ft, longitudinal ratings indicated that pilots perceived this axis to be uncontrollable. The monotonic one-sided character of rating versus gain is in contrast with the expected U-shaped trend. It is believed this is because of the pilot's low sensitivity to the high frequency/low amplitude disturbances when the display sensitivity is low. Taking in concert the performance data of Figure 5.1 and the subjective data in Figure 5.4, a case can be made that the optimum display gain lies in the vicinity of 3 mrad/ft.

It is proposed that similar use of subjective scores and simulation performance could be made in identifying the region of optimum gain for different vehicle dynamics and/or task requirements. A preliminary flight display design would use these values as starting points for configuration gains, subject to later flight test and validation. Experience with previous flight displays indicates that the flight gains would be somewhat lower than the optimum gains identified during simulation (personal communication with McRuer).
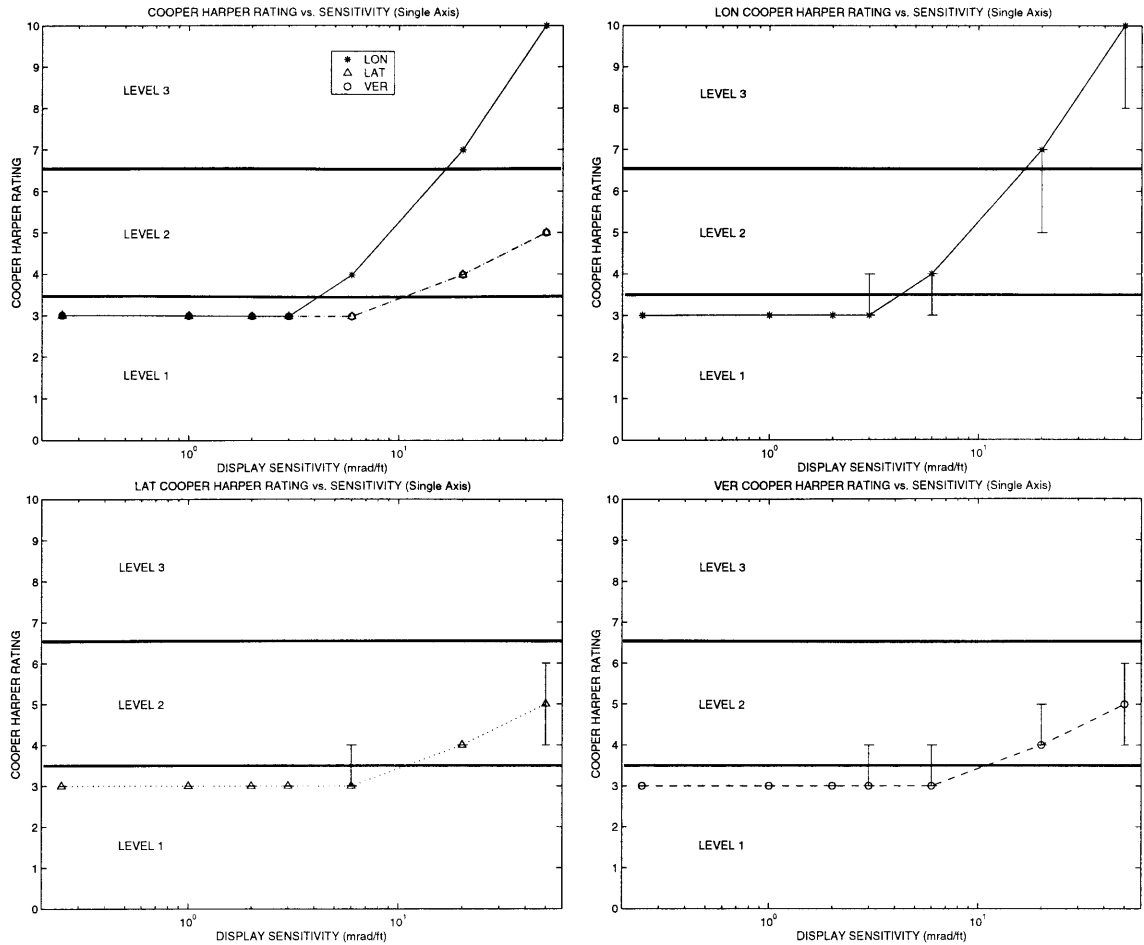
Figure 5.4. Subjective rating versus display sensitivity.

5.1.3   Frequency Domain Data

Figure 5.5 shows crossover frequency increasing with display sensitivity in the longitudinal and lateral axes until 3 mrad/ft followed by a general leveling until 6 mrad/ft, after which crossover appeared to increase. The vertical axis increased monotonically and appeared to yield the highest crossover out of all axes at all sensitivities. Crossover for the lateral and longitudinal axes appear to match one another until 6 mrad/ft.

Referring back to the performance data of Figure 5.1, error performance is seen to stabilize above 2 mrad/ft, and the Crossover Model states that in this range of stable

performance the crossover frequency is expected to likewise remain approximately constant. The data in Figure 5.5, however, seems to indicate that the crossover invariance rule given by the Crossover Model does not apply here. It appears that inner-loop crossover (attitude and/or translation rate for the longitudinal and lateral axes, translational rate for vertical) is being driven up by increasing display sensitivity. Later in §5.1.4 the implications of this will be discussed in more detail.
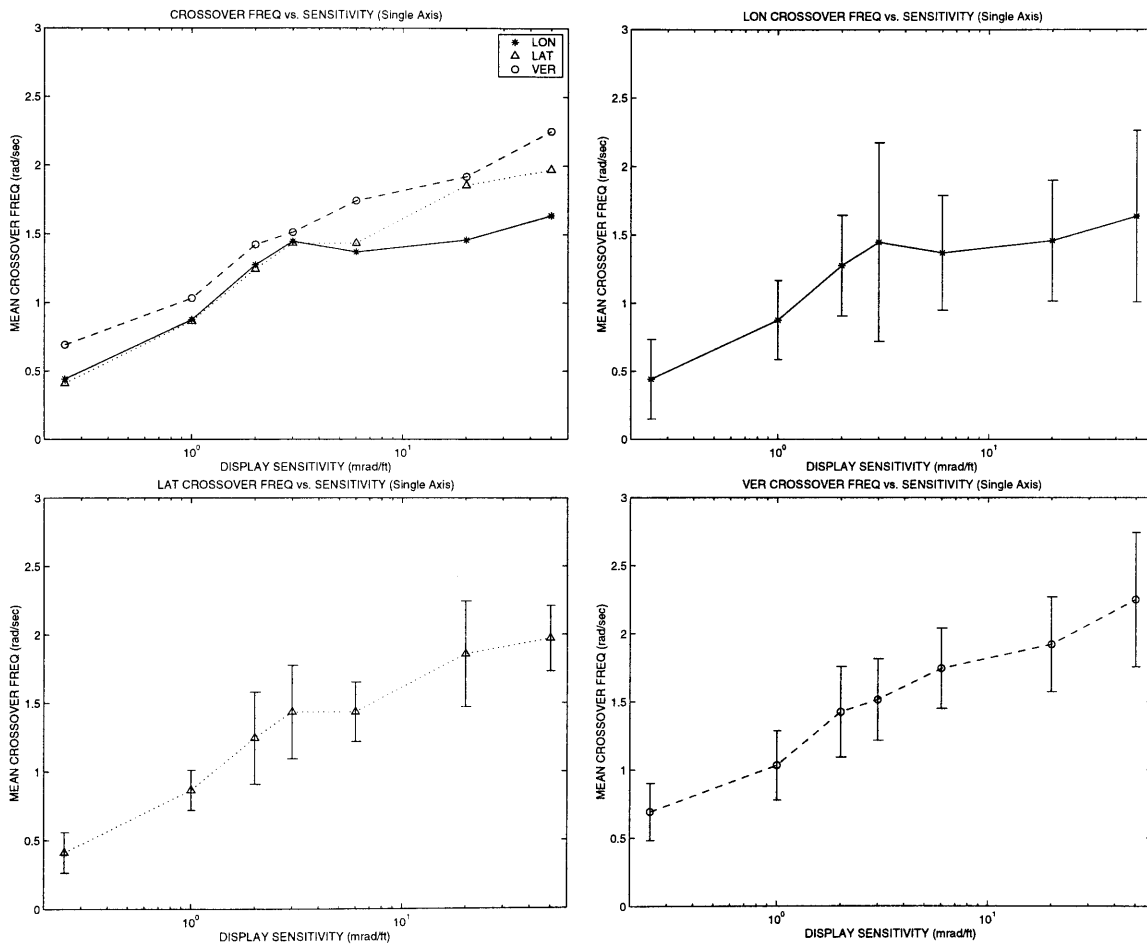
Figure 5.5. Crossover frequency versus display sensitivity.

90

In Figure 5.6 the phase margin for all axes is seen to be relatively invariant with sensitivity above 2 mrad/ft, stabilizing at about 53 degrees. Despite a perceived near uncontrollability for a longitudinal sensitivity of 50 mrad/ft, longitudinal phase margin is still above 50 degrees.
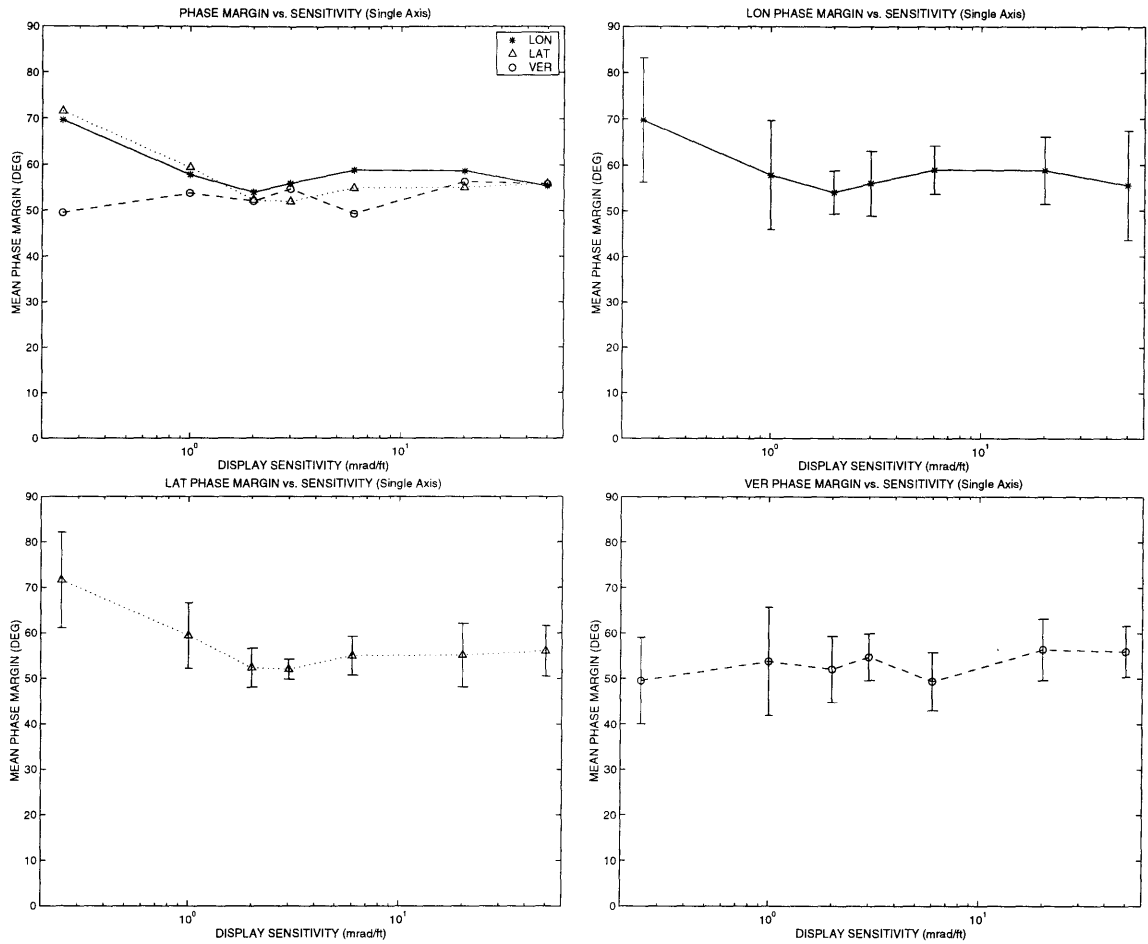
Figure 5.6. Phase margin versus display sensitivity.

In Figure 5.7 the amplitude ratio slopes appear to gradually flatten with increasing

sensitivity, stabilizing at approximately –20 dB/dec. This would indicate that the

Crossover Model is an appropriate model for this task.
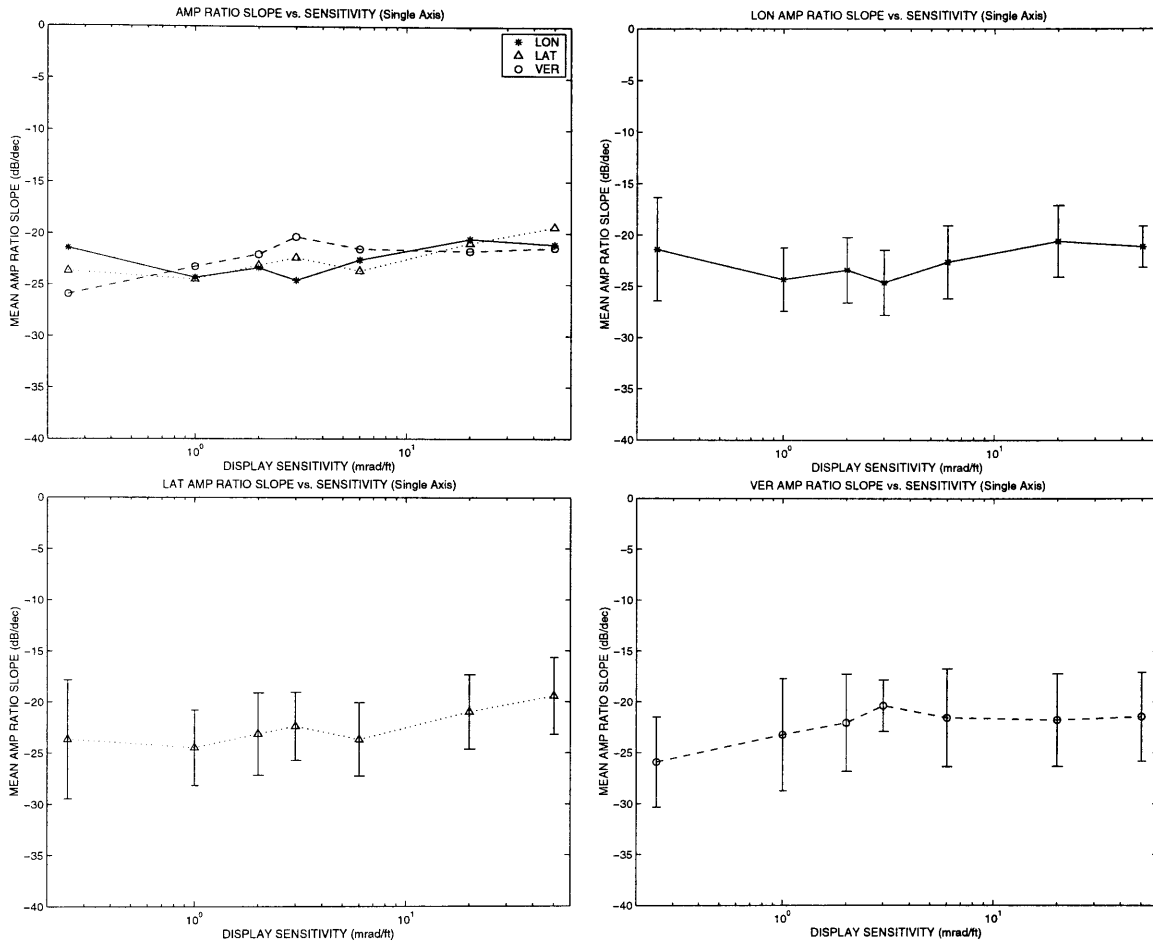
Figure 5.7. Amplitude ratio slope versus display sensitivity.

Figure 5.8 shows examples of DC observation noise, break frequency, and roll-off, which are terms used to describe power spectra. The DC noise level is computed using the mean value of noise (the noise computed at the forcing function frequencies was not used in the mean) out to 0.5 rad/s. A best-fit line from approximately 2 to 20 rad/s defines the roll-off slope, and the intersection of these two lines' projections is defined to be the break point.
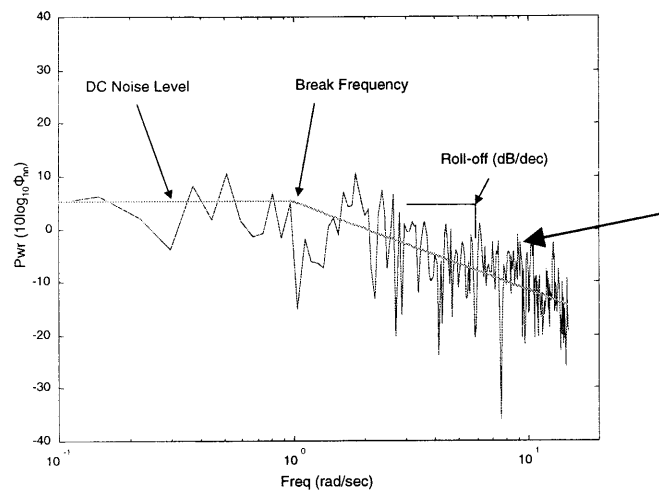
Figure 5.8. Example spectrum of observation noise.

Figure 5.9 shows DC observation noise normalized with the variance of the tracking error. The standard deviation of the normalized noise is generally very small. Except for the lowest sensitivity, normalized DC remnant appears to be invariant with display gain. The data also shows DC remnant to scale with the square of the tracking error (variance). Both of these results agree with previous work (Jex, 1969) - given the large differences between previous work and this study in the general nature of the tracking task, as well as in the complexity of the visual cues, this agreement is unexpected.
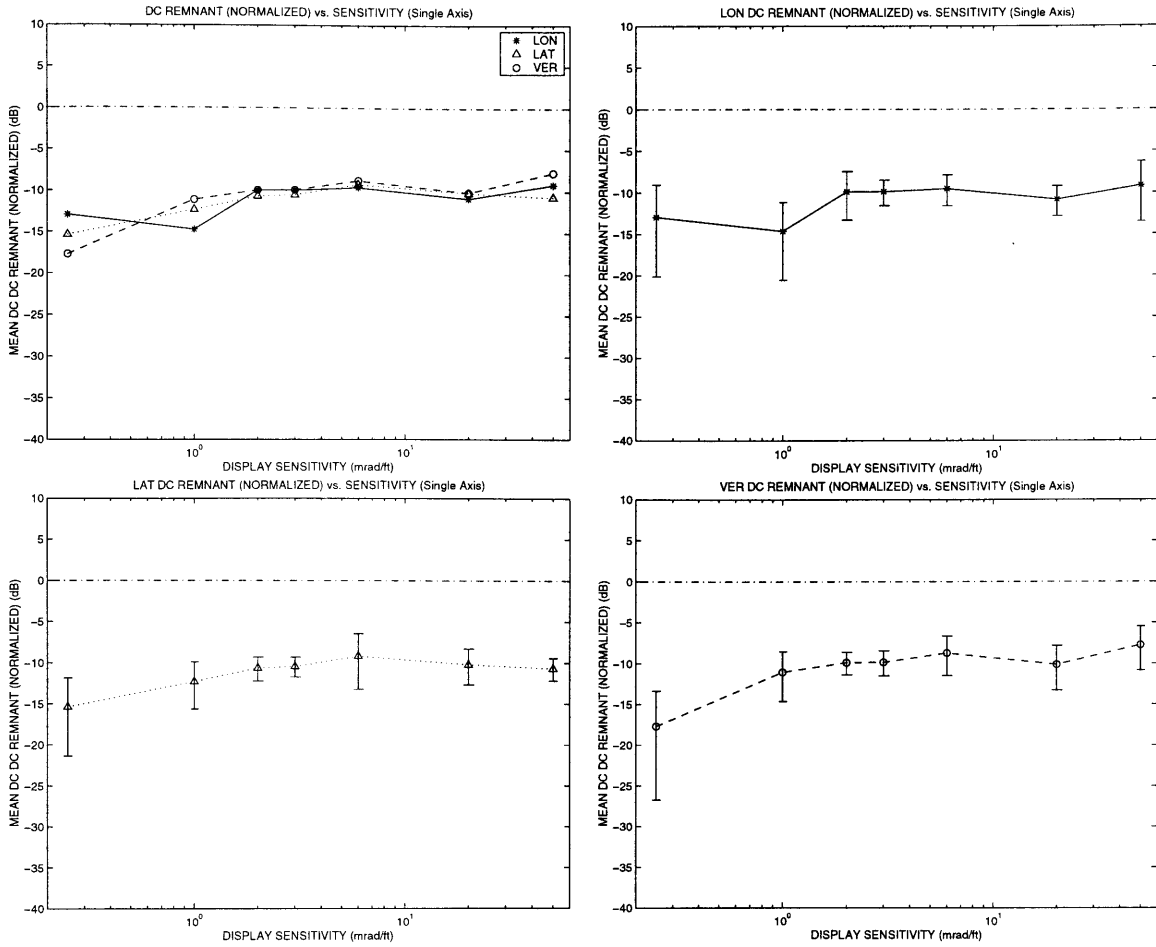
Figure 5.9. Normalized DC observation noise versus display sensitivity.

Figure 5.10 shows the break frequency of the observation noise generally to be invariant with display sensitivity. Prior studies showed the break to occur at approximately 3 rad/sec, slightly higher than the values observed in this experiment.
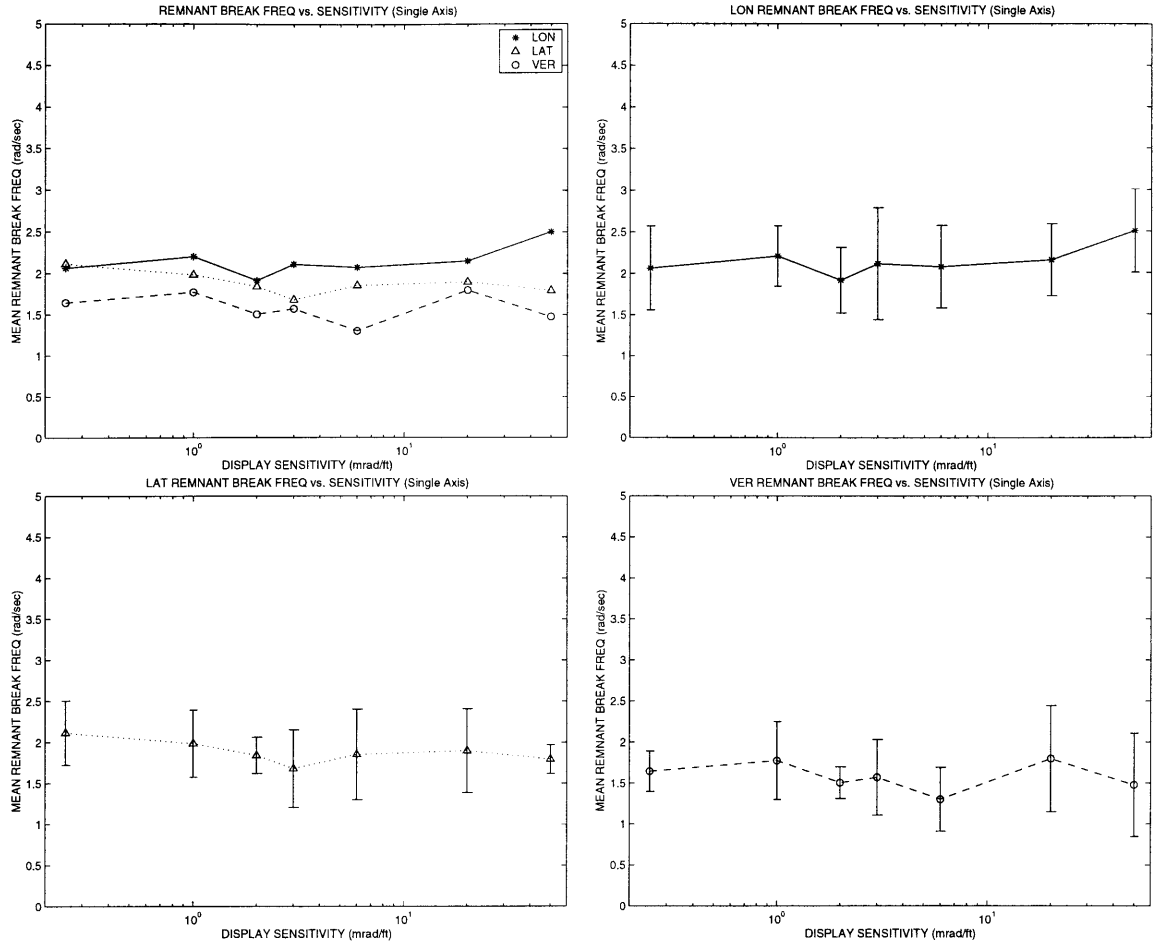
Figure 5.10. Break frequency of observation noise versus display sensitivity.

In Figure 5.11 the observation noise roll-off for the vertical axis appears to be less

steep than the other two axes.
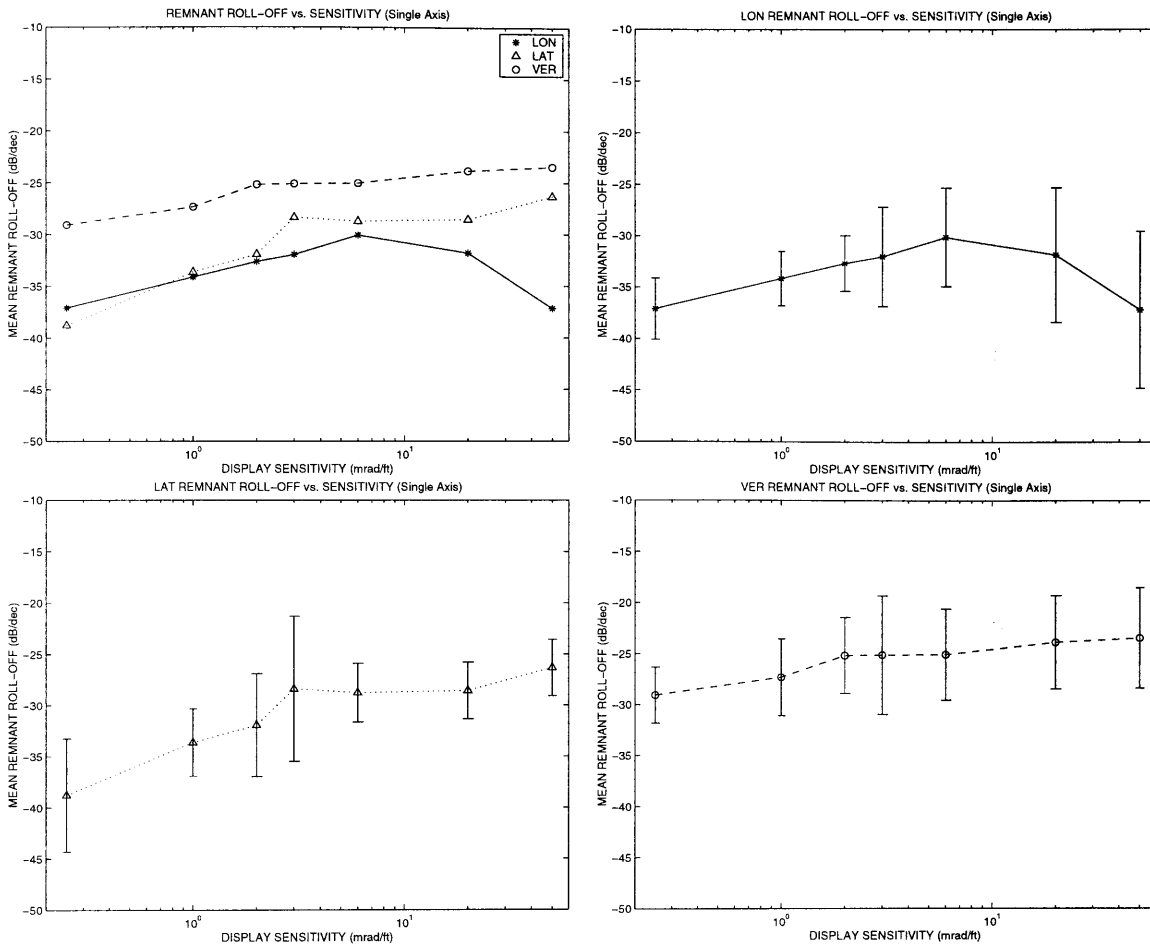
Figure 5.11. Observation noise roll-off versus display sensitivity.

Relative remnant is shown in Figure 5.12. The vertical axis appears to have higher remnant than the other axes for all display sensitivities. The lateral and longitudinal axes are very similar in remnant activity.
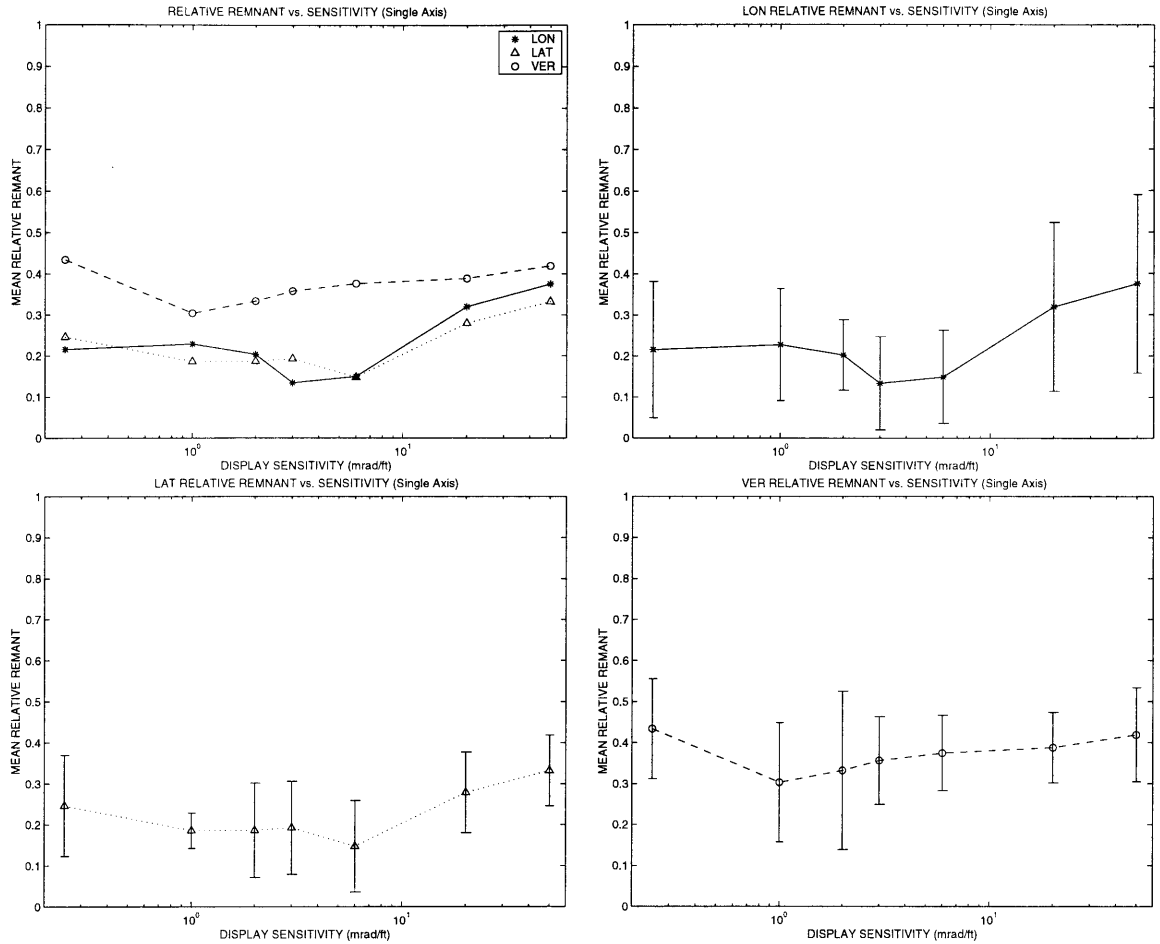
Figure 5.12. Relative remnant versus display sensitivity.

5.1.4   Discussion of Single Axis Results

5.1.4.1   Effect of Display Pixellization

To examine the effects caused by quantization of the displayed position error, an analysis of attenuation, time delay, and stability was conducted. The pixel width for the hardware used was 3 mrad, or 3.6 arcminutes. In Figure 5.13 the disturbance i is assumed to have a Gaussian distribution, and the open-loop element is assumed to have the form N/s (from the Crossover Model). The spectral function of the closed-loop transfer function can be written as a ratio of polynomials in s^2 (Brown, 1983), and this is used along with the relation between power spectral density and variance to identify N (Gelb, 1968), where N represents the gain attenuation associated with a uniform quantizer (stair-step function) of width 3 mrad.
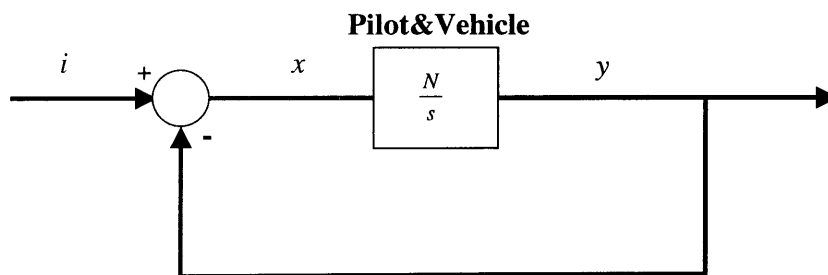
Figure 5.13. Block diagram representing closed-loop system.

Figure 5.14 shows that the effective system gain is reduced by approximately 50% when using a display sensitivity of .25 mrad/ft, and above 0.7 mrad/ft the attenuation is negligible.
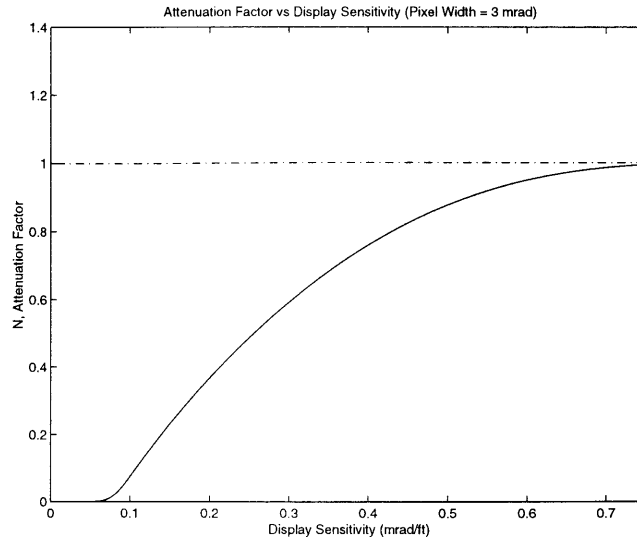
Figure 5.14. Effective gain attenuation as a function of display sensitivity.

The combined effect of display error quantization and time delay on tracking

performance is shown in Figure 5.15, where a pixel width of 3 mrad and time lags of .5, .7,

and .9 seconds were used. Modeling simulation was employed to generate the performance

plots, where the same input signals, pixel width, and vehicle dynamics were employed as

those in the experiment. The time lags and crossover frequencies were inserted into the

Crossover Model to model the pilot. Normalizing the crossover frequency with the time lag

shows that all three time lags yield the same phase margin at the point when mean squared

error begins to build with increasing crossover. Note this occurs well before the minimum

RMS error and dynamic stability limit of $\pi/2$ that would be applicable if the power spectrum

of the forcing function were rectangular. The reason for the decreased performance in

Figure 5.15 is the presence of remnant created by quantization. From Figure 5.15 it can be

seen that time delay does not influence the magnitude of remnant.
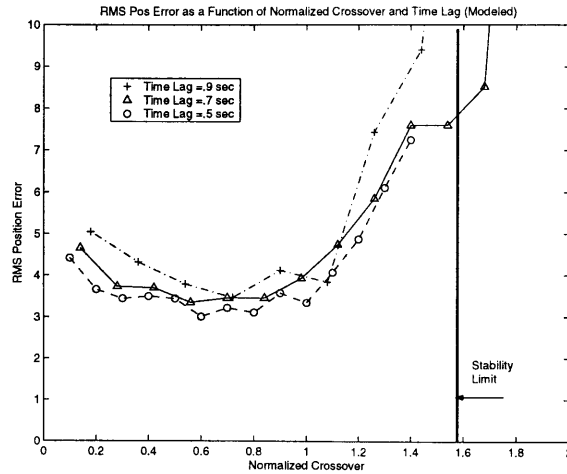
Figure 5.15. Effect of pilot time delay on stability (pixel width = 3 mrad)

Figures 5.15 and 5.16 show the dynamic effect (again using modeling simulation)

of varying pilot time delay and display sensitivity, where the time delays used were

approximately those observed in the experiment. In Figure 5.16 pixel width is seen to

have a significant effect on minimum tracking error only at the lowest sensitivity of .25

mrad/ft (as was predicted in Figure 5.14) - at 1 mrad/ft and above, the minimum RMS

position errors are essentially identical. Decreasing time delay is seen to increase the

maximum crossover.
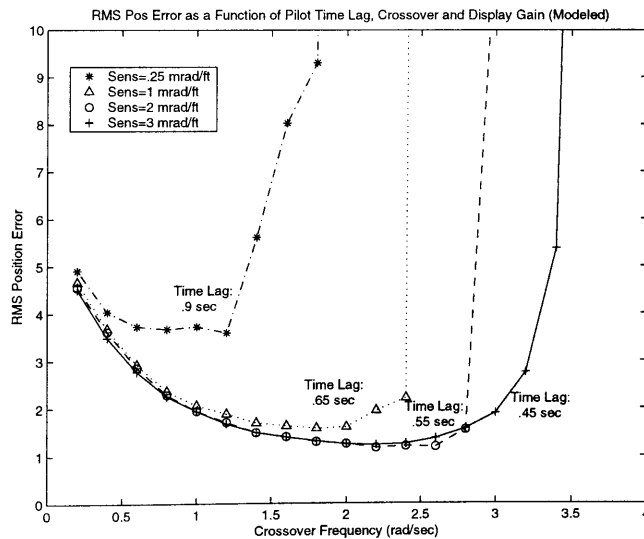
Figure 5.16. Effect of time delay, display sensitivity and crossover on performance
(pixel width = 3 mrad).

100

The effect of remnant originating from the pilot (i.e., apart from quantization effects) in Figure 5.15 would be to shift the crossover frequency for minimum error toward the left (which in turn would raise phase margin in order for real stability margin to exist) and would also increase minimum performance error. From Figure 5.17 we see that display sensitivities of 1 mrad/ft and above yield approximately equivalent minimum-error normalized crossover frequencies.
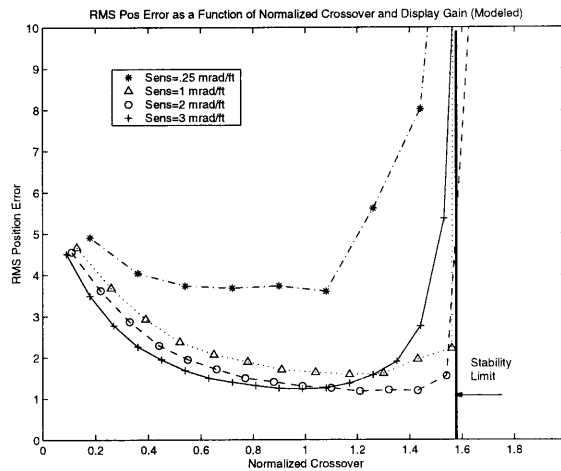
Figure 5.17. Effect of time delay and display sensitivity on stability (pixel width = 3 mrad).

For a given display sensitivity, the spatial displacement between pixel jumps (3 mrad) will correspond to an incremental length of time that varies over the length of the error signal. An average time increment can be computed and halved to yield a mean 'pixel delay' associated with the quantization of the display error. This mean pixel delay decreases linearly with increasing sensitivity for display gains of 1 mrad/ft and higher. At 1 mrad/ft, the mean pixel delay is approximately .66 sec, and .33 sec for a display gain of 2 mrad/ft. If these pixel time delays contribute to total effective time delay then minimum-error crossover should increase with display gain, since the time delay used to normalize crossover is strictly the time lag computed by cross-correlating position error

101

with stick. A difference in minimum-error crossover of approximately 0.5 (normalized crossover) should be seen in going from a display gain of 1 mrad/ft to 2 mrad/ft. However, Figure 5.18 shows minimum-error crossover to be independent of sensitivity at 1 mrad/ft and above. From this it is concluded that the only kind of time delay that affects instability is the one that can be measured through cross-correlation – quantization affects control response only in magnitude.

5.1.4.2 Interpretation of Single-Axis Performance and Frequency Domain Results

Two factors that determine the upper limit on pilot gain are time delay and remnant. Time delay establishes the maximum crossover frequency will for a time delay-normalized crossover stability limit of $\pi/2$. The effect of remnant is to shift the maximum open-loop crossover for minimum error to lower frequencies, and to increase tracking error. Two factors that appear to influence pilot time delay are perceptual threshold (which include display quantization effects), and task demands (which affect neuromuscular tightening). The data suggests that perceptual effects manifest themselves at the lowest display gains in the form of heightened time delay sensitivity to changes in display gain, as compared to lower time delay sensitivity due to task demands. Display quantization and perceptual threshold is thus believed to account for the low crossover frequencies seen at the display gain of 0.25 mrad/ft, after which perceptual thresholding accounts for crossover increasing monotonically until 3 mrad/ft. Because of low pilot gain and large time lag associated with the lower display gains, tracking performance is correspondingly poor. System modeling in Figure 5.15 shows that as crossover is increased, performance improves and then stabilizes over a limited region. This behavior was observed in the experimental results, where performance stabilized at a gain of

102

approximately 3 mrad/ft corresponding to a crossover of about 1.4 rad/sec. Time delay sensitivity to display gain for all three axes also appears to lessen near a display gain of 3 mrad/ft, which would indicate that above this gain perception does not improve appreciably.

The point at which error perception stabilizes is where the Crossover Model rule of tracking error and crossover frequency invariance would be expected to apply. In the lateral and vertical axes error performance was approximately steady for display gains ranging from 3 to 50 mrad/ft. However, in the longitudinal axis cue motion saturation began to occur at 20 mrad/ft, and became more prominent at 50 mrad/ft. Saturation degrades tracking error performance most notably at higher crossover frequencies, and this is believed to be the reason for the increase in longitudinal tracking standard deviation at the two highest display gains.

For the lateral and longitudinal axes, crossover appeared to stabilize from 3 to 6 mrad/ft, but then resumed increasing with display gain, whereas the vertical axis exhibited monotonic crossover growth with display gain. Both position and position rate were subject to the same display gains; however, attitude (pitch and roll) remained at a fixed gain for all display sensitivities. In actual helicopter hover, attitude control is given more attention than the outer velocity and position loops since attitude closure determines the stability of the outer loops. It is therefore reasonable to assume that, the lateral and longitudinal axes in this experiment used attitude as the primary inner-loop state (which for the dynamics used was also a surrogate state for position rate). When error perception stabilized at a gain of 3 mrad/ft, it is conjectured that the pilot was able to maintain constant crossover from 3 to 6 mrad/ft of display gain by maintaining constant inner-loop (attitude) gain and halving his outer-loop (position) gain. Beyond 6 mrad/ft the velocity

cues were so compelling due to rapid, large amplitude motion that they likely replaced attitude as the inner-loop control state. Since the inner-loop state was no longer independent of display gain at this point it appears that the pilot's inner-loop gain was driven by the increasing position rate gain, which raised open-loop crossover. This appears to be supported by the monotonic increase in crossover with display gain for the vertical axis, where throughout operation the only inner-loop control state available was position rate.

An effect of saturation is to reduce crossover frequency since the pilot's response at the forcing function frequencies is effectively reduced. This likely accounts for why longitudinal crossover did not rise in the same manner as the lateral axis at gains of 20 and 50 mrad/ft – the lateral axis experienced no saturation at these display gains.

Most of the experiments that were used in the development of the Crossover Model involved attitude-like tracking tasks, where primarily one control loop was closed. From the data presented in §5.1.1--§5.1.3 it appears that the crossover and error invariance rule may still hold for multi-loop tasks, where the inner-loop display gains are constant. However, when the inner-loop gain is varied, pilot inner-loop gain will follow, raising open-loop crossover. This may or may not incur a change in tracking performance, depending on cue saturation and pilot workload.

Of course, in the experiments presented here the task is not single loop attitude control, but multi-loop control of position. The overall key result is that the inner loop is closed such that position error is kept almost constant over a very broad range of display gains.

The normalized DC noise was comparable to levels found with previous work (Jex: 1969, Levison: 1968). These previous experiments generally used a stationary line

or reference point with a moving line or reference point as a target, whereas the patterns observed by the pilot here were considerably more complex, so that the general agreement in DC noise between the two is perhaps surprising. Past results indicated a break point of approximately 3 rad/s for tasks not requiring lead, and the break point observed in these results tended to be in the region of 2 rad/s for all axes. Noise roll-off was generally steeper than the -20 dB/dec observed in past studies. Normalizing the DC noise with the system error variance resulted in very low standard deviation and relative invariance with display sensitivity, agreeing with the previous studies.

Finally, the Crossover Model appears to be an appropriate model for this single axis tracking task. Amplitude ratio slope agreed closely with the model's predicted –20 dB/dec slope, and modeled tracking error using measured parameters (time delay, cross-over) in the Crossover Model closely matched actual tracking error (see Figures 5.1, 5.4 and 5.15).

5.1.4.3   Interpretation of Single-Axis Subjective Ratings

At low display gains only the large amplitude/low frequency components of the disturbance signal are perceived, and are acted upon with relative ease (especially given that the pilot compensation in this experiment was essentially pure-gain). This is given evidence by the Level 1 Cooper Harper ratings at low display gains for all axes. Increased display gain magnifies and makes perceptible the high frequency disturbance content that the pilot attempts to track. After 3 mrad/ft the ratings sharply rose in the longitudinal axis, and rose more gradually in the lateral and vertical axes. The subjective scores showed that longitudinal station-keeping is clearly perceived by the pilots to be a more difficult task than the other two axes for display sensitivities greater than 3 mrad/ft.

Transverse motion with this display shifts cues parallel the direction of the error. It appears that the radial, symmetric expansion or contraction of the display cues that accompany longitudinal motion are controlled with more effort.

Finally, based on the subjective scores and tracking performance, it appears that an optimum display sensitivity in the vicinity of 3 mrad/ft is shared by all three axes for the single axis tracking task used in this experiment. The location of this optimum point could be expected to be most influenced by factors affecting pilot time delay (or error perception) at the low end of display gain. For example, if the task were conducted in an actual helicopter or a full motion simulator, vestibular feedback would reduce the pilot reaction times. This in turn would allow for higher crossover at lower display gain, thus shifting the optimum point toward a lower gain. On the other hand, any increase in time delay originating from sensors, display, vehicle, or pilot would increase optimum display sensitivity.

5.2 The Effect of Display Motion Gain on Multi-Axis Station-Keeping

The objective of this experiment was to observe pilot response to display motion gain using the Synthetic Cue display when attention is simultaneously divided among the three axes of translation to regulate helicopter position. These results will be compared later with the baseline pilot response when full attention was devoted to regulating helicopter position along single axes of translation.

5.2.1 Time Domain Data

Figure 5.18 shows RMS station-keeping error data for all seven subjects as a function of display sensitivity for each of the axes of translation. Display sensitivities were 0.25, 1, 2, 3, 6, 20 and 50 milliradians/foot. The mean data show decreasing error in all three axes with increasing sensitivity until a collective minimum is reached near 3 mrad/ft. Figure 5.19 shows total RMS position error (root square sum of each axis' error) at a minimum at 3 mrad/ft gain. This multi-axis minimum also corresponds with the single axis mimima found for the three axes. Longitudinal error rapidly increases beyond 6 mrad/ft sensitivity.

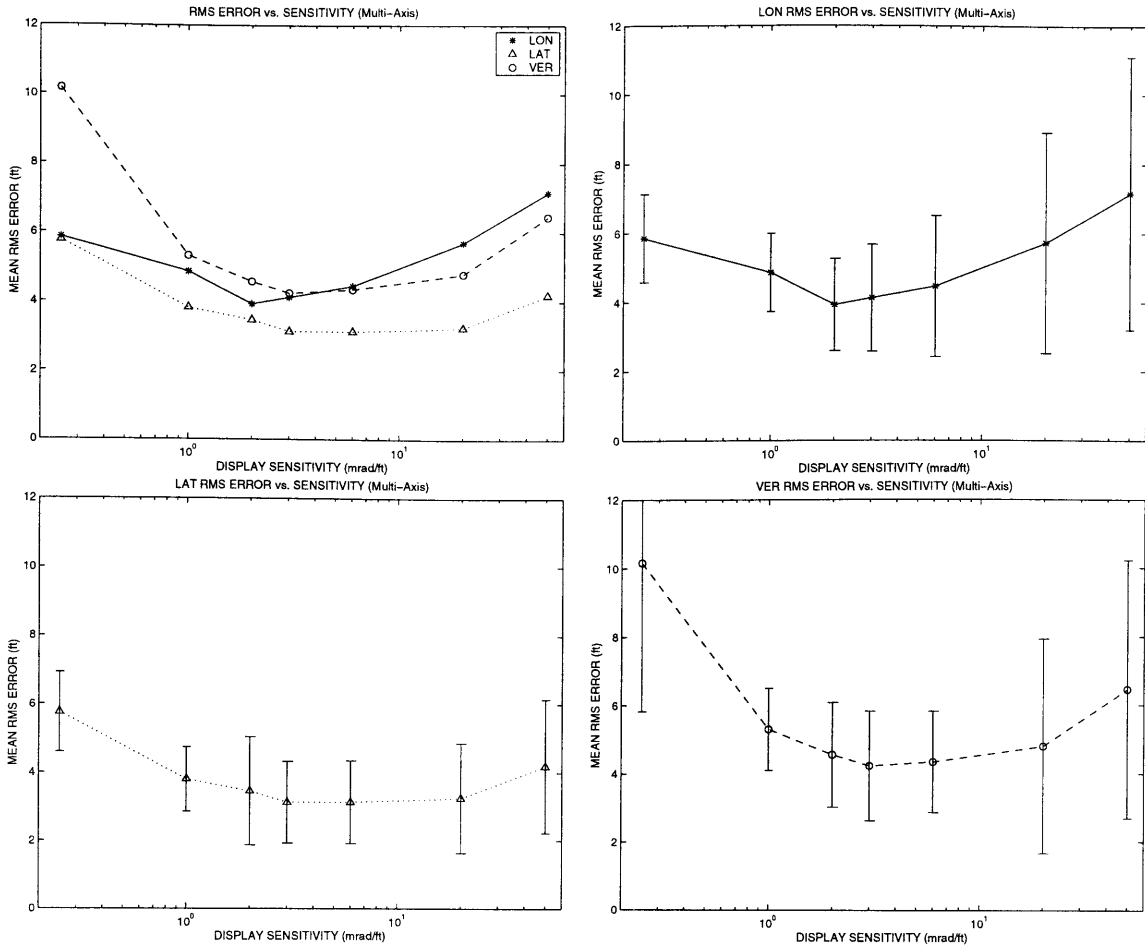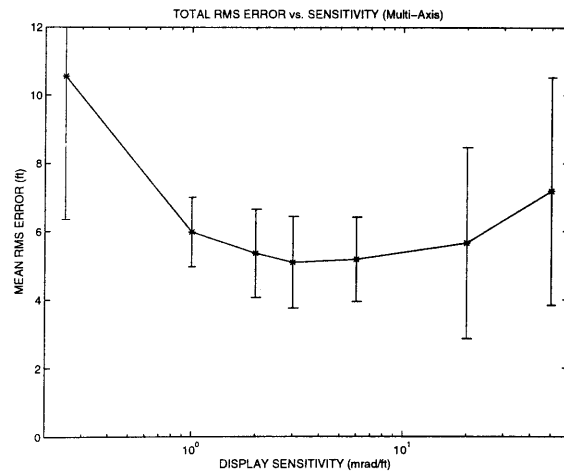**Figure 5.18. Position RMS error versus display sensitivity.**

Figure 5.19. Total position RMS error versus display sensitivity.

108

Pilot time delay is shown in Figure 5.20. There appears to be a general transition in slope in the vicinity of 2 mrad/ft. When compared with single-axis results, multi-axis seems to increase pilot time delay by 50%.
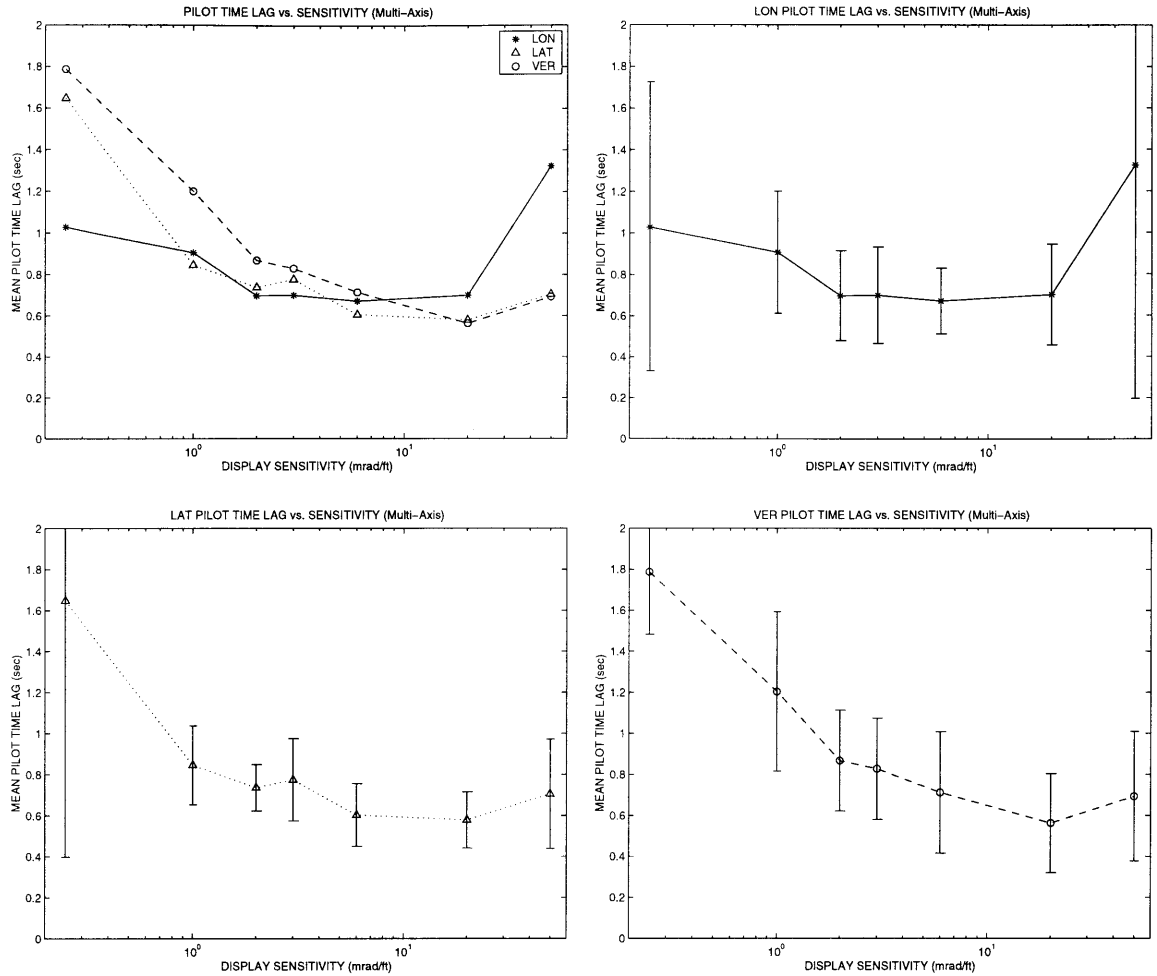
Figure 5.20. Pilot time delay versus display sensitivity.

Figure 5.21 shows that all three axes exhibit saturation at 20 mrad/ft.
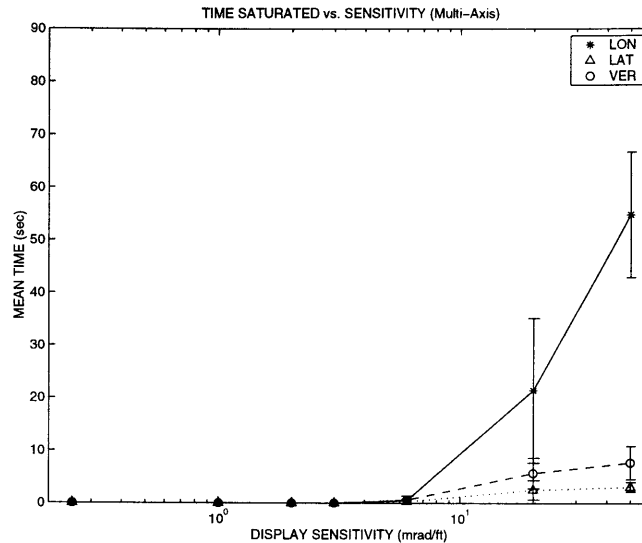
Figure 5.21. Operating times for when cue motion was saturated (90-second total run time).

The forcing function frequencies were slightly different between axes so that the position disturbance RMS would be nearly equivalent across axes. However, one frequency was kept significantly different in the longitudinal axis from the lateral and vertical to allow for measurement of cross-axis coupling at a forcing function frequency. In Figure 5.22 the ratio of pilot response magnitude between primary axes and cross axis is shown. In general, there is little cross-coupling except at display gains of .25 and 6 mrad/ft for the longitudinal axes. Note that the minimum cross-coupling for all axes appears to occur at the optimum display sensitivity of 3 mrad/ft.
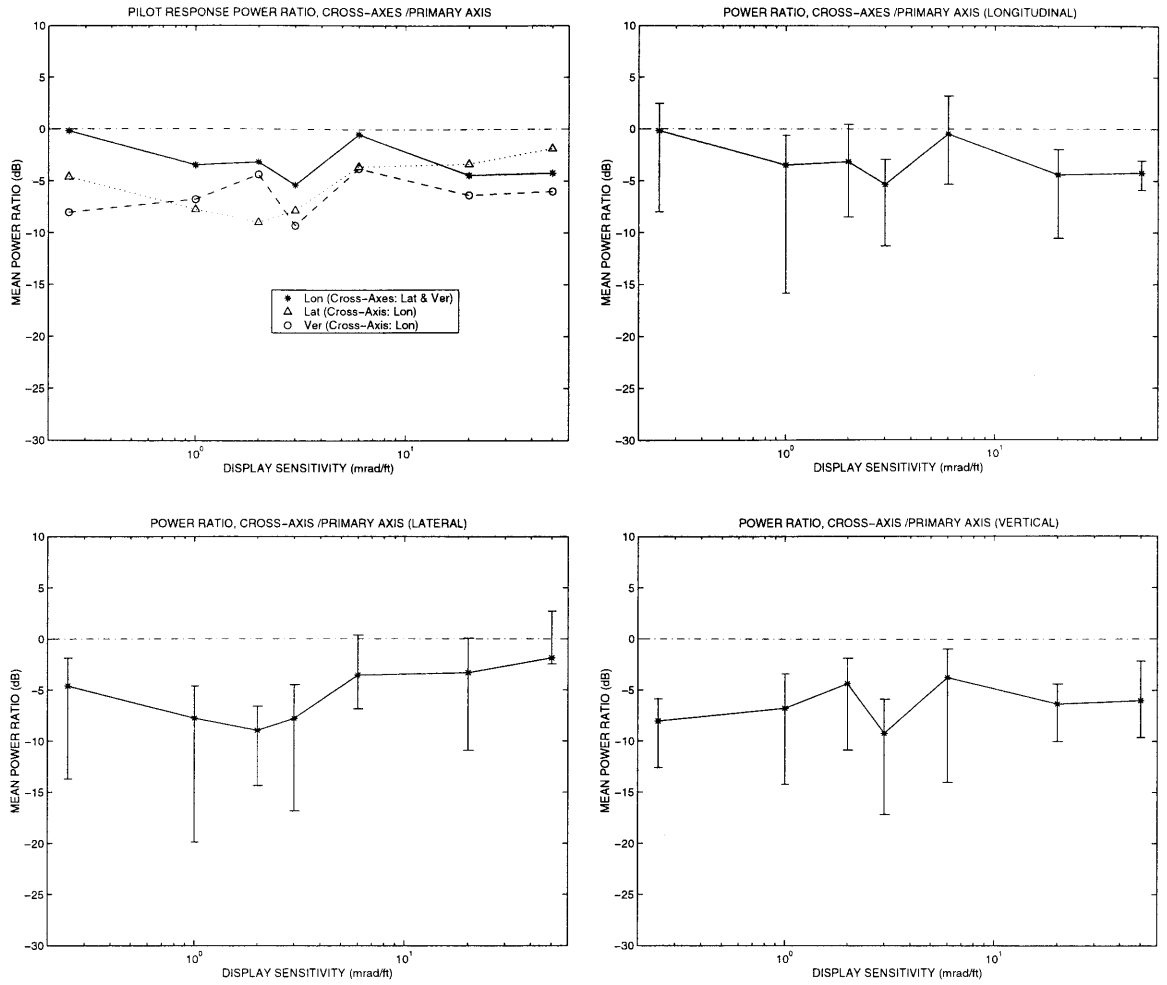
Figure 5.22. Cross-axis coupling versus display sensitivity.

111

5.2.2 Subjective Scores

The Cooper-Harper ratings for aircraft/display handling qualities are presented in Figure 5.23. The ratings are stable from 2 to 6 mrad/ft (this region includes the single-axis optimal gain), followed by a rapid worsening. Note ratings are higher in the 2-6 mrad/ft region than the single axis ratings by about 1 point. From the multi-axis subjective and performance results, it appears that the optimum display gain is also in the vicinity of 3 mrad/ft.
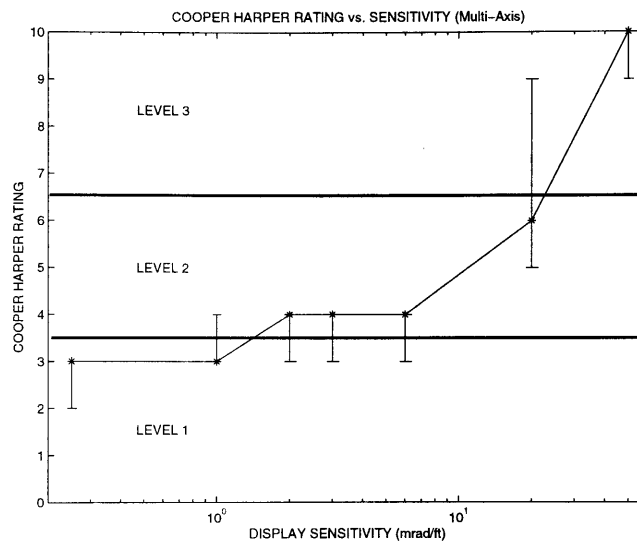
Figure 5.23. Subjective rating versus display sensitivity.

5.2.3   Frequency Domain Data

Figure 5.24 shows crossover frequency increasing with sensitivity in all three axes

until 6 mrad/ft. The vertical axis seems to have the highest crossover, with the

longitudinal axis having the lowest. At the highest sensitivity of 50 mrad/ft, there

appears to be a reduction in crossover for the lateral and longitudinal axes. Single axis

crossover was higher for all display sensitivities than for multi-axis operation, as

expected.
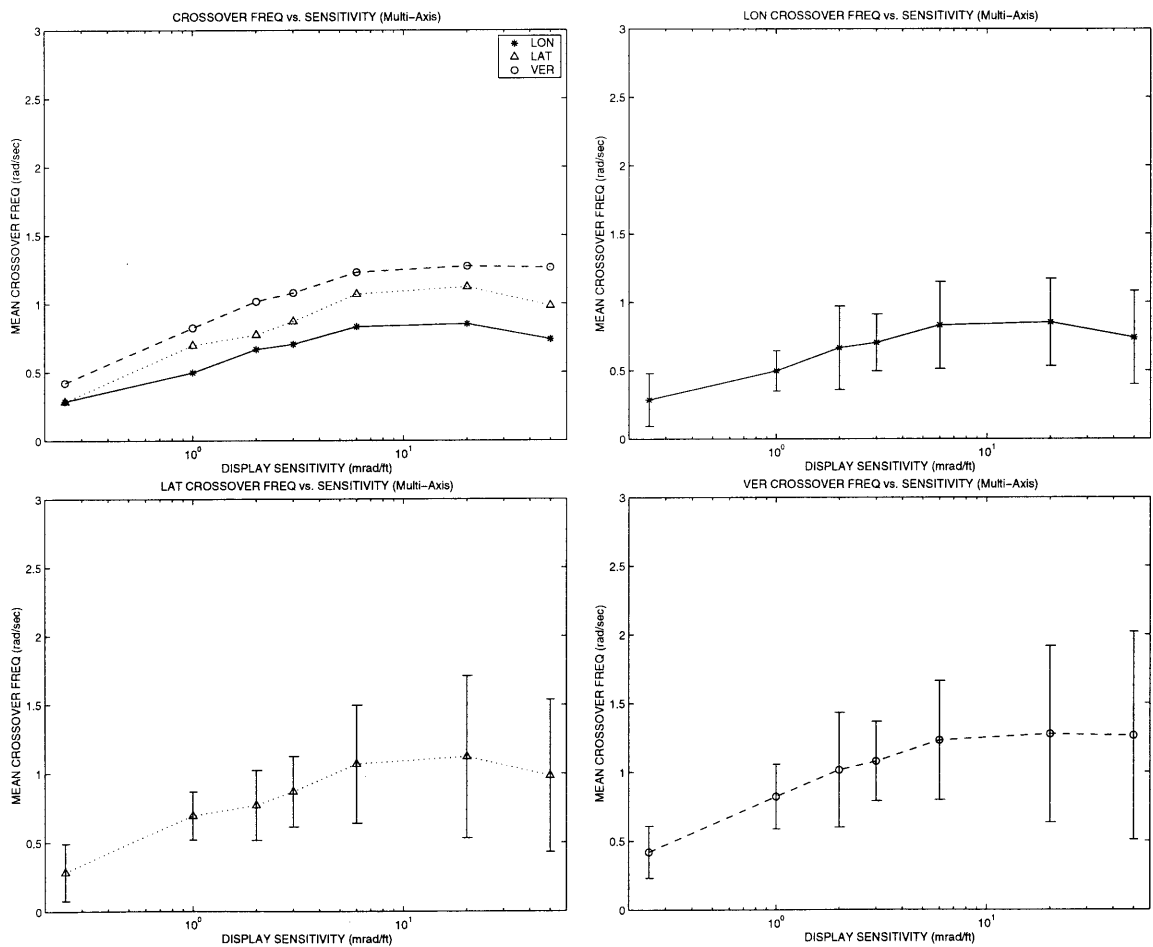
Figure 5.24. Crossover frequency versus display sensitivity.

In Figure 5.25 the phase margin for the longitudinal axis appears to be greatest for all but the highest display sensitivity, while the vertical axis seems to have the lowest phase margin. Comparison of multi with single axis operation shows the standard deviation for multi-axis to be very large, implying a high degree of fluctuation in attention between axes.
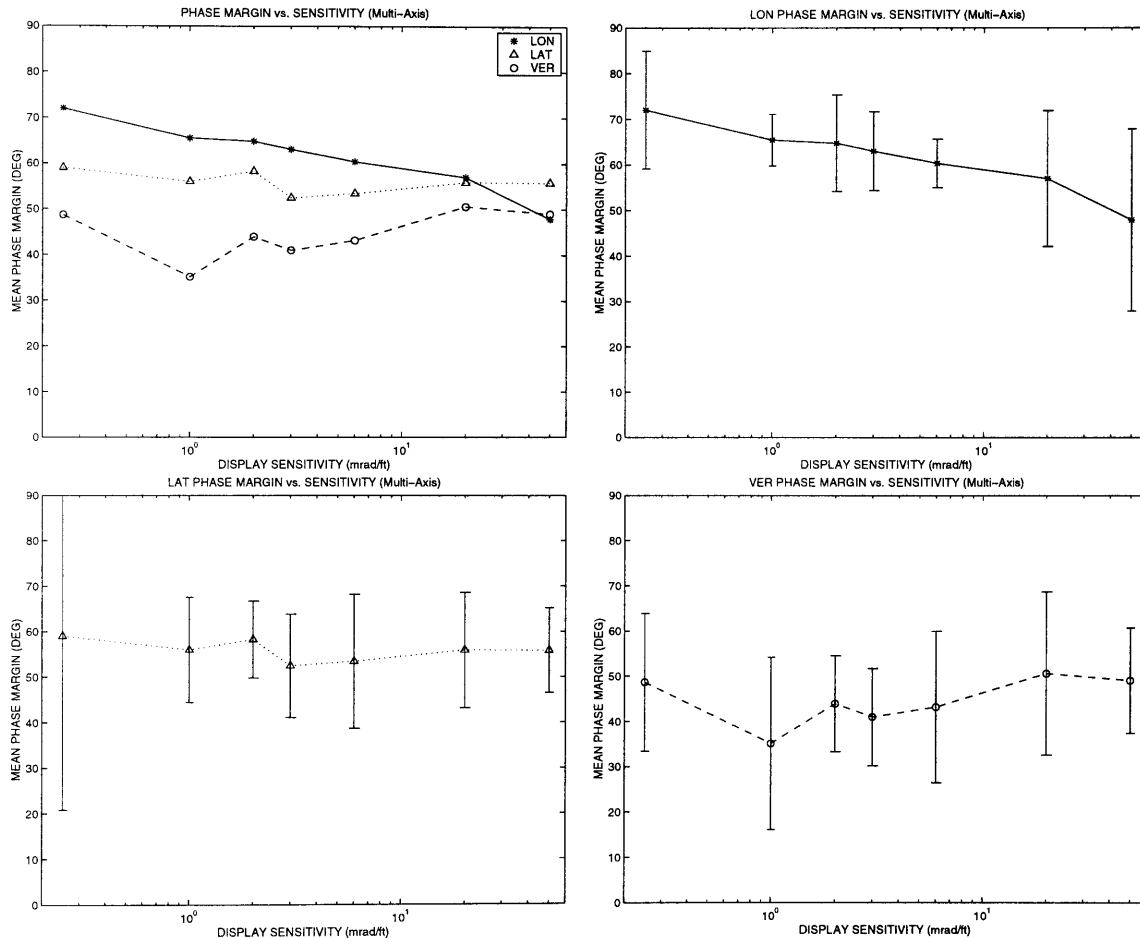
Figure 5.25. Phase margin versus display sensitivity.

In Figure 5.26 the amplitude ratio slope for all axes tends to steepen until

approximately 3 mrad/ft, after which the slope is seen to flatten toward –20 dB/dec.

These slopes exhibit greater departures from the Crossover Model than was observed in

the single axis results, with the greatest departure (-26 to –30 dB/dec) occurring at the

optimum display gain.
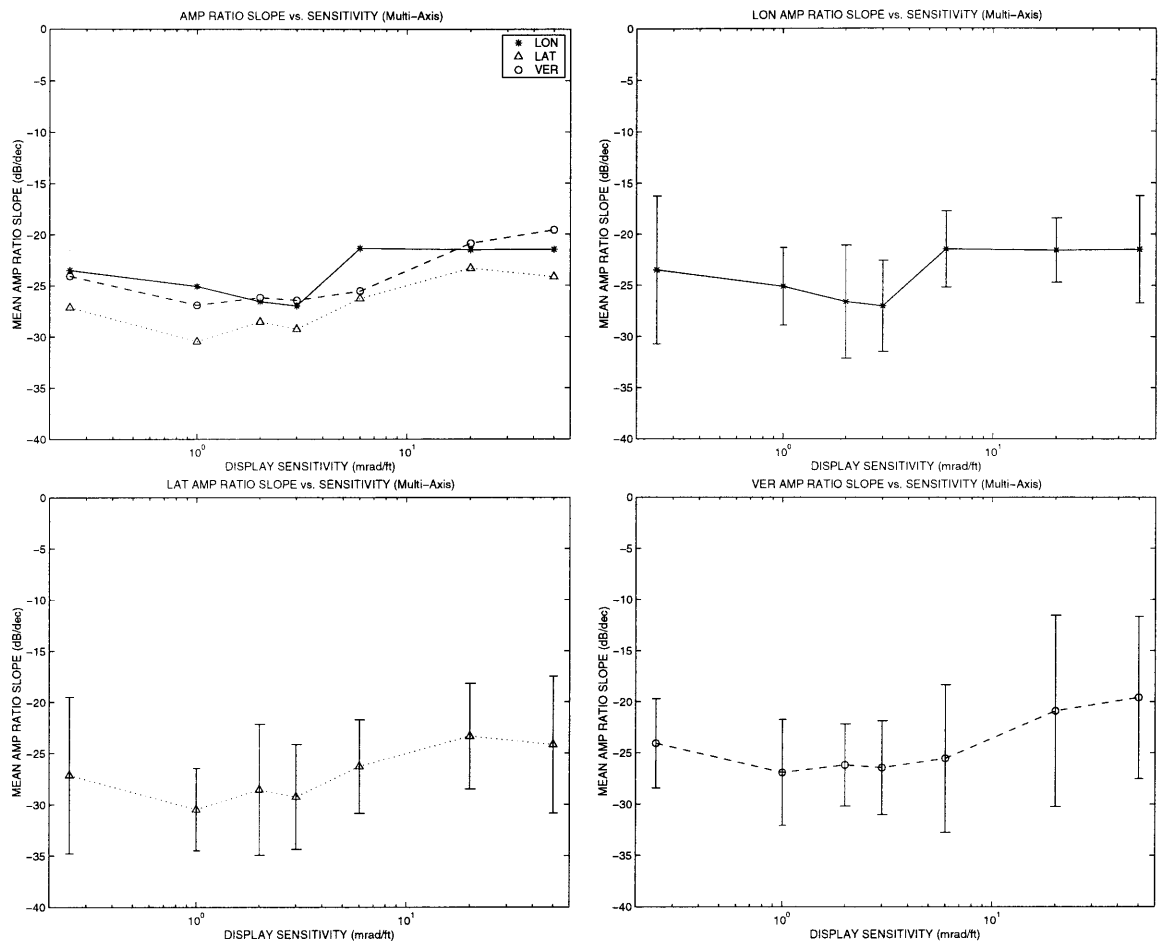
Figure 5.26. Amplitude ratio slope versus display sensitivity.

In Figure 5.27 the multi-axis normalized noise is comparable to the single axis cases,

indicating that low frequency relative remnant does not increase for multi-axis operation.
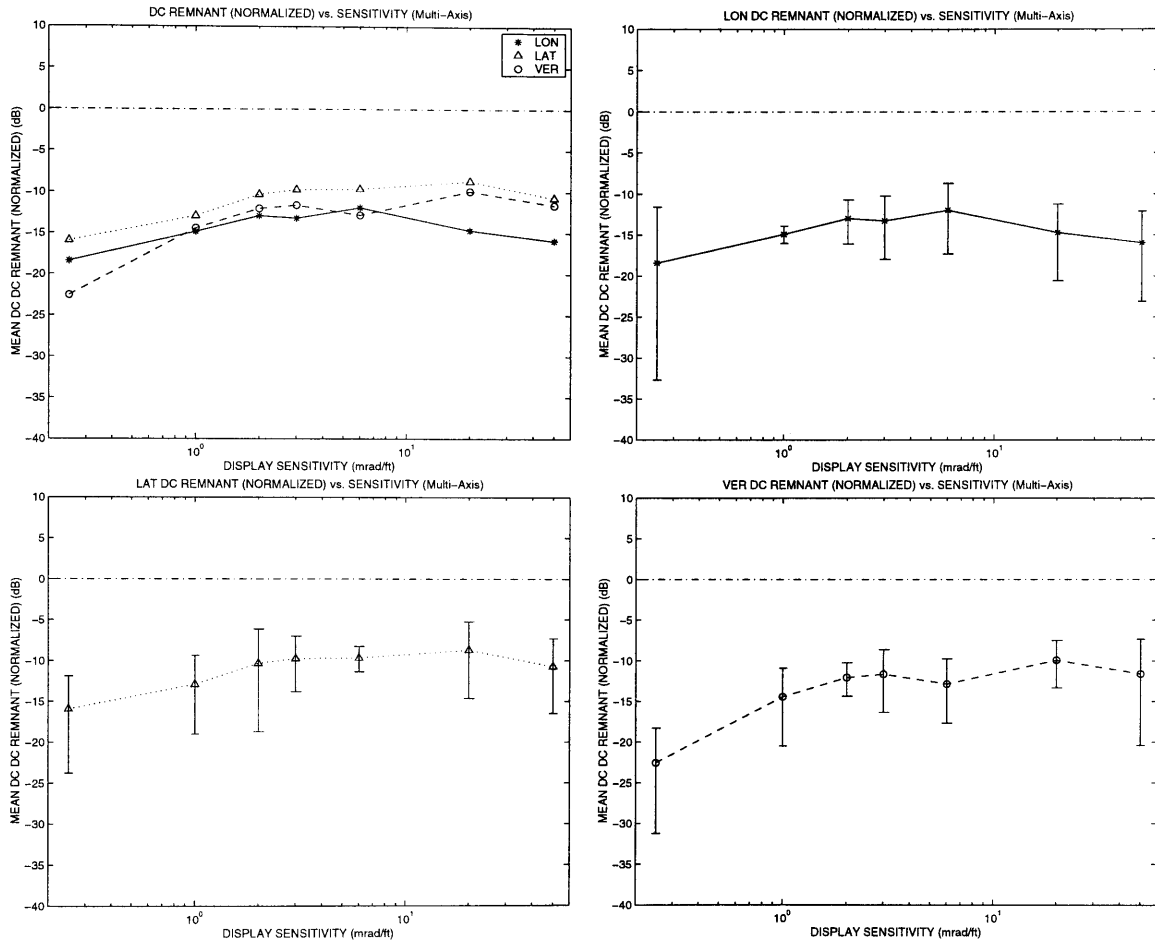
Figure 5.27. Normalized DC observation noise versus display sensitivity.

116

In Figure 5.28 the observation noise break frequencies appear to be relatively

invariant with display sensitivity, as was seen with single axis operation.
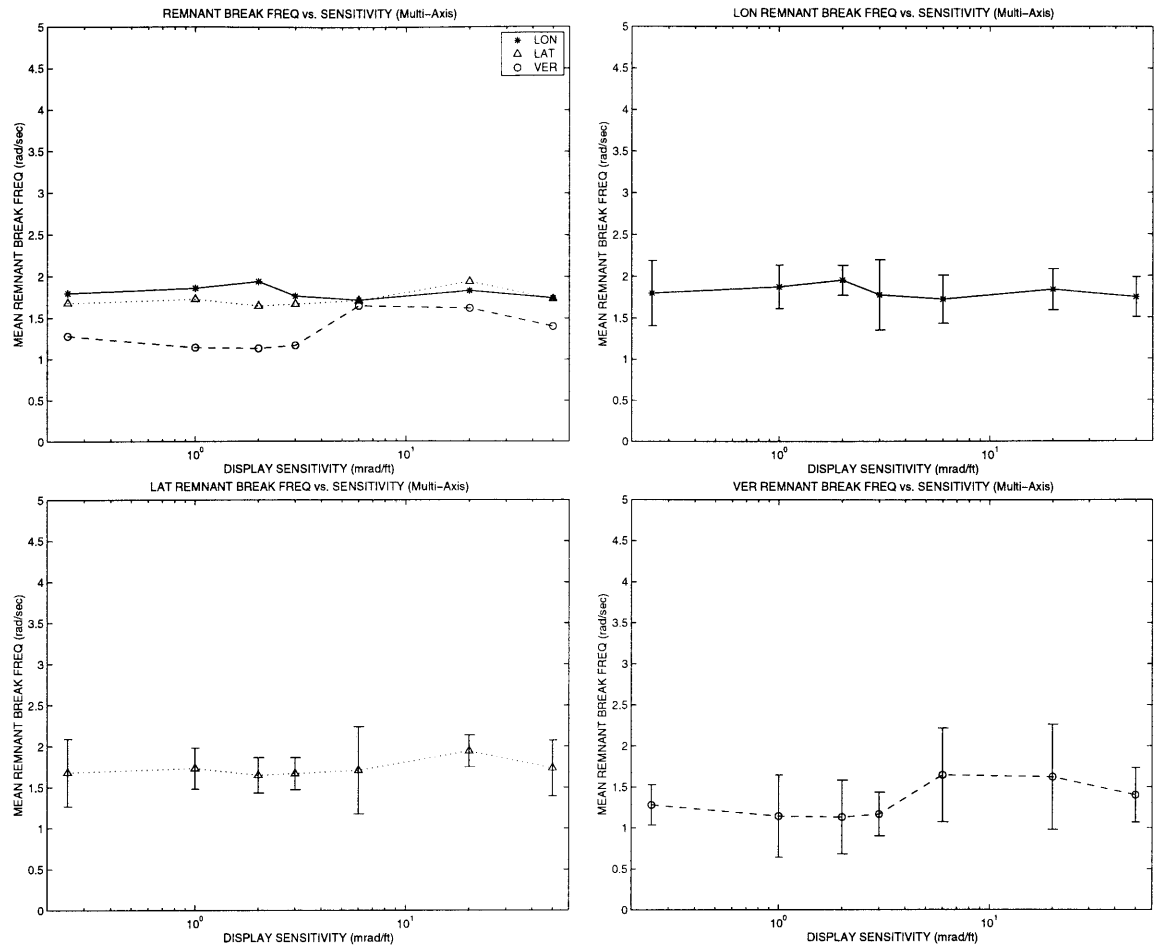
Figure 5.28. Break frequency of observation noise versus display sensitivity.

Figure 5.29 shows the high frequency slope of the observation noise to be

generally less steep for the vertical axis than the lateral and longitudinal. Roll-off

appears relatively invariant with display gain, except for an increase in steepness in the

vertical at 3 mrad/ft.
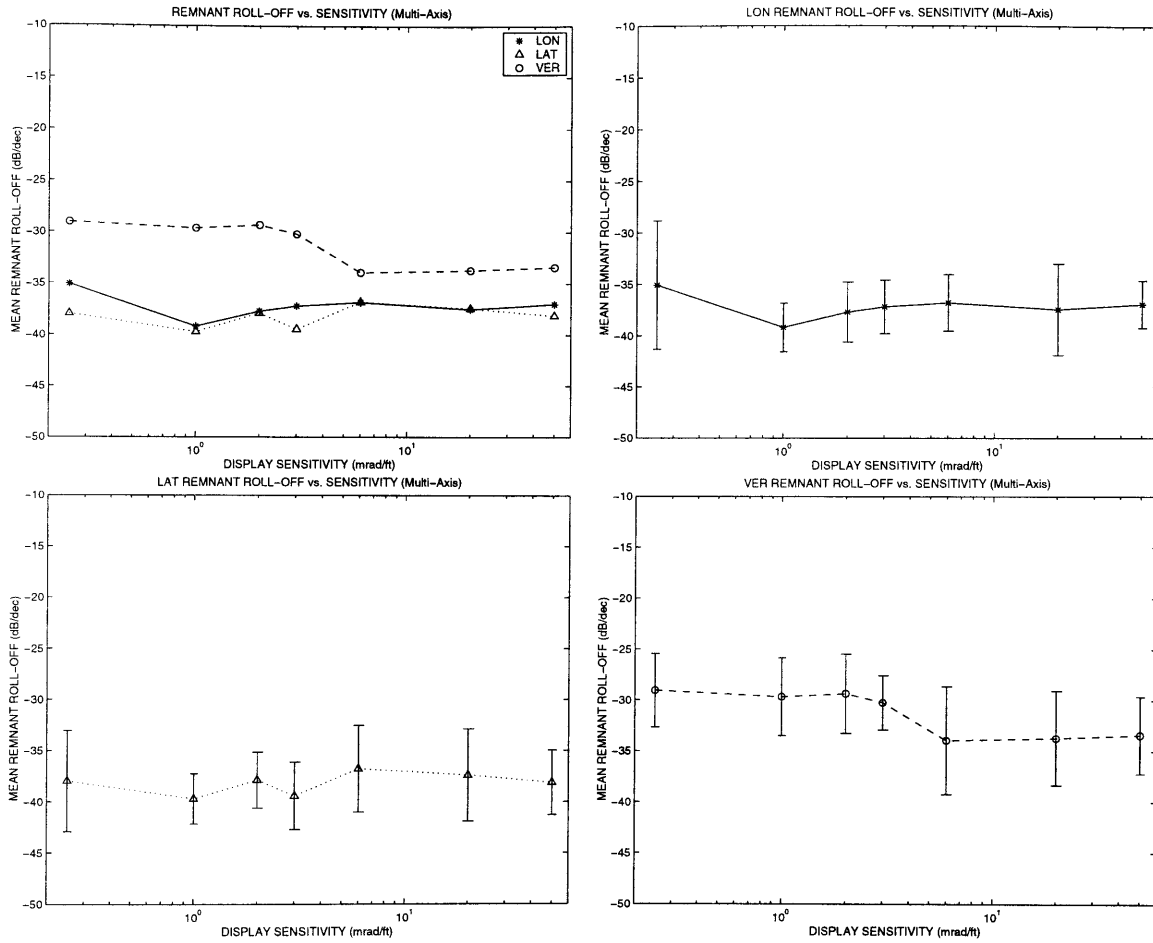
Figure 5.29. High frequency slope of observation noise versus display sensitivity.

Relative remnant is shown in Figure 5.30. As with the single axis results, the vertical axis here appears to have higher remnant for all display sensitivities than the other axes. The lateral and longitudinal axes are generally similar in remnant activity.
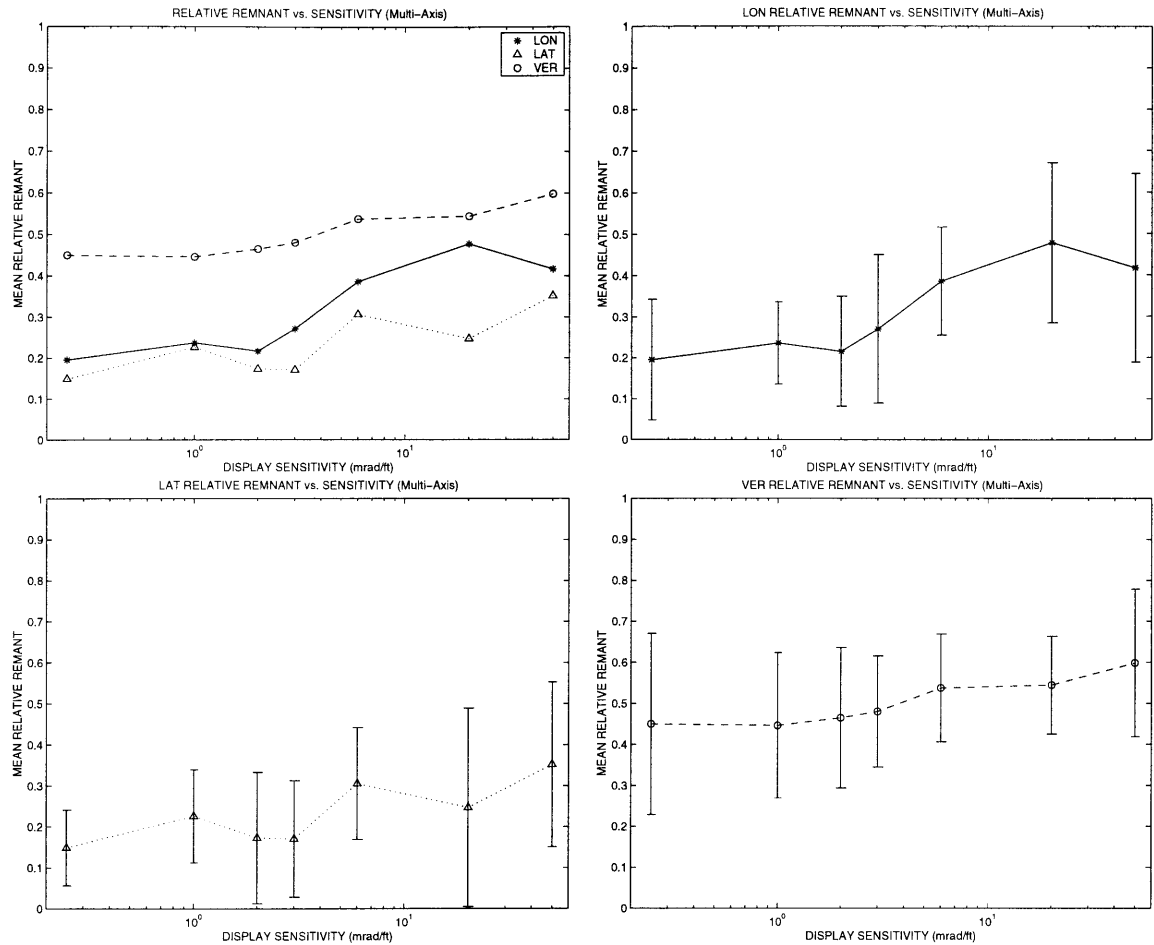
Figure 5.30. Relative remnant versus display sensitivity.

5.2.4 Discussion of Multi-Axis Results

5.2.4.1 Interpretation of Multi-Axis Performance and Frequency Domain Results

As was previously observed in the single-axis results, two factors appear to be influencing pilot time delay: (1) perceptual threshold (which includes display quantization effects), and (2) task demands (which affect neuromuscular tightening). The data suggests that perceptual thresholding has an effect until a display gain of 2 mrad/ft, after which changes in time delay are largely due to task demand. At the highest display gain time delay appeared to increase for all axes, which indicates that time delay may be subject to the U-shaped behavior that is normally seen with performance with increasing task demands.

Comparison with the single axis cases suggests that division of attention can have profound effects on time delay. Previous work on scanning (Clement, 1971) found that performing a foveally viewed tracking task simultaneous with a parafoveally viewed tracking task had the effect of increasing remnant (compared with the single foveal task) and reducing loop gain, without producing time delay increases. However, placing three control tasks in the foveal vision appears to introduce increased processing delays on all three tasks as seen in this experiment. For all three axes crossover reached a maximum at a display gain 6 mrad/ft, although tracking error continued to increase beyond that gain. At the highest display gain, a combination of saturation and increased time delay most likely contributed to a marked decrease in tracking performance. Single axis operation showed virtually no performance degradation due to saturation, however divided attention in combination with saturation is seen to have a dramatic effect.

120

Despite appearing to have a higher crossover at all display gains, the vertical axis yielded performance that was consistently worse than the lateral axis, indicating higher remnant in the vertical. However, the vertical phase margin is lower than the lateral, which in turn suggests that the actual stability margin of the vertical axis is even lower than the phase margins indicate. This is believed to be a consequence of the velocity cues (which have the same gains as the position cues) driving the pilot's inner-loop gain higher than the inner-loop gains of the lateral and longitudinal axes, which probably relied on the constant-gain attitude cues.

Looking at the subjective scores, amplitude ratio slopes, and crossover frequencies, the region between 3 and 6 mrad/ft appears to be a transition region. At the lowest display sensitivity crossover frequency is approximately .4 rad/sec and remnant break frequency is approximately 1.5 rad/sec. As crossover increases with display sensitivity, noise (remnant) that is generated by the pilot will be amplified and will increasingly affect performance. One way the pilot can attenuate the effects of noise in this situation is to decrease (make more negative) the amplitude ratio slope so that noise beyond the crossover frequency is more rapidly attenuated. Decreasing this slope will reduce phase margin stability (McRuer, 1973), but at low sensitivities stability is not an issue. From 1 to 3 mrad/ft the slopes are significantly steeper than −20 dB/dec, but at 6 mrad/ft all axes have reached their maximum crossover. Remnant and time delay reduce stability thus limiting crossover to low frequencies, and at 6 mrad/ft noise attenuation appears to be traded for stability as there is a general decrease in amplitude ratio slope.

Thus it is proposed that the strategy adopted by the pilot for low display sensitivities for multi-axis control is one of noise suppression, whereas the transition point from 3 to 6 mrad/ft marks a shift in strategy toward stability preservation.

5.2.4.2   Interpretation of Multi-Axis Subjective Ratings

At 3 mrad/ft the Cooper-Harper ratings for multi-axis operation were higher than the single axis ratings by about 1 point, indicating, as expected, that multi-axis control was perceived as more difficult. Based on the subjective scores and tracking performance, it appears that an optimum display sensitivity is in the vicinity of 3 mrad/ft. Once again, the location of this optimum point could be expected to be influenced most by factors affecting system time delay (i.e., error perception) at the low end of display gain. Task demands would be expected to drive the performance level at that optimum gain.

The pilot ratings predicted by Anderson's (1970) "Paper Pilot" (that appears in §2.3) were compared with the actual subjective ratings collected in this study. The match was found to be very poor, which is not surprising since the pilot lead constants were essentially constant for all display gains - only the motion sensitivity changed. In Anderson's study pilots were observing actual performance, whereas in this study pilots could only view displayed error - actual error remained relatively constant over much of the gain region where subjective ratings were changing most rapidly.

122

5.3 Comparison Between Single-Axis and Multi-Axis Station-Keeping Results

5.3.1 Time Domain Data

In Figure 5.31, the single axis mean position errors between axes are similar in profile, as is the case with the multi-axis control. The three axes reach a minimum near 3 mrad/ft for both single and multi-axis. The minimum RMS error for single axis is approximately 2 ft, and further increases in display sensitivity have little effect on position error. For multi-axis, the minimum RMS error shifts up to approximately 4 ft. Increasing sensitivity above 3 mrad/ft results in rapid growth of the longitudinal error while the other two axes' errors increase less rapidly.
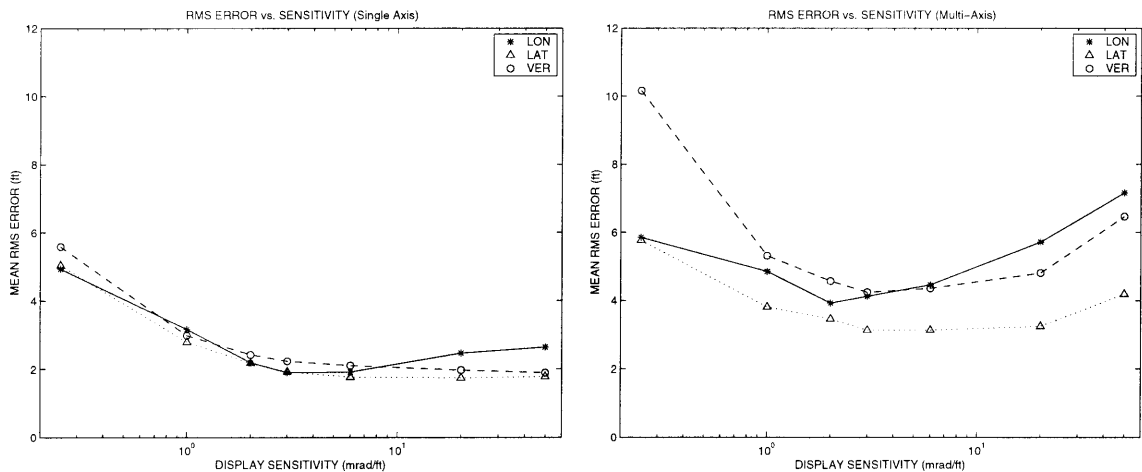
Figure 5.31. Position RMS error versus display sensitivity, single axis and multi-axis.

In Figure 5.32, the single axis minimum time delays are approximately 0.25, 0.25, and 0.4 seconds lower than multi-axis delay for the longitudinal, lateral, and vertical axes, respectively.
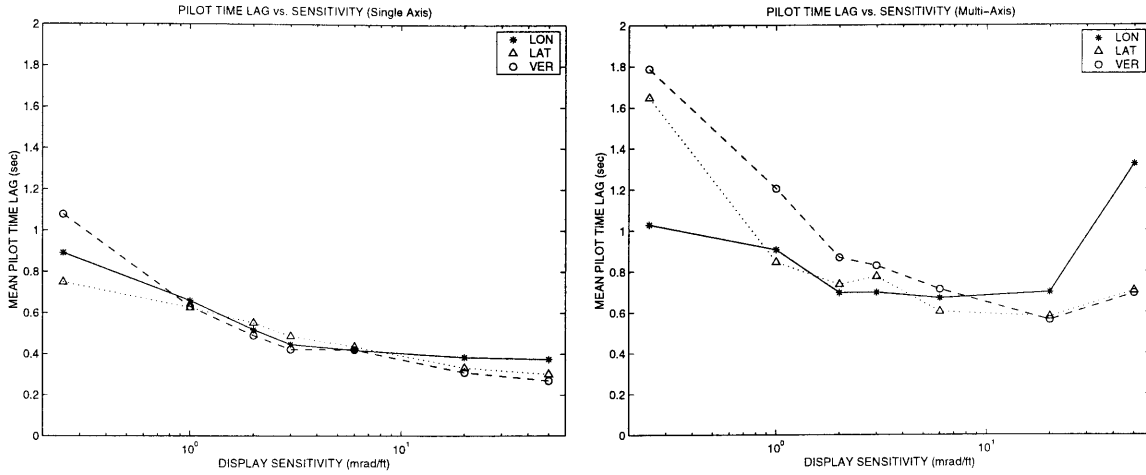
Figure 5.32. Pilot time delay versus display sensitivity. single axis and multi-axis.

In Figure 5.33 saturation is seen to affect all axes at 20 mrad/ft during multi-axis operation, and at 50 mrad/ft the longitudinal axis has saturated approximately 60% of the time.
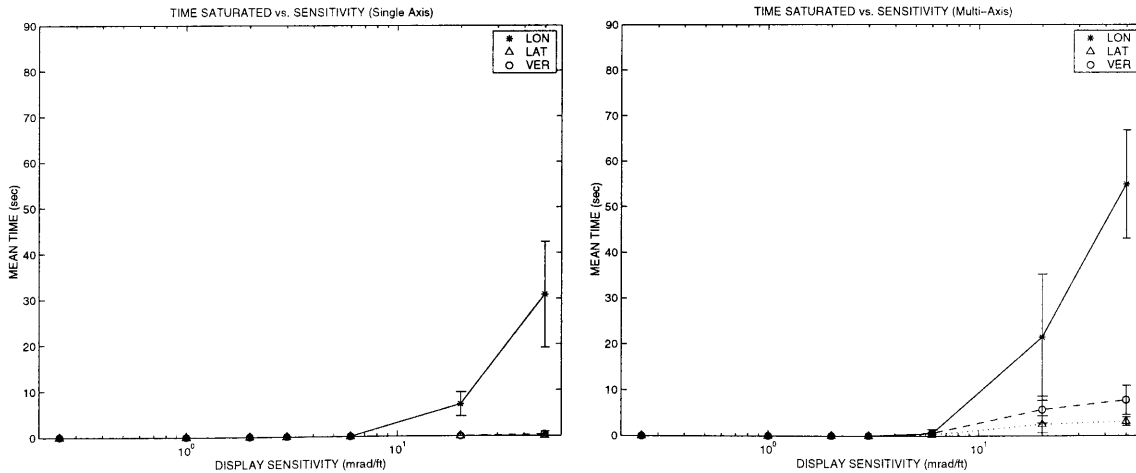
Figure 5.33. Operating times for when cue motion was saturated (90-second total run time).

5.3.2 Subjective Scores

Figure 5.34 shows that for a sensitivity of 6 mrad/ft and higher, the single axis longitudinal subjective scores closely match the multi-axis scores.
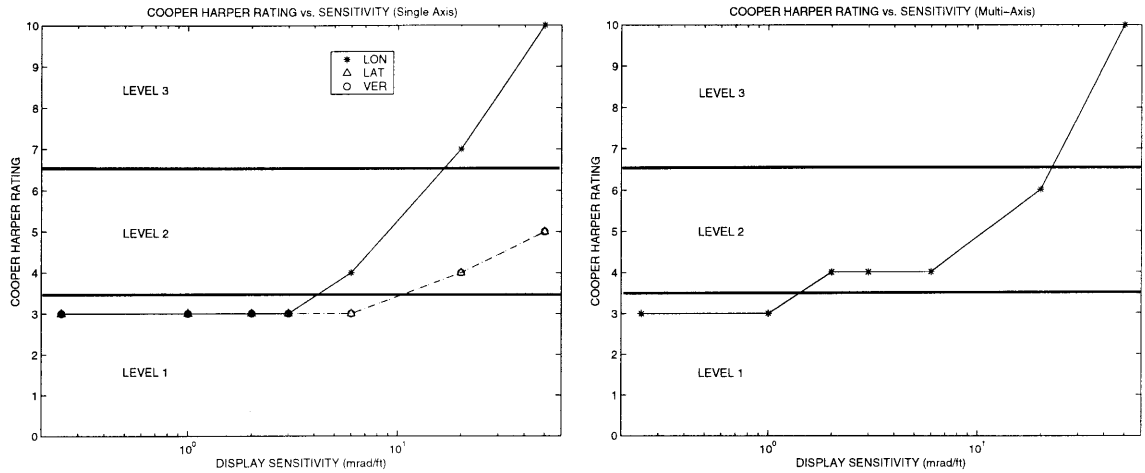
Figure 5.34. Subjective rating versus display sensitivity, single axis and multi-axis.

5.3.3 Frequency Domain Data

In Figure 5.35, the single axis crossover frequencies are uniformly higher than the multi-axis crossover frequencies. At a sensitivity of 50 mrad/ft, multi-axis crossover has regressed, whereas single axis crossover frequencies at 50 mrad/ft still appear to be rising. For both single axis and multi-axis, vertical crossover is generally highest.
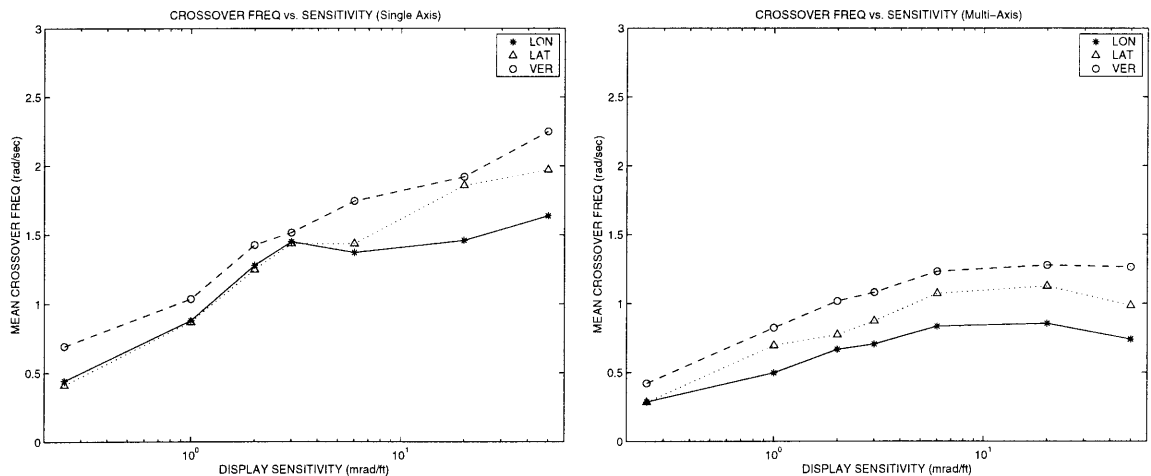
Figure 5.35. Crossover frequency versus display sensitivity, single axis and multi-axis.

125

Figure 5.36 shows the ratios for crossover frequency between multi-axis and single axis (within subjects). At the optimum gain of 3 mrad/ft the vertical axis exhibits the largest ratio, followed by lateral, with longitudinal showing the lowest ratio.

In Figure 5.37, the single axis phase margins for all axes coalesce to approximately 50 degrees. The vertical multi-axis phase margin in general is lower than the other axes' margins, and the longitudinal multi-axis margin appears to be decreasing with increasing sensitivity.
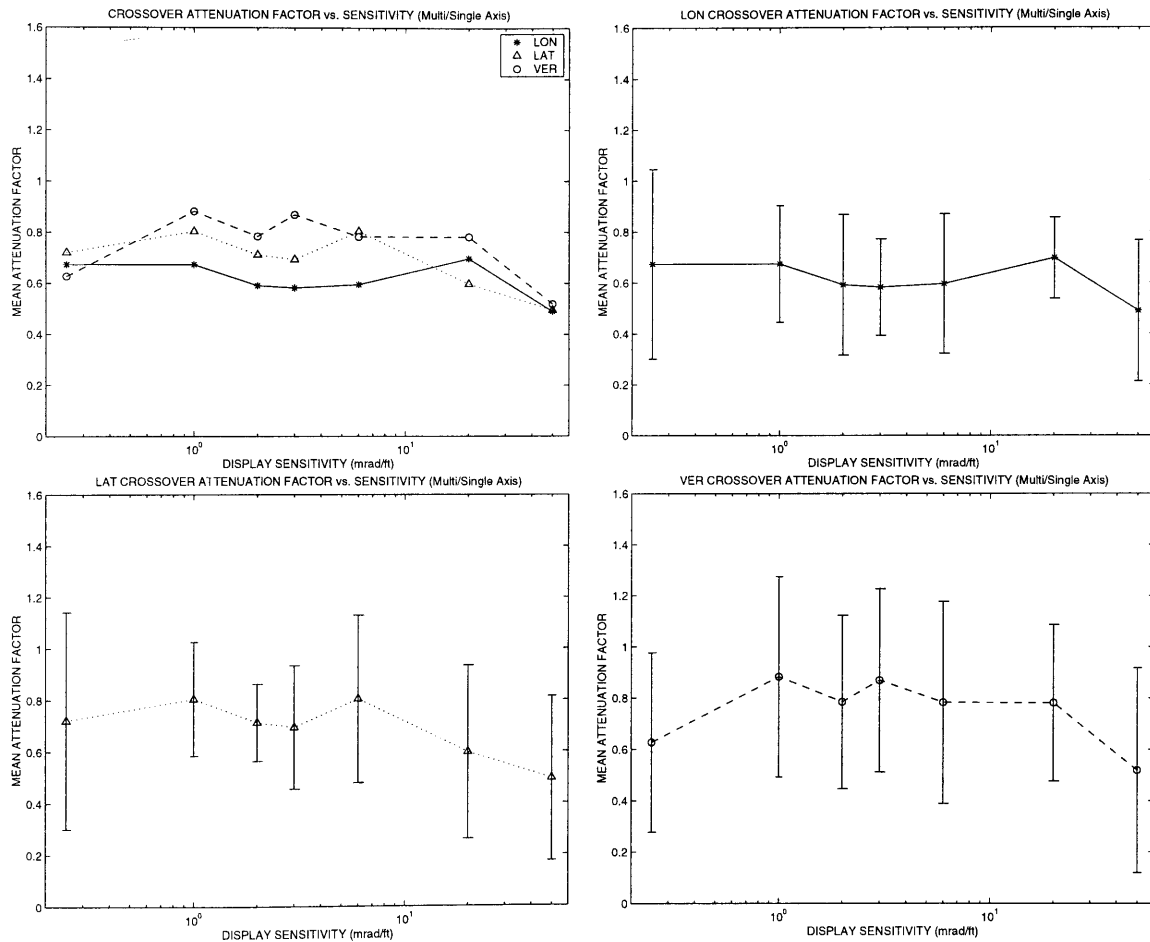
Figure 5.36. Crossover frequency ratios (multi/single-axis)
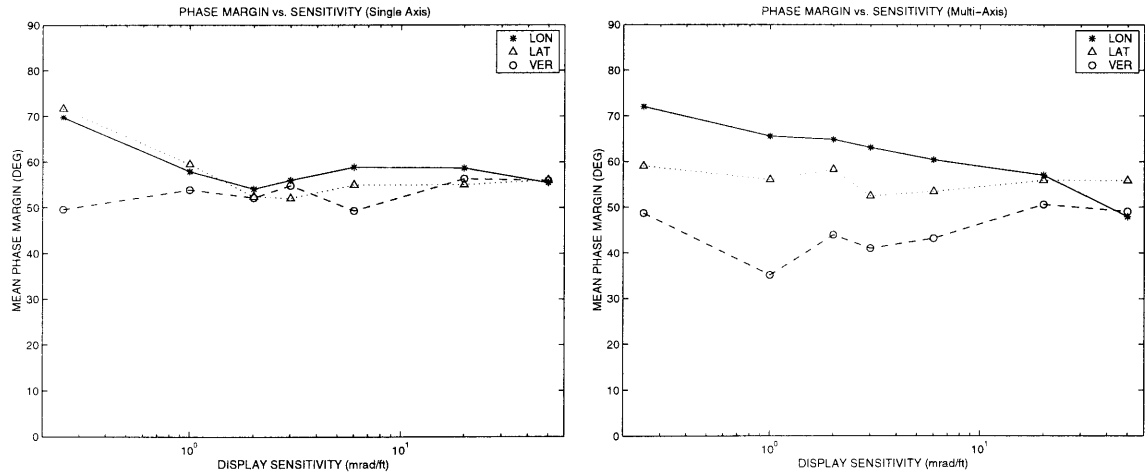
Figure 5.37. Phase margin versus display sensitivity. Single axis and multi-axis.

In Figure 5.38 the single axis amplitude ratio slopes generally flatten toward -20 dB/dec with increasing sensitivity. Multi-axis slopes initially are seen to steepen with increasing sensitivity and then flatten beyond 3 mrad/ft.
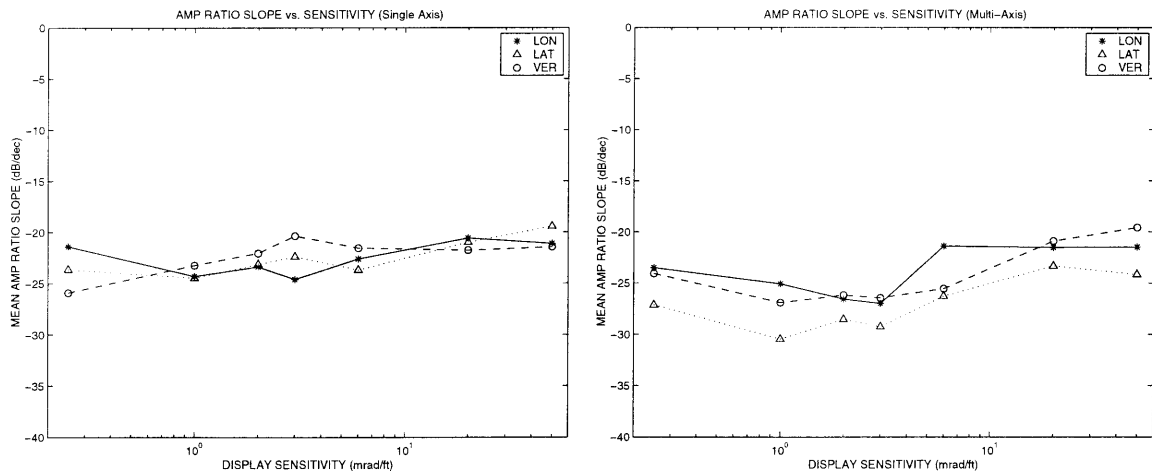
Figure 5.38. Amplitude ratio slope versus display sensitivity. Single axis and multi-axis.

Figure 5.39 shows the single axis and multi-axis normalized DC observation noise

to be very similar in magnitude and shape.
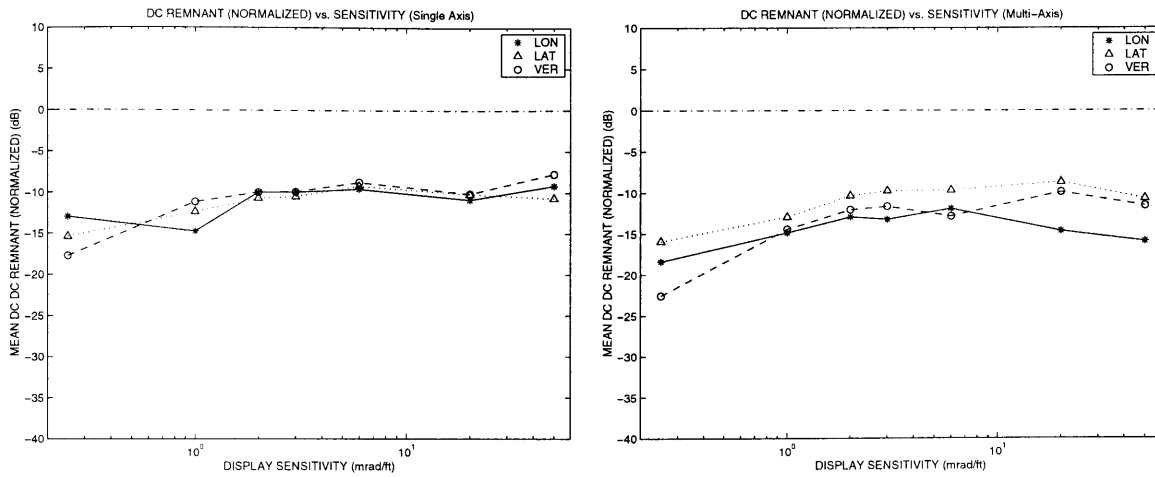
Figure 5.39. Normalized DC observation noise versus display sensitivity single axis and multi-axis.

In Figure 5.40 break frequencies are similar for single and multi-axis control,

showing relative invariance with display gain.
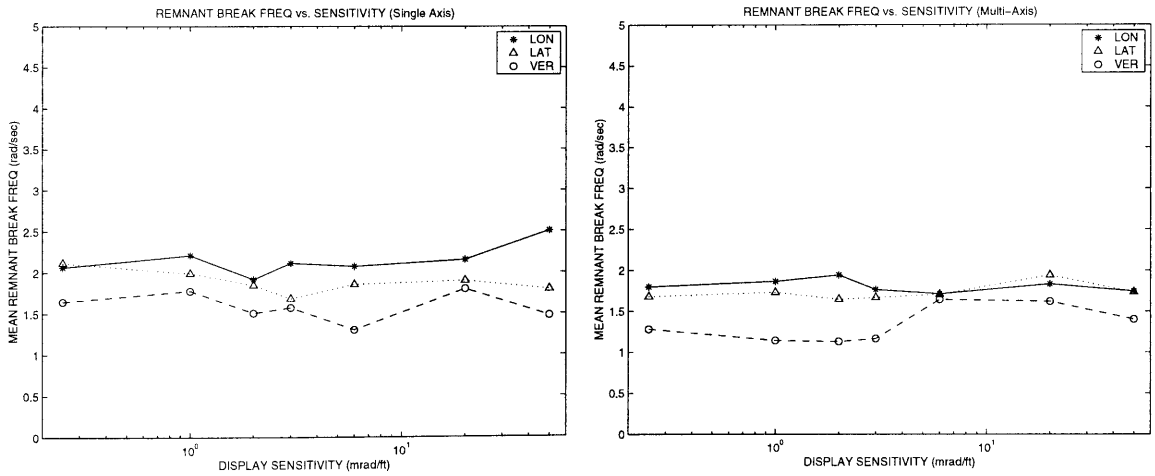
**Figure 5.40. Break frequency of observation noise versus display sensitivity, single axis
and multi-axis.**

In Figure 5.41 both the single axis and multi-axis vertical axis slopes appear to be less steep than the other axes. For the single axis case, display sensitivity appears to have a flattening effect on slope up until 6 mrad/ft.
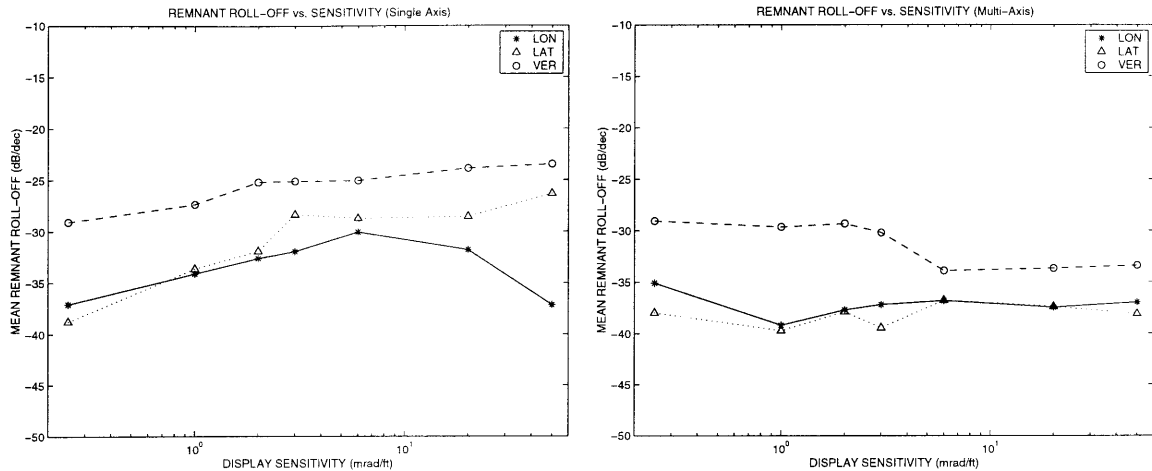
Figure 5.41. High frequency slope of observation noise versus display sensitivity, single axis and multi-axis.

In Figure 3.41 relative remnant for multi-axis control appears to be higher than single axis remnant for all display gains in the vertical axis, and above 3 mrad/ft in the longitudinal axis. Remnant in the lateral axis appears to be relatively unaffected by divided attention.
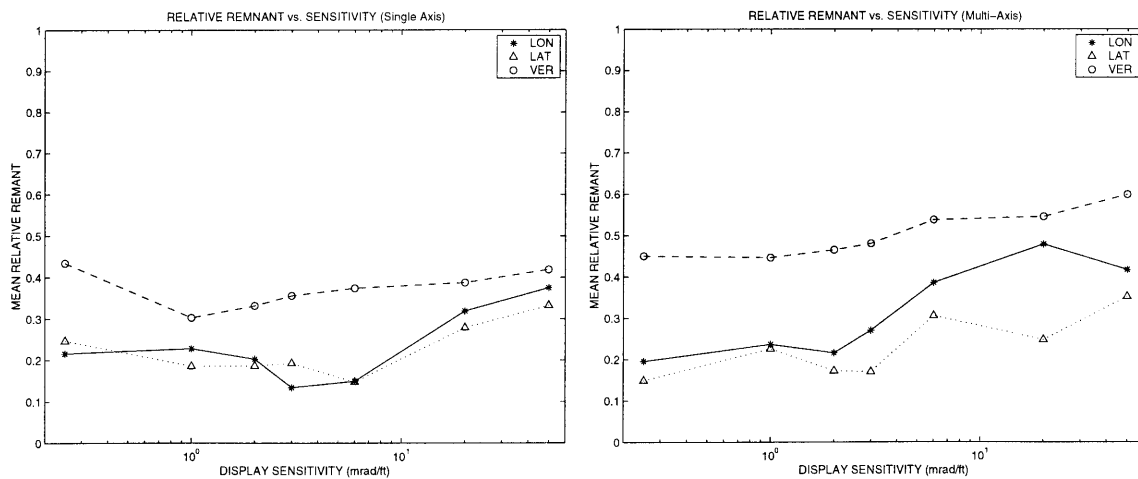
Figure 5.42. Relative remnant versus display sensitivity, single axis and multi-axis.

Discussion on the comparison between single and multi-axis results will be presented following the results of the next section.

5.4 Performance Tradeoff Varying Display Motion Gains Between Axes

Figure 5.43 shows the results for the performance tradeoff study, and Table 5.1 presents the results of a multivariate repeated measures analysis performed on the position RMS data. Independent variables were sensitivity (1 and 3 mrad/ft) and axis of sensitivity (longitudinal, lateral, and vertical). Changes in longitudinal sensitivity are seen to significantly affect performance in the other axes, with a similar result for changes in lateral sensitivity. As an example, the first display condition is compared with the second in Figure 5.43. Longitudinal sensitivity is increased from 1 to 3 mrad/ft while the other axes remain at 1 mrad/ft. As expected, performance in the longitudinal axis improves, however performance in the two cross-axes degrades.

Time delays in each axis during single axis control were comparable to one another, however, the increase in time delay in going to multi-axis operation appeared to be greater in the vertical than the other two axes. In order to maintain the same single-axis stability margins during multi-axis operation crossover frequency would have to be reduced in all axes due to the increased latencies (and remnant, when it increased). As
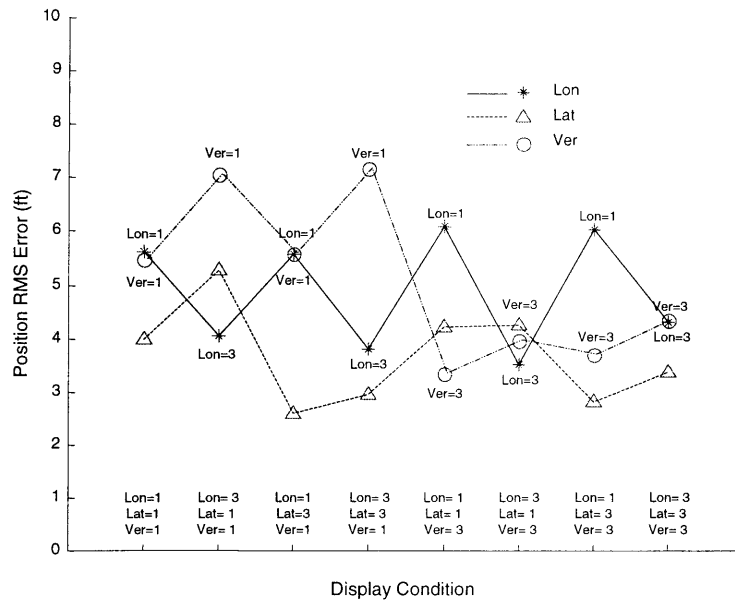
Figure 5.43. RMS errors for sensitivity tradeoff study.

Table 5.1. Multivariate repeated measures analysis results.

	p
Main effect of axes across all sensitivities	0.006
Main effect of lon sensitivity across all axes	0.061
Main effect of lat sensitivity across all axes	0.038
Main effect of ver sensitivity across all axes	0.208
Effect of lon sensitivity on each axis	0.007
Effect of lat sensitivity on each axis	0.040
Effect of ver sensitivity on each axis	0.203

the vertical axis had the highest latency, it might be expected that this axis would have

had the smallest multi/single crossover ratio. Instead, it exhibited the highest ratio of the

three axes, as well as the lowest phase margin.

Longitudinal axis sensitivity was seen to have the most significant effect on cross-

axis performance, and the longitudinal axis also appeared to have the smallest multi-to-

single crossover ratio. These results might be indicative of a different control strategy for

the vertical than the longitudinal and lateral axes, where task-sharing is appropriating more attentional resources to longitudinal and lateral axes.

5.5 The Effect of Synthetic Cues on Station-Keeping Using a Simulated NVG Environment

The primary objective of this experiment was to compare station-keeping performance using the baseline NVG display and the Synthetic Cue display. A secondary objective was to determine if perceptual conflict occurs when synthetic cues are assigned translational gains that are different from those in the natural background scene. The display conditions that were flown are shown in Table 5.2.

The ground tracks of the seven pilots are overlaid on one another in Figure 5.44 for the six display conditions. All pilots initiated flight at the (0, 0) point denoted by the intersecting dashed lines. The *NVG* far-field condition yielded a much wider area of ground drift compared with the far-field *NVG*/Synthetic Cue display condition, the latter

Table 5.2. Matrix of display conditions flown.

Display	Lon Gain	Lat Gain	Ver Gain	Field Type
NVG/Synthetic Cue	3	3	3	Near
NVG/Synthetic Cue	3	3	3	Far
NVG/Synthetic Cue	3	1	3	Near
NVG/Synthetic Cue	3	1	3	Far
NVG	*	*	*	Near
NVG	*	*	*	Far

producing a well-defined region of drift centered tightly about the initial hover point. The near-field *NVG* condition shows a pronounced rearward drift whose axis is centered on the lateral starting position. Lateral error is seen to become progressively worse as drift increases rearward, which is consistent with the decreasing angular error the pilot

observes (for the same lateral displacement) as distance from the near-field objects increases. The *NVG/* Synthetic Cue display condition using near-field objects produced a ground track profile essentially identical to the one seen when far-field objects were used.

The mean RMS errors corresponding to the ground tracks of Figure 5.44 are shown in Figure 5.45. There is a significant effect of the synthetic cues on longitudinal position for both near and far-field conditions, and a significant effect on lateral position for the far-field case. Synthetic cues were not found to have an effect on altitude control, presumably due to the fact that an altimeter could be viewed on the instrument panel while looking forward out the cockpit.

In Figure 5.46 the crossover frequencies are shown for the display conditions. Longitudinal crossover for the *NVG* condition appears to be less than half of what the *NVG*/Synthetic Cue condition yielded. Note that longitudinal crossover standard deviation at the 3/3/3 (lon/lat/ver) sensitivity condition (near-field objects) is considerably larger than for the 3/1/3 other display condition. This appears to indicate that higher consistency in the longitudinal axis is achieved by trading lateral performance. Note that in Figure 5.40 lateral performance did not differ very much between the 3/3/3 and 3/1/3 conditions.

Far-Field Objects
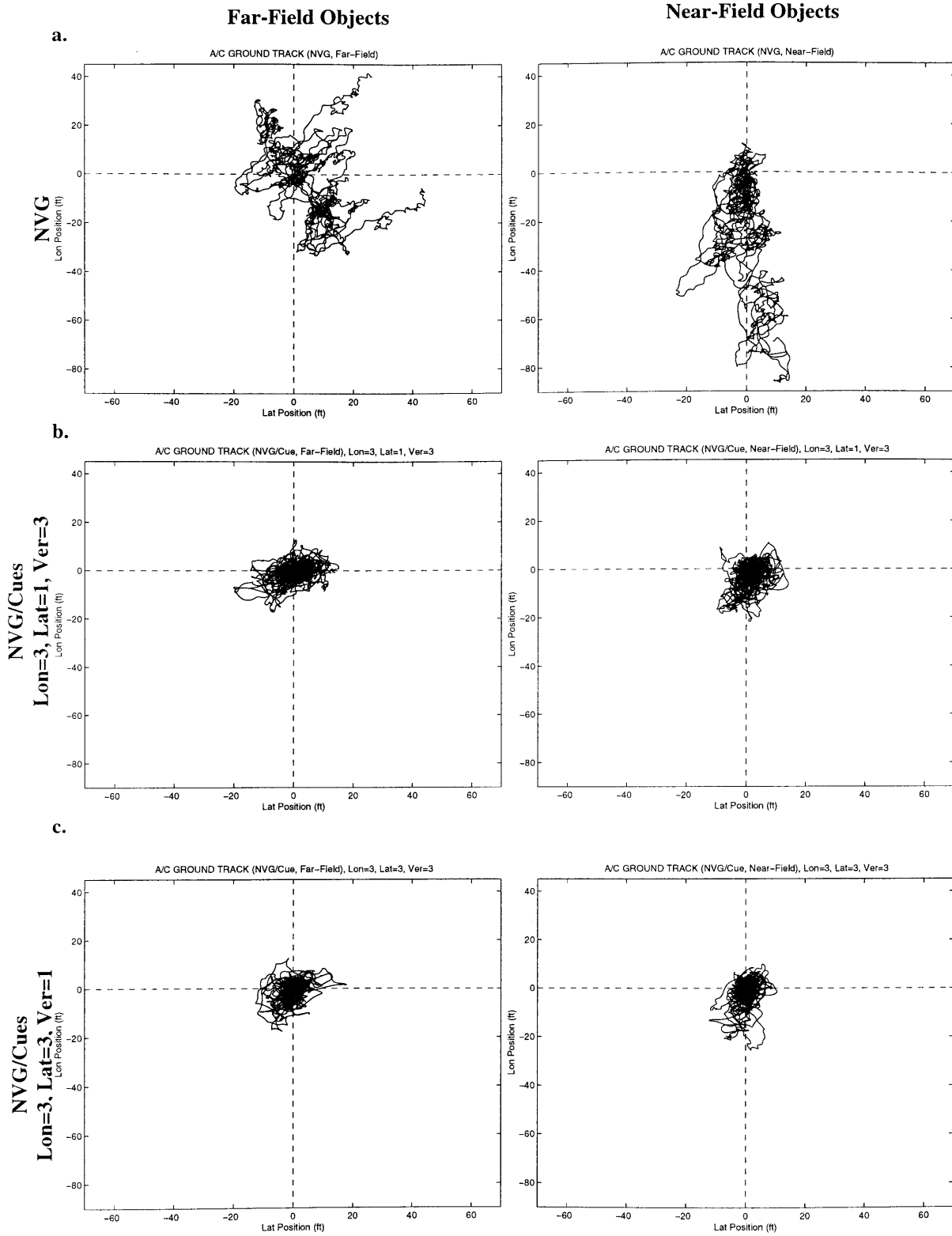
Near-Field Objects

Figure 5.44. Hover ground tracks using: a) NVG display condition; b) and c) NVG/Synthetic Cue display condition, near-field and far-field objects in view.

134
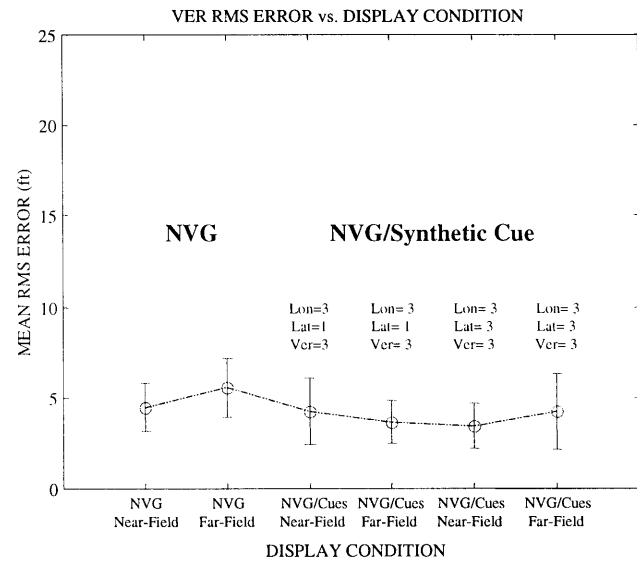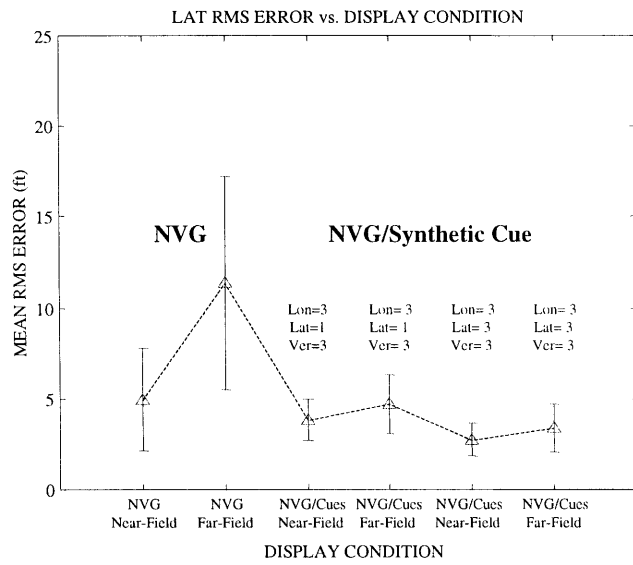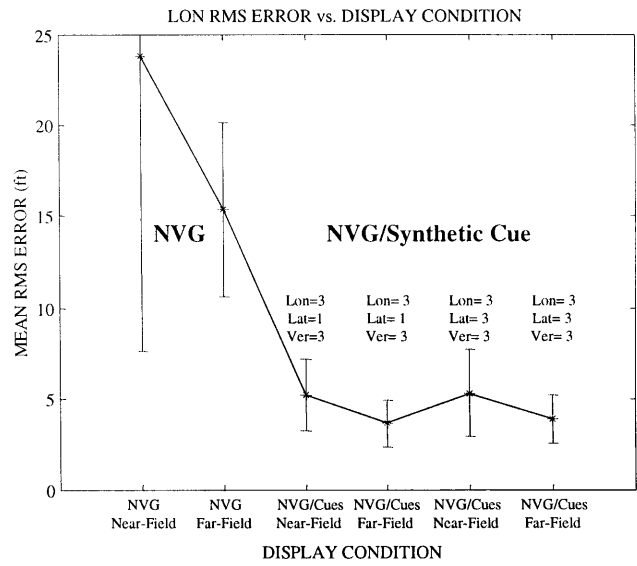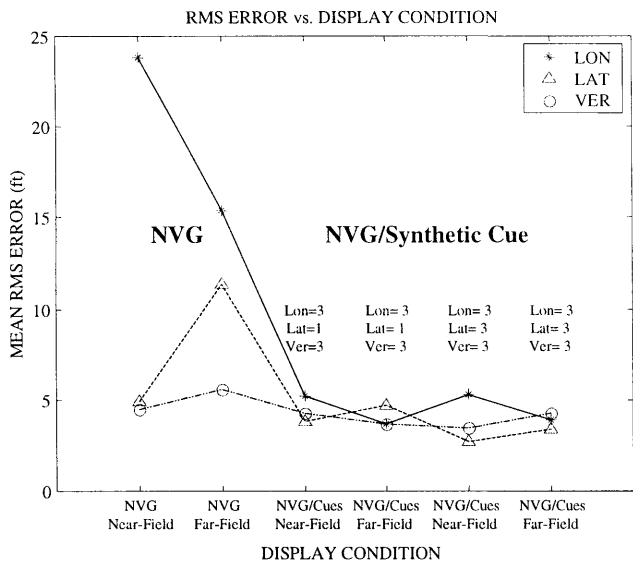
Figure 5.45. Station-keeping performance showing effect of synthetic cues and presence of near-field objects.
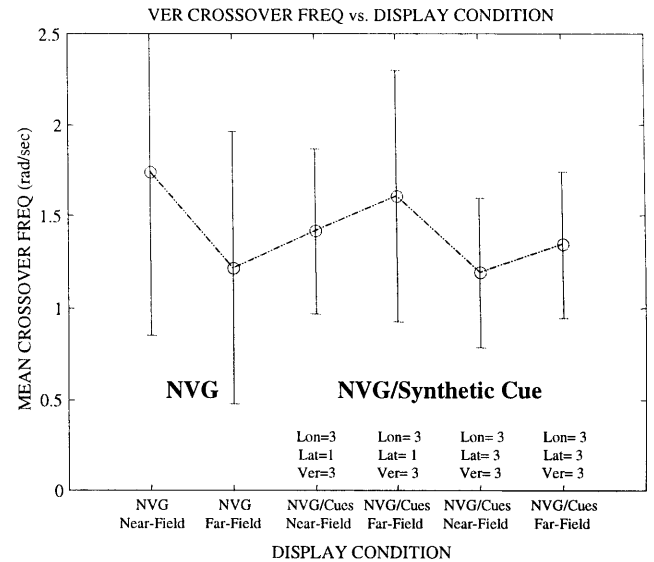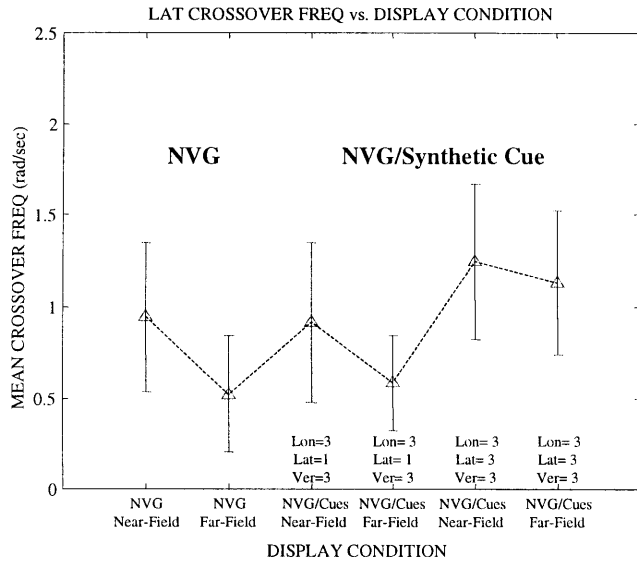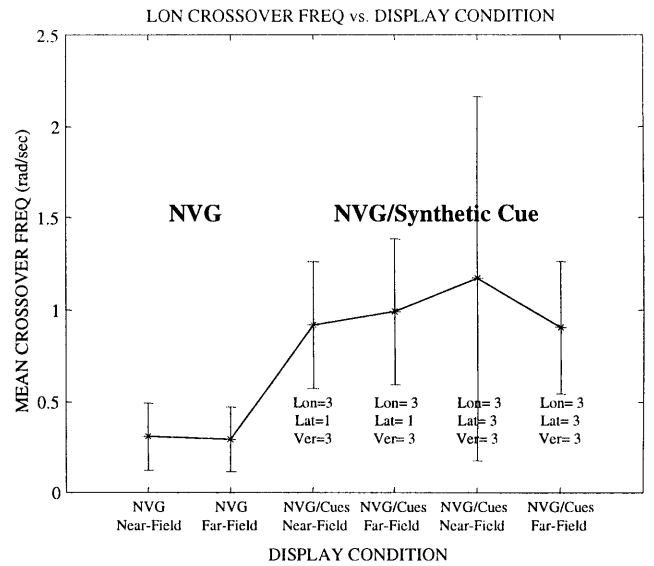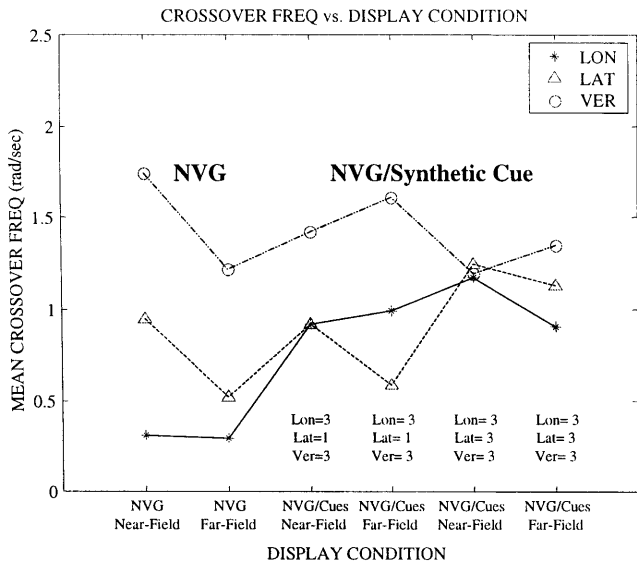
Figure 5.46. Crossover frequency showing effect of synthetic cues and presence of near-field objects.

The subjective ratings for the six display conditions are shown in Table 5.3. In addition to the ratings, pilots were questioned about any perceptual or physical discomfort they might have experienced while flying with the overlaid synthetic cues. No adverse reactions were reported. In post flight briefings, the pilots were very surprised when shown groundtracks – while using the NVG display in-flight, none of them had apparently been aware of gross drift for either the near-field or far-field viewing conditions.

Table 5.3. Subjective ratings (Cooper-Harper) for display conditions flown.

Display	Lon Gain	Lat Gain	Ver Gain	Field Type	MedianCooper-Harper Rating
NVG/Synthetic Cue	3	3	3	Near	4
NVG/Synthetic Cue	3	3	3	Far	4
NVG/Synthetic Cue	3	1	3	Near	4
NVG/Synthetic Cue	3	1	3	Far	4
NVG	*	*	*	Near	4
NVG	*	*	*	Far	4

Chapter 6

Summary and Conclusions

6.1 Summary

This thesis identified a need for synthetic cueing in the night vision flight environment, and based on an integrated approach a prototype ecological cue set was developed. This cue set raised the potential problem of differential perceived sensitivity between the longitudinal and transverse axes, which led to the development of a synthetic enhancement technique for perceiving longitudinal error. This in turn brought up issues of perception and performance due to non-conformality. In order to investigate these and other issues, as well as cue system performance, a unique simulation facility was developed which incorporated state-of-art helicopter dynamic characteristics with a realistic hover environment. This allowed pilot perception and control of each axis to be independently probed for frequency content and performance.

A set of single-axis control experiments was conducted using the prototype cue set to establish baseline pilot perception and control. The data indicated that: (1) an optimal gain common to all three axes appeared to exist, (2) pilot time lags associated with all three axes were similar, (3) the longitudinal axis was more difficult to control (based on subjective ratings) and exhibited the worst performance at high sensitivities, (4) the vertical axis appeared to have the highest spurious control activity, and the highest crossover frequency (indicative of highest internal pilot gain), and (5) the lateral axis was the easiest to control, based on subjective ratings.

138

In order to establish the best set of cue motion gains for use with the prototype cue set in NVG flight, another experiment was conducted that looked at the effect of display motion sensitivity on pilot response during multi-axis control. The results of this experiment indicated that: (1) an optimal gain common to all three axes seemed to correspond to the same optimal gain seen in the single-axis control case, (2) multi-axis operation was more difficult to control at lower sensitivities than single-axis, based on increased subjective ratings - at higher sensitivities, subjective ratings appeared to be driven by the longitudinal axis (similar profile as single-axis ratings), (3) across all axes performance and crossover frequency decreased, while pilot time delay and spurious control activity increased, (4) the longitudinal axis exhibited the lowest crossover, (5) the vertical axis showed the highest spurious noise activity, highest crossover frequency, largest pilot time delay increase, and the lowest phase margins (lowest stability), and (6) the lateral axis exhibited the best performance at all sensitivities.

A third experiment was conducted investigating the performance tradeoff when mixing gains between axes. This study indicated that: (1) changes in longitudinal (and lateral) sensitivity significantly degraded performance in the other two axes, (2) the longitudinal and lateral axes appeared relatively insensitive to changes in vertical sensitivity, (3) there was a control strategy where the vertical axis is given less attention but higher gain than the other axes (hence less stable), and the longitudinal axis is given highest priority.

A fourth and final experiment was conducted that compared hover using the baseline NVG image against the synthetic cue set using the optimal gains determined in the multi-axis study. The results of this study indicated that: (1) synthetic cues designed around compensatory task were found to significantly improve hover performance when

139

overlaid on a simulated NVG environment, (2) the effect of near-field objects in NVG visible scene was that all subjects backed away, consistent with a number of NVG-related accidents involving rearward flight into trees or ground, (3) synthetic cues allowed pilots to compensate for the fear of forward drift and collision with near-field tree, (4) the effect of non-conformal box displacement did not appear to be an issue, and (5) synthetic cues can be manipulated in an ecological, pseudo-conformal manner to significantly enhance hover performance in a visually degraded environment, even in regimes of high-threat.

In this study display sensitivity appeared to have a direct effect on pilot time delay. Time delay establishes the maximum crossover frequency for a time-delay-normalized crossover frequency stability limit of $\pi/2$. Two factors that appear to influence pilot time delay are perceptual threshold (which include display quantization effects), and task demands (which affect neuromuscular tightening). The data suggest that perceptual effects manifest themselves at the lowest display gains in the form of heightened time delay sensitivity to changes in display gain, as compared to lower time delay sensitivity due to task demands. Time delay appeared to increase for all axes at the highest display gain during multi-axis operation, which indicates that time delay may be subject to the U-shaped behavior that is normally seen in performance with increasing task demands.

Comparison of single and multi-axis control suggest that division of attention can have profound effects on time delay, thus on maximum crossover and performance. Single axis operation showed virtually no performance degradation when saturation occurred, however divided attention in combination with saturation was seen to dramatically decrease performance.

Despite a higher crossover at all display gains during multi-axis control, the vertical axis yielded performance that was consistently worse than the lateral axis, agreeing with the higher remnant observed in the vertical. Additionally, phase margin in the vertical appeared to be lower than the lateral, and because of remnant actual stability margin of the vertical axis would be lower than the phase margins indicated. The high gain/low stability response is believed to be a consequence of the velocity cues (which have the same gains as the position cues) driving the pilot's vertical inner-loop gain higher than the inner-loop gains of the lateral and longitudinal axes, which probably relied on constant-gain attitude cues.

One possible factor contributing to the difference in control (multi-axis) between the vertical and the other two axes is pilot conditioning. The vertical dynamics in a real helicopter tend to be relatively stable due in part to ground effect, whereas the longitudinal and lateral axes require fairly tight attitude control for stability. Attitude was a surrogate state for lateral and longitudinal position rate in this study, but rather than use the rate cues for all but the highest display gains pilots appeared to have used attitude for inner-loop control, which would be expected from force of habit. The phenomenon of error and crossover invariance that has previously been observed for single-loop, compensatory tasks does not appear to hold at high gains when the display motion gain of the inner-loop is subject to the same gain as the outer position loop cues.

The Crossover Model holds up remarkably well for the tasks considered here, in particular since the display configuration differed markedly from those on which the original model was based. A modest departure from the nominal –20 dB/dec slope occurred when low display sensitivities were used and for multi-axis operation, perhaps to accomplish noise filtering. The Crossover Model proved an invaluable tool for

modeling and analyzing pilot control behavior, and in conjunction with the guidelines developed in Chapter 2 it provides the means for an intuitive, analytical approach toward compensatory task display design.

6.2   Conclusions

This thesis has shown that significant gains in hover performance can be achieved through appropriate use of synthetic cues. By careful design a cueing system was developed that can match different axis gains with the human's perception and control characteristics, as well as with the task requirements. These cues were presented such that position performance could be maintained relatively constant over a very wide range of display conditions, but subjective ratings were not constant. Indeed, an optimal gain set appears to exist, which should depend on such factors as vehicle dynamics, task demands, and flight environment. While the cueing system developed here worked very well, a number of issues would have to be explored before final implementation, including: (1) obscuration and clutter, (2) cue color selection, (3) cue fixation, (4) sensor (i.e., head tracking, GPS) integration and reliability, and (5) initiation of display cue set (i.e., pilot-triggered, remotely programmed). In addition, such a display would have to be matched with the task requirements. As this display is limited to the hover task, other cueing may be required for flight phases transitioning into and out of hover.

The results of this study have demonstrated that, even while operating in a visually complex environment, humans appear to close control loops in a manner consistent with the Crossover Model. Use of such knowledge can greatly assist in the development and evaluation of future display designs. If done correctly, it is anticipated

that implementation of synthetic cues in night vision systems could significantly reduce both training time and fatigue due to workload while improving performance.

The display used in this thesis was set up for non-coupled, tightly attitude-controlled helicopters. State-of-the-art helicopter design already employs these dynamics – the challenge today is presenting the proper synthetic visual cues to improve impoverished Usable Cue Environments. On a display/control tradeoff, it is proposed that the display concept employed in this thesis could be used with state-of-art helicopter dynamics to provide a Usable Cue Environment of 1.

Strong consideration should be given to integrating synthetic cueing systems into current and future helicopter Night Vision Device systems. The enhanced hover performance and dynamic situation awareness should serve to reduce the risk of NVD accident and subsequent loss of life.

References

Allen, Wade R. and Duane T. McRuer, *The Man/Machine Control Interface – Pursuit Control*, System Technology, Inc., Paper No. 243, Apr. 1979.

Anderson, Ronald O., *A New Approach to the Specification and Evaluation of Flying Qualities*, Technical Report AFFDL-TR-69-120, June 1970.

Bachelder, Edward N. and R. J. Hansman, "Issues in Simultaneous HMD Display of Multi-Reference Frames for Helicopter Applications," SPIE Proceedings: Enhanced and Synthetic Vision; Paper No. 2736-23, 1995.

Bode, H. W., *Network Analysis and Feedback Amplifier Design*, Van Nostrand, New York, 1945.

Brown, Rober G., *Introduction to Random Signal Analysis and Kalman Filtering*, John Wiley & Sons, New York, 1983.

Bruce, Vicki, Patrick R. Green, and Mark A. Georgeson, *Visual Perception: Physiology, Psychology, and Ecology*, Psychology Press, United Kingdom, 1996.

Clement, Warren F., Hoh, Ferguson, et al., *Flying and Ground Handling Qualities Requirements for Military Rotorcraft* – MIL-H-8501 Revised, Systems Technology, Inc., TR-1194-1-I, Jan. 1984.

Cooper, G. E., and R. P. Harper, Jr., *The Use of Pilot Ratings in the Evaluation of Aircraft Handling Qualities*, NASA TN D-5153, Apr. 1969.

Crowley, J., Rash, C. and R. Stephens, "Visual Illusions and other Effects with Night Vision Devices," *SPIE,* Vol. 1695, Helmet Mounted Displays III, 1992.

Cutting, James E., and Peter M. Vishton, *Perceiving Layout and Knowing Distances: The Integration, Relative Potency, and Contextual Use of Different Information about Depth.* In W. Epstein & S. Rogers (Eds), *Handbook of Perception and Cognition. Vol. 5: Perception of Space and Motion*, San Diego, CA, 1995.

Dornheim, Michael A., "Ames YAV-8B Demonstrates ASTOVL Landing Concepts," *Aviation Week & Space Technology*, Apr. 10, 1995.

Gelb, Arthur and Wallace E. Vander Velde, *Multiple-Input Describing Functions and Nonlinear System Design*, McGraw-Hill Book Company, New York, 1968.

Gillingham, Kent K. and Fred H. Previc, *Spatial Orientation in Flight*, Armstrong Laboratory, Final Technical Report for Period January 1982 – January 1993, Nov. 1993.

Heffley, Robert K. (System Technology, Inc), *A Compilation and Analysis of Helicopter Handling Qualities Data*, NASA – Ames Research Center, Vol.2, Aug. 1979.

Heffley, Robert K., Clement, Ringland et al., *Determination of Motion and Visual System Requirements for Flight Training Simulators*, Department of the Army – ARI, Report STI-TR-1162-1, Aug. 1981.

Hess, Ronald A. and Peter J. Goder, *Design and Evaluation of a Cockpit Display for Hovering Flight*, AIAA Paper No.88-4495, Sept. 1988.

Hoh, Roger H. (System Technology, Inc), *Investigation of Outside Visual Cues Required for Low Speed and Hover*, National Aeronautics and Space Administration Ames Research Center, Report No. 1213-1, Jun. 1984.

Hoh, Roger H. (System Technology, Inc), "Handling Qualities Criterion for very Low Visibility Rotorcraft Noe Operations," *AGARD Flight Mechanics Panel Meeting Rotorcraft Design for Operations*, Paper No. 392, Amsterdam, The Netherlands, Oct. 1986.

Jex, H. R., and R. E. Magdaleno, "Corroborative Data on Normalization of Human Operator Remnant," IEEE Trans., Vol. MMS-10, No. 4, Dec. 1969.

Kemp, Gordon G., *A VTOL Prediction Display*, S.M.E.A.A. Thesis, Massachusetts Institute of Technology, Sep. 1969.

McCann, R. S. and D. C. Foyle, "Scene-Linked Symbology to Improve Situation Awareness," AGARD Conference Proceedings, No.555, 1995.

McRuer, Duane T., Ashkenas, Irving, and Dunstan Graham, *Aircraft Dynamics and Automatic Control*, Princeton, NJ: Princeton University, 1973.

McRuer, Duane T., Clement, Warren F., Thompson, Peter M., and Raymond E. Magdaleno, *Minimum Flight Qualities – Volume II: Pilot Modeling for Flying Qualities Applications*, Flight Dynamics Laboratory – Wright Research and Development Center, Report WRDC-TR-89-3125, Vol. II, Jan. 1990.

McRuer, Duane T. and D. K. Schmidt, "Pilot-Vehicle Analysis of Multi-Axis Tasks," AIAA Guidance, Navigation and Control Conference, Monterey, CA, Aug. 1987.

Miller, Robert E., Provines, Block, et al., *Comparative Visual Performance with AN/PVS-5A Night Vision Goggles under Starlight Conditions*, USAFSAM-TR-84-28, Brooks AFB, Texas, Nov. 1984.

Miller, Robert E. and Thomas J. Tredici, *Night Vision Manual for the Flight Surgeon*, Ophthalmology Branch, Armstrong Laboratory, Report AL-SR-1992-0002, Aug. 1992.

Mulder, Max, "Cybernetics of Tunnel in the Sky Displays," Delft, The Netherlands: Delft University, 1999.

National Research Council, *Aviation Safety and Pilot Control, Understanding and Preventing Unfavorable Pilot-Vehicle Interactions*, National Academy Press, Washington, D.C., 1997.

Newman, R. L., *Helmet-Mounted Display Symbology and Stabilization*, Crew Systems Tech. Report 93-19A, Apr. 1994.

Ockier, C., *Pilot-Induced Oscillations in Helicopters – Three Case Studies*, Report No. IB 111-96/12. Braunschweig, Germany: DLR Institut für Flugmechanik.

Riegler, J.T., Whiteley, J.D., Task, H.L., and J. Schueren, "The Effect of Signal-to-Noise Ratio on Visual Acuity through Night Vision Goggles," *AL/HSD*, Wright-Patterson AFB, Ohio, Mar. 1991.

Ringland, Robert F., Clement, Warren F., and Henry R. Jex, "Factors in Determining Visual and Motion Fidelity Requirements for Training Simulators," System Technology, Inc., Working Paper No. 1162-4, Dec. 1980, Revised Mar. 1981.

Stapleford, Robert L., Clement, Heffley et al., *Flight Control/Flying Qualities Investigation for Lift/Cruise Fan V/STOL – Vol. I: Analytical Development*, Naval Air Development Center, Report TR-1122-1-I, Aug. 1979.

Task, H. L., "Apparent Field of View versus Eye Relief," *HSD/YA*, Brooks AFB, Texas, Nov. 1991.

U.S. Army, *Handling Qualities Requirements for Military Rotorcraft.* ADS-33D. St. Louis, Missouri: U.S. Army Aviation Troop Command, 1994.

Vicente, K. J. and J. Rasmussen, "Ecological Interface Design: Theoretical Foundations," IEEE Trans. On Systems, Man and Cybernetics, Vol. 22, No. 4, Jul. 1992.

Warren, William H. and Kenneth J. Kurtz, "The Role of Central and Peripheral Vision in Perceiving the Direction of Self-Motion," *Perception and Psychophysics*, 1992.

Wier, D. H. and C. K. Wojcik, *Simulator Studies of the Driver's Dynamic Response in Steering Control Tasks*, Driving Simulation, Highway Research Record No. 364, 1971.

Wickens, C. D., "Frame-of-Reference in Displays for Flight Path Guidance and Navigation: Implications for the Design of HUDS, Approach Plates, and Rehearsal Flight Training," *U.S. Air Force Academy Symposium on Applied Psychology, Keynote Lecture*, 1994.